Politecnico di Milano

SCHOOL OF INDUSTRIAL AND INFORMATION ENGINEERING

Master of Science in Energy Engineering

POLITECNICO
MILANO 1863

Analysis of flow field design for Vanadium Redox Flow Batteries through the development and validation of CFD codes

Supervisor: Dr. Matteo Zago
Co-supervisor: Ing. Mirko Messaggi

Patrizio Canzi 836800

April 2017

Abstract

The recent penetration of renewable sources in the energy system caused a transformation of the needs of the distribution system and amplified the need of energy storage systems to properly balance the electricity grid. Among electrochemical energy storage devices, all vanadium flow batteries are one of the most promising technologies due to their high efficiency, long lifetime, reliability and independence between installed power and storage capacity. Oppositely, the low energy density and the high costs are preventing this technology from spreading at commercial level, even if many are the opportunities of improvement.
If research on materials is working towards better and cheaper components, other works are meant to improve the performance of the system by means of a smart stack configuration or optimizing the operating condition. This work deals with the impact on the performance of the battery of a single part of the system, the flow field, and, in order to accomplish the desired purpose, numerical models have to be implemented and validated on experimental data. The knowledge of the fluid dynamic and electrochemical phenomena is intended as a tool for the optimization of the geometrical characteristics of the flow field. Starting from a fitting procedure performed on a bidimensional model, a threedimensional code to solve fluid dynamics and electrochemistry will be developed using a commerical CFD code: "ANSYS Fluent". It will be used to characterize a *5 cm x 5 cm* hydrogen-vanadium battery, a particular cell setup aimed at enlightening the losses of just the positive electrode of a Vanadium Redox Flow Battery. Various geometries are simulated, including a serpentine flow field, a parallel flow field and an interdigitated flow field, while a novel geometry will be proposed. A dedicated procedure to analyze the impact of the flow field considering both the electrochemical performance and the pressure drop of the component is refined.
By means of the hydrogen-vanadium cell in $MRT\ Fuel\ Cell\ Lab$, four different flow fields are tested to understand which could be the optimal flow field configuration in a real system and to experimentally validate the numerical results.

Keywords: VRFB, Flow Battery, CFD, ANSYS Fluent, Mathematical model, Experimental study.

Abstract (different language)

La recente penetrazione di fonti rinnovabili all'interno del sistema energetico ha causato un cambiamento nelle necessità del sistema di distribuzione e ha messo in luce l'esigenza di sistemi di accumulo per bilanciare la rete. Tra i dispositivi elettrochimici, le batterie a flusso al vanadio rappresentano una delle migliori tecnologie a causa della loro alta efficienza, la lunga vita utile, l'affidabilità e l'indipendenza tra potenza installata e capacità immagazzinata. La scarsa densità energetica e gli alti costi non permettono ancora uno sviluppo su scala commerciale di questi sistemi, tuttavia sono presenti margini di miglioramento.
Se la ricerca nel campo dei materiali porta allo sviluppo di componenti più performanti ed economici, altri lavori sono intesi aumentare la prestazione del sistema attraverso una gestione intelligente dell'architettura dello stack oppure ottimizzando il punto di funzionamento. Questo lavoro quantifica l'impatto sulla prestazione della batteria di un singolo componente, il distributore, e, per ottemperare a questo obiettivo, sono stati sviluppati dei modelli numerici. La comprensione dei fenomeni fisici è intesa essere strumento per l'ottimizzazione delle caratteristiche geometriche del distributore. Partendo da una procedura di fitting usando un modello bidimensionale, un modello tridimensionale capace di risolvere fluidodinamica ed elettrochimica sarà sviluppato usando un codice CFD commerciale: "ANSYS Fluent ® ". Esso sarà usato per caratterizzare una cella idrogeno-vanadio di *5 cm x 5 cm*, un particolare setup sperimentale atto all'analisi delle perdite del solo elettrodo positivo di batterie a flusso al vanadio. Saranno simulate differenti geometrie, partendo da una geometria a serpentina e da una geometria in parallelo fino a una geometria interdigitated, mentre una nuova geometria verrà proposta. E' sviluppata una procedura per quantificare tenendo conto dei consumi degli ausiliari l'efficienza del sistema. Usando la cella idrogeno-vanadio presente nel laboratorio $MRT\ Fuel\ Cell\ Lab$, quattro distributori sono testati per capire quale sia la miglior configurazione per il distributore in un sistema reale e per validare sperimentalmente i risultati numerici.

Parole chiave: VRFB, Batterie a flusso, CFD, ANSYS Fluent, Modello matematico, Studio Sperimentale.

Extended Abstract

The recent penetration of renewable sources in the energy system caused a transformation of the needs of the distribution system and amplified the need of energy storage systems to properly balance the electricity grid. Among electrochemical energy storage devices, all vanadium flow batteries are one of the most promising technologies due to their high efficiency, long lifetime, reliability and independence between installed power and storage capacity. Oppositely, the low energy density and the high costs are preventing this technology from spreading at commercial level, even if many are the opportunities of improvement. If research on materials is working towards better and cheaper components, other works are meant to improve the performance of the system by means of a smart stack configuration or optimizing the operating condition. This work deals with the impact on the performance of the battery of a single part of the system: the flow field. It has to be said that in the beginning of the development of the technology of flow batteries the flow field was not used and electrolytes were just injected into the porous electrode. This configuration, called flow through, was common some years ago but than it was abandoned due to its disadvantages: high pressure drop and low performance. One of the most influencing articles on this topic was published by M.M Mench [1] and dealt with the analysis of the improvement of the performance of the system due to the use of a flow field and a cell architecture similar to the one used in fuel cells. The most utilized shapes of flow field present for fuel cells technologies were used in the field of flow batteries and are reported in figure 0.1: the main geometries are a serpentine one, the parallel geometry and the interdigitated shape.

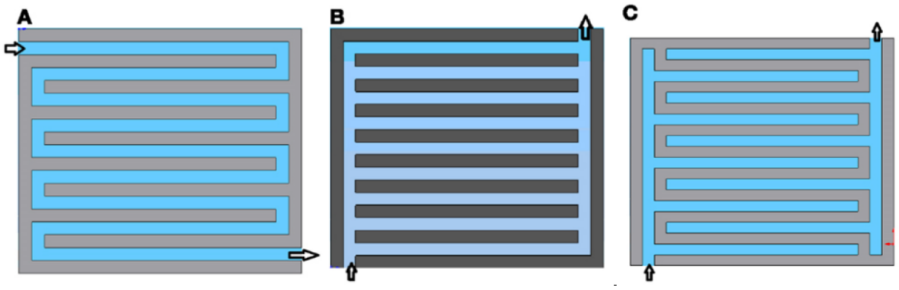

Fig. 0.1: Flow fields present in the literature: a)Serpentine, b)Parallel , c) Interdigitated

The determination of the properties of the flow field has to be considered using a particular experimental setup aimed at enlightening the losses of just the positive electrode of a Vanadium Redox Flow Battery: the hydrogen-vanadium cell present in $MRT\ Fuel\ Cell\ Lab$. A complete VRFB would not provide clear insights on the problem as the losses of two flow fields would be measured at the same time. What is more,in order to quantify the impact of this component, numerical models have to be implemented and validated against experimental data. The knowledge of the fluid dynamic and electrochemical phenomena is intended as a tool for the optimization of the geometrical characteristics of the flow field. Starting from a fitting procedure performed on existing experimental data using a bidimensional model in "$COMSOL\ Multiphysics^{®}$", a threedimensional code to solve fluid dynamics and electrochemistry will be developed using a commerical CFD code: "ANSYS Fluent ®". It will be used as an instrument for the characterization of a *5 cm x 5 cm* hydrogen-vanadium battery. Various geometries are simulated, including a serpentine flow field, a parallel flow field and an interdigitated flow field, while a novel geometry will be proposed, as visible in figure 0.2.

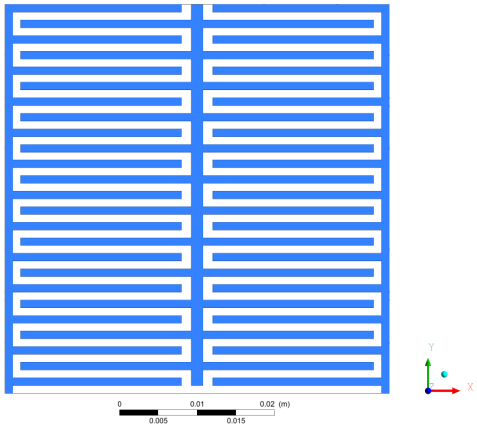

Fig. 0.2: Novel geometry proposed in this work

A dedicated procedure to analyze the impact of the flow field considering both the electrochemical performance and the pressure drop of the component is refined.
By means of the experimental setup in $MRT\ Fuel\ Cell\ Lab$, four different flow fields are tested in an hydrogen-vanadium cell to understand which could be the optimal flow field configuration in a real system.
The first part of the work dealt with the development of a bidimensional model using $COMSOL\ Multiphysics^{®}$ simulating in a potentiostatic way the performance of a cell tested in a previous work. The fitting procedure brought to the determination of a set of parameters used throughout the work and gave the opportunity to understand which are the most influencing phenomena and how they are modelled using the constitutive equations of the electrochemical cell. The weight of the parameters on the cell behaviour was clarified and a procedure to solve together electrochemistry and fluid dynamics was

developed. The characteristics of the electrode were its active area, the mean pore radius, the permeability and the porosity. These last two influence the fluid dynamic behaviour of the electrode while active area and mean pore radius are involved in the electrochemical reaction kinetics. Other key parameters were the reaction rate and the value of charge transfer coefficient and the influence of the numerical entity of parameters was very high. The results of the second chapter enlighten how it is difficult to relate the local behaviour of species' fluxes to the overall performance of the cell and how convection plays a major role in the porous domain. A threedimensional code has been developed using $ANSYS\ Fluent$ with the use of $User\ Defined\ Functions$ and $User\ Defined\ Scalars$. This model solves both electrochemistry and fluid dynamics inside a *5 cm x 5 cm* domain. The first case studied is the serpentine channel: the pressure distribution inside the cell is heavily influenced by the geometry of the flow field and forces some fluid to pass under the rib in certain zones close to the switchbacks. Such level of detail allows the visualization of the phenomena that occur in the porous electrode and in the channels. For example a variation of the state of charge of the battery on a plane at mid height of the porous electrode is reported in figure 0.3 along with the values of velocity in the same position of the porous medium (for more detailed information see chapter 3).

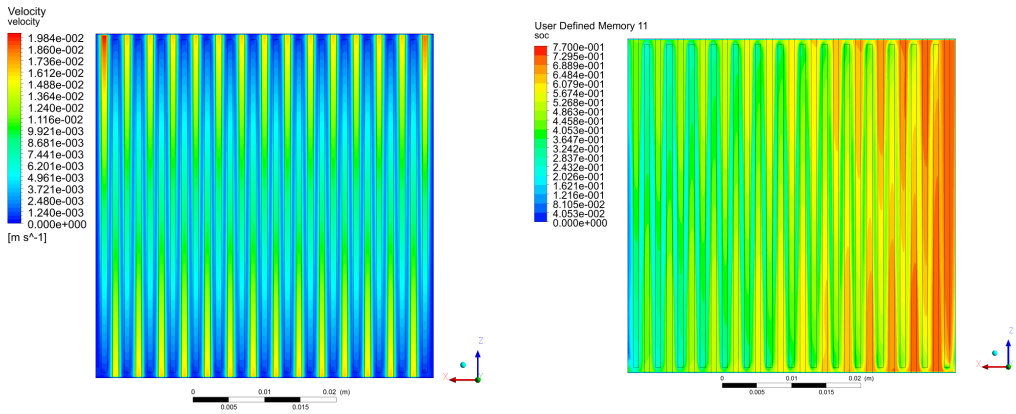

Fig. 0.3: Velocity (left) and state of charge (right) on a plane at half height of the porous medium

What emerges is that the flow in porous medium is not easy to be modelled and its link with electrochemical quantities is complicated: the solid part of the domain is not physically present in the models. Anyway this work clarifies, according to the assumptions made, the phenomenon of the under the rib fluxes, visualizing this quantity inside the electrode domain. The analysis presented is relevant from the scientific point of view as just one example of a fully coupled and full cell threedimensional model is found to exist in the literature [37] and therefore the knowledge of the problem is not fully investigated. Not much effort has been done to relate locally the performance of the cell to the fluid dynamic condition whereas in this work this aspect is analyzed. The fluid dynamic condition inside the porous domain changes the capability of the system to actively convert reactants and the mechanism through which this occur is through the effective movement

of the solution into the porous medium. On the other hand the potential values are imposed in the zones where there is a rib and therefore also this aspect has to be taken into account as the reaction depends effectively on the local value of the overpotential, determined by the geometrical architecture and the electric properties of the material. The geometrical characteristics of the domain have been investigated performing a sensitivity analysis with respect to the channel dimension pointing out that for a serpentine flow field the smaller the channel the higher the performance for a given flow rate and state of charge. According to the experimental analysis present in the literature a parallel flow field is presented as an example of a situation in which mass transport phenomena are limiting heavily the performance of the battery. A different design is presented: the interdigitated. Its different properties force all electrolyte to move under the rib to reach the outlet. A sensitivity analysis with respect to the dimension of the channel is proposed and the trends of main quantities are also critically analyzed, it is found that there is a dimension of the channel that maximizes the performance of the cell for a given flow rate. There are significant differences between the velocity values among the channels for the interdigitated geometry while the variability of reaction rate and state of charge is heavily dependent on both the geometry of the flow field, the state of charge and the flow rate. The comparison between the interdigitated and serpentine flow field forecast a better performance of the interdigitated flow field for a given flow rate and state of charge. Thanks to the experience gained in the initial phase of the modelling part a novel geometry is proposed as a modification of the interdigitated flow field shaping a double outlet geometry. The ideas that drove the process were aimed at giving a direction to the pressure gradient between inlet and outlet and limiting the unevenness of velocity in the channels. The numerical results forecast a certain trend of electrochemical performance but also quantified the pressure drop of the cell, a key parameter for the operation of a real cell as it impacts on the consumption of the auxiliaries and hence has an impact on the energy efficiency of the system. It was found that serpentine design introduces a pressure loss that is one order of magnitude larger than the interdigitated's one in all working conditions. A dedicated procedure was developed to quantify both the energy efficiency of the system and the efficiency with respect to an ideal distributor. The conclusion of this process was that the influence of the flow field has to be taken into account along with the operating condition of the cell and, since in these system there is the possibility of recirculating the electrolyte, in order to have more uniform distribution of reactants one has to operate the cell at low current density or increase the excess of the reaction by means of a higher flow rate. The flow field has to guarantee a uniform distribution of reactants limiting the pressure drop. The serpentine, due to its higher pressure drop is not in this sense the optimal solution to this problem. The trend forecast by the model were confirmed by the experimental campaign regarding the performance of the three flow fields derived from an interdigitated design: a base case, the double outlet and an interdigitated flow field with smaller rib and higher number of channels. The influence of a smaller rib is quantified to be penalizing the cell as on one side it has a lower area of the cell over which the potential is fixed and on the other side it causes a higher unevenness

of the velocity in the channels giving a lower velocity component in the central digits. The double outlet design is proved to improve the performance of the cell with respect to the interdigitated base case when operated at low state of charge and low flow rate: this is one of the major results of this work as no similar flow field is found to exist in the literature. The experimental campaign pointed also out how the serpentine flow field, whose performance was numerically forecast to be lower than the interdigitated, outperformed all other flow fields in all working conditions tested. The values of pressure drop measured in the experimental facility had the same trend of ones of the simulated cells even if the numerical values were not the same. As a last procedure, since no dedicated fitting procedure was performed on the threedimensional model, an attempt to understand the numerical entity of the performance was considered. Despite the fact that the performance of the serpentine was fitted with a new set of parameters, the simulation regarding the interdigitated were still favoring this last flow field. Effort has been made to understand which could be the reason of such behaviour and it was found out that the way in which mass transport was modelled could effectively change the shape of the performance of the simulated cells. A new fitting procedure was therefore put in place considering a convective model for the characterization of mass transport inside the porous medium and this brought to a better pairing with the experimental data.

Extended Abstract (different language)

La recente penetrazione di fonti rinnovabili all'interno del sistema energetico ha causato un cambiamento nelle necessità del sistema di distribuzione e ha messo in luce l'esigenza di sistemi di accumulo per bilanciare la rete. Tra i dispositivi elettrochimici, le batterie a flusso al vanadio rappresentano una delle migliori tecnologie a causa della loro alta efficienza, la lunga vita utile, l'affidabilità e l'indipendenza tra potenza installata e capacità immagazzinata. La scarsa densità energetica e gli alti costi non permettono ancora uno sviluppo su scala commerciale di questi sistemi, tuttavia sono presenti margini di miglioramento.
Se la ricerca nel campo dei materiali porta allo sviluppo di componenti più performanti ed economici, altri lavori sono intesi aumentare la prestazione del sistema attraverso una gestione intelligente dell'architettura dello stack oppure ottimizzando il punto di funzionamento. Questo lavoro quantifica l'impatto sulla prestazione della batteria di un singolo componente, il distributore. E' necessario ricordare come, all'inizio dello sviluppo della tecnologia delle batterie a flusso, il distributore non era presente e la soluzione elettrolitica veniva iniettata all'interno del mezzo poroso. Questa configurazione era comune qualche anno fa, ma fu abbandonata a causa di due svantaggi: l'alta perdita di pressione e la bassa prestazione. Uno dei più influenti articoli riguardanti questo aspetto fu pubblicato da M.M. Mench [1] e riguardava l'analisi del miglioramento delle prestazioni del sistema a causa dell'adozione di un sistema di distribuzione simile a quello usato nel campo delle celle a combustibile.

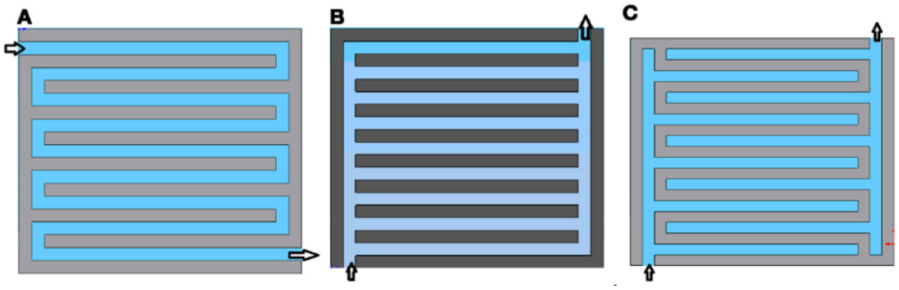

Fig. 0.4: Distributori presenti nella letteratura: a) Serpentina, b) Parallelo , c) Interdigitated

Le geometrie più usate nel campo delle celle a combustibile furono utilizzate per le batterie a flusso e sono riportate nella figura 0.4: le geometrie sono serpentina, in parallelo e interdigitated. Lo studio delle proprietà del distributore deve essere considerato usando una particolare configurazione sperimentale, atta a evidenziare le perdite del solo elettrodo positivo di una batteria a flusso al vanadio: la cella idrogeno-vanadio presente all' $MRT\ Fuel\ Cell\ Lab$. Una batteria completa non porterebbe chiarimenti univoci sul problema siccome verrebbero misurate contemporaneamente le perdite di due distributori. Oltre a questo, per quantificare l'impatto di questo componente, si devono implementare modelli numerici ed è necessario validarli con dati sperimentali. La conoscenza dei fenomeni fluidodinamici ed elettrochimici è intesa essere strumento per l'ottimizzazione delle caratteristiche geometriche del distributore. Partendo da una procedura di fitting effettuata su dati sperimentali esistenti con un modello bidimensionale in $COMSOL\ Multiphysics^{®}$, un modello tridimensionale capace di risolvere fluidodinamica e elettrochimica sarà sviluppato usando un codice CFD commerciale: $ANSYSFluent^{®}$. Verrà usato come strumento per la caratterizzazione di una batteria idrogeno-vanadio di *5 cm x 5 cm*.

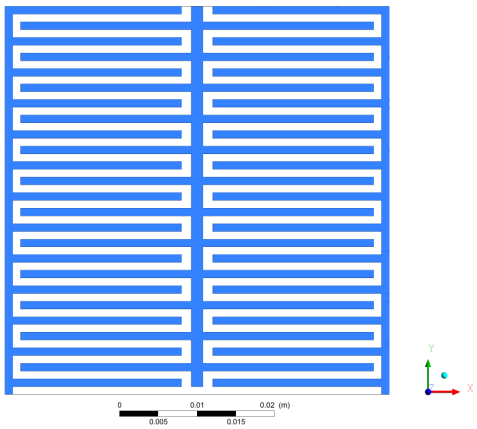

Fig. 0.5: Geometria innovativa proposta in questo lavoro

Sono simulate diverse geometrie, inclusa una geometria a serpentina, un distributore in parallelo mentre una geometria innovativa verrà proposta, come visibile nella figura 0.5. Verrà anche messa a punto una procedura dedicata per analizzare l'impatto del distributore considerando sia la prestazione elettrochimica che la perdita di pressione introdotta dal componente. Usando l'apparato sperimentale presente nell' $MRT\ Fuel\ Cell\ Lab$, sono testati quattro distributori per capire quale sia la miglior configurazione per il funzionamento in sistema reale. Nella prima parte del lavoro si è sviluppato un modello bidimensionale usando $COMSOL\ Multiphysics^{®}$, simulando in maniera potenziostatica il funzionamento di un sistema testato in un lavoro precedente. La procedura di calibrazione ha portato alla determinazione di un set di parametri usati in tutto il lavoro e ha dato l'opportunità di capire quali siano i fenomeni più influenti e come siano modellati usando le equazioni cos-

titutive della cella elettrochimica. E' chiarificato il peso dei parametri sul comportamento della cella ed è stata sviluppata una procedura per risolvere in maniera accoppiata la fluidodinamica e l'elettrochimica. Le caratteristiche dell'elettrodo sono identificate essere l'area attiva, il raggio medio dei pori, la permeabilità e la porosità. Queste ultime due influenzano il comportamento fluidodinamico dell'elettrodo mentre l'area attiva e il raggio medio dei pori sono inclusi nella cinetica della reazione elettrochimica. Altri parametri importanti si sono rivelati essere la velocità della reazione e il valore del coefficiente di trasferimento di carica mentre è molto elevata la rilevanza dei valori numerici dei parametri. I risultati del secondo capitolo mettono in luce come sia difficile relazionare il comportamento locale dei flussi delle specie alla performance globale della batteria e come la convezione giochi un ruolo maggioritario nel mezzo poroso. Un codice tridimensionale è stato sviluppato usando $ANSYSFluent^{®}$ con l'uso di $User\ Defined\ Functions$ e $User\ Defined\ Scalars$. Questo modello risolve contemporaneamente elettrochimica e fluidodinamica all'interno di un dominio *5 cm x 5 cm*. Il primo caso studiato è stato la serpentina: la distribuzione della pressione all'interno della cella è fortemente influenzata dalla geometria e forza una parte del flusso a passare sotto la spalla del distributore in alcune zone vicine alle curve. Tale livello di dettaglio permette di osservare i fenomeni che avvengono nel mezzo poroso e nei canali. Per esempio la variazione dello stato di carica della batteria su un piano a metà dell'elettrodo è riportata nella figura 0.6 accanto ai valori della velocità nella stessa posizione (per maggiori informazioni si può consultare il capitolo 3).

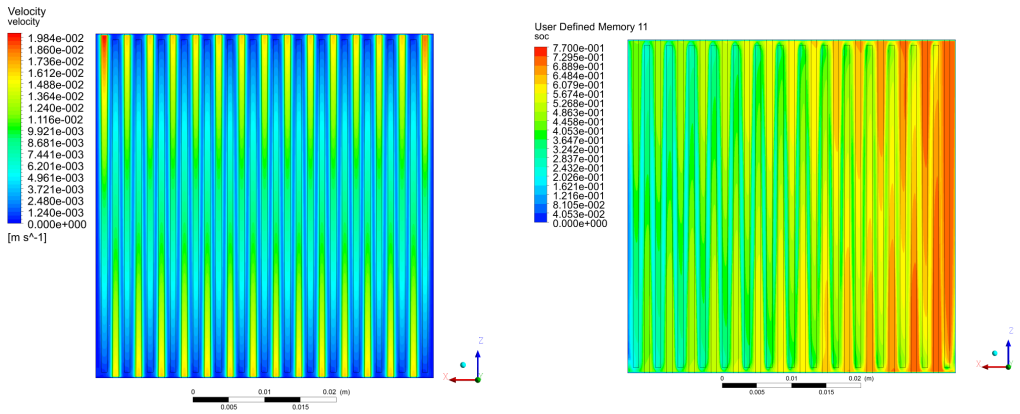

Fig. 0.6: Velocità (sinistra) e stato di carica (destra) su un piano a metà dell'elettrodo poroso.

Quello che emerge è che il campo di moto all'interno del setto poroso non è semplice da modellare e il collegamento con le quantità elettrochimiche è complesso: la parte solida del dominio non è fisicamente presente nei modelli. Tuttavia questo lavoro chiarifica, coerentemente con le assunzioni fatte, il fenomeno dei flussi under the rib, visualizzando questa quantità all'interno dell'elettrodo. L'analisi presentata è rilevante dal punto di vista scientifico siccome esiste in letteratura soltanto un esempio di modello tredimensionale della cella completa che risolve fluidodinamica ed elettrochimica e il problema non è

completamente analizzato. Non è stato svolto molto lavoro per collegare localmente la prestazione della cella alla condizione fluidodinamica mentre questo aspetto è analizzato in questo lavoro. La condizione fluidodinamica all'interno del mezzo poroso cambia la capacità del sistema di convertire attivamente i reagenti e il meccanismo attraverso il quale esso avviene è l'effettivo movimento della soluzione all'interno del setto poroso. D'altra parte, nelle zone in cui vi è la spalla del distributore, vengono imposti i valori del potenziale e questo aspetto è da tenere in considerazione siccome il grado di reazione dipenderà effettivamente dal valore locale del sovrapotenziale, determinato dalle caratteristiche geometriche e dalle proprietà elettriche del materiale. Le caratteristiche geometriche del distributore sono state analizzate con l'uso di una analisi di sensitività sulla dimensione del canale, trovando che per una geometria a serpentina più piccolo il canale più alta la prestazione per un dato stato di carica e portata. Coerentemente con le analisi presenti in letteratura una geometria in parallelo è presentata come esempio di una situazione in cui i problemi di trasporto di massa limitano fortemente la prestazione del sistema. Una geometria differente è presentata: l'interdigitated. Le differenti proprietà forzano tutto l'elettrolita a passare sotto le spalle per raggiungere l'outlet. Una analisi di sensitività rispetto alla dimensione del canale è riportata e gli andamenti delle maggiori quantità sono criticamente analizzati trovando che esiste una dimensione del canale che massimizza la prestazione del sistema. Ci sono differenze significative tra i valori della velocità dei canali per la geometria interdigitated mentre la variabilità di grado di reazione e stato di carica sono molto influenzate dalla geometria del distributore, lo stato di carica iniziale e la portata. Il confronto tra la geometria a serpentina e interdigitated prevede una miglior prestazione del distributore interdigitated per una data portata e stato di carica. Grazie all'esperienza maturata nella fase iniziale della parte di modellazione una geometria innovativa viene proposta come una modifica del distributore interdigitated: la geometria con un doppio scarico. Le idee che hanno guidato il processo avevano lo scopo di dare una direzione alla gradiente di pressione tra ingresso ed uscita limitando l'irregolarità della velocità nella canali. I risultati numerici prevedono una certa tendenza di prestazioni elettrochimiche ma quantificano anche le perdite di carico della cella, un parametro fondamentale per il funzionamento di un sistema reale siccome esso ha un impatto sul consumo degli ausiliari e quindi sull'efficienza energetica del sistema. Si è constatato che la geometria a serpentina introduce una perdita di pressione che è un ordine di grandezza più grande di quella delle geometrie interdigitated in tutte le condizioni operative. Una procedura dedicata è stata sviluppata per quantificare sia l'efficienza energetica del sistema sia l'efficienza rispetto ad un distributore ideale. La conclusione di questo processo è che l'influenza del distributore deve essere presa in considerazione insieme alla condizione di funzionamento della batteria e, dal momento che in questi sistemi c'è la possibilità di ricircolo dell'elettrolita, in modo da avere una distribuzione più uniforme dei reagenti si deve operare la cella a bassa densità di corrente o aumentare l'eccesso della reazione mediante una portata maggiore. Il distributore deve garantire una distribuzione uniforme del reagenti limitando la caduta di pressione. Gli andamenti previsti dal modello sono stati confermati dalla campagna sperimentale per quanto riguarda le prestazioni dei tre

distributori derivati da un disegno interdigitated: un caso base, la doppia uscita e una geometria interdigitated con piccola spalla e alto numero di canali. L'influenza di una spalla più piccola è quantificata penalizzare la cella per due ragioni: da un lato ha una superficie inferiore della cella sopra la quale il potenziale è fissato e dall'altro provoca una disuniformità superiore della velocità nei canali dando una componente di velocità inferiore nei canali centrali. Il disegno doppia uscita è dimostrato migliorare le prestazioni del sistema rispetto la situazione di base quando si opera a basso stato di carica e bassa portata: questo è uno dei principali risultati di questo lavoro siccome nessun distributore simile è risultato esistere nella letteratura. La campagna sperimentale ha sottolineato, inoltre, come la geometria a serpentina, la cui performance è stata numericamente prevista essere inferiore all'interdigitated, garantisce una prestazione migliore di tutti gli altri distributori in tutte le condizioni di lavoro testate. I valori della caduta di pressione misurati nella struttura sperimentale hanno avuto lo stesso andamento di quelle dei sistemi simulati anche se i valori numerici non sono esattamente uguali. Come ultima procedura, dal momento che nessuna procedura dedicata di calibrazione è stata eseguita sul modello tridimensionale, un tentativo di capire l'entità numerica della prestazione è stato considerato. Nonostante il fatto che la prestazione della serpentina sia stata simulata adeguatamente con un nuovo insieme di parametri, la simulazione per quanto riguarda la geometria interdigitated prevedeva una migliore prestazione di quest'ultima. Un grande sforzo è stato fatto per capire quale potrebbe essere la ragione di tale comportamento e si è scoperto che il modo in cui si modella il trasporto di massa può effettivamente cambiare la forma delle prestazioni della cella simulata. E' stata svolta una nuova procedura di calibrazione considerando un modello convettivo per la caratterizzazione dei problemi di scambio di massa all'interno del setto poroso e ha portato a un miglior accoppiamento con i dati sperimentali.

Acknowledgement

Molte sono state le ore e le energie che ho speso per portare a compimento questo lavoro, ultimo atto della mia esperienza nel campo accademico prima di muovermi verso il prossimo passo. Porsi obiettivi ambiziosi è secondo me necessario per migliorare se stessi anche se giocare a spostare i propri limiti finisce inevitabilmente per presentarteli quotidianamente. Non è però un percorso che ho affrontato da solo: vorrei esprimere un ringraziamento al mio relatore, il Dottor Matteo Zago, per l'aiuto datomi e per non aver lasciato procedere il lavoro senza supervisione. Vorrei anche ringraziare l'Ing. Mirko Messaggi perchè è stato molto stimolante lavorare con un ragazzo tanto sveglio, paziente e competente. Senza ombra di dubbio i compagni di avventura all'interno dell' $MRT\ Fuel\ Cell\ Lab$, Domenico, Giorgia, Matteo e Matteo, così come gli studenti di dottorato, Eugenio, Claudio and Andrea, mi daranno un piacevole ricordo per lungo tempo, siccome è stata una grande squadra di cui esser parte. Ricordo e ringrazio Matteo Tagliabue, chi mi ha anticipato nello studio di queste materie, per il suo aiuto personale nelle prime fasi del lavoro e perchè con il suo studio chiaro e completo ha rappresentato per me un vero e proprio punto di riferimento. Spero che questo lavoro possa essere lo stesso per qualcuno che in futuro si addentrerà nello studio di questi dispositivi. Ai miei amici Francesco, Alberto e Samuele, Riccardo e Fabio va un pensiero speciale perchè sei anni fa ci siamo seduti vicini alla prima lezione di Ingegneria e siamo diventati compagni in questo lungo percorso. Al di fuori dell'università, ringrazio la mia famiglia per avermi supportato sempre anche quando il cammino sembrava decisamente in salita. Li ringrazio anche per avermi insegnato a lavorare sempre con il massimo impegno, con la massima puntualità e la massima qualità. Li ringrazio di avermi dato il privilegio di poter studiare. Agli zii di Mandello va un pensiero speciale perchè mi hanno sempre voluto un gran bene. I miei amici sono sempre nella mia mente quando si tratta di ricordare chi devi ringraziare siccome è con loro che ho passato i momenti migliori: Mik, Tommaso e Alessio per essere stati con me più di quattro amici e aver registrato un EP a maggio 2016 come "Charlirancol", Ambrogio per essere Ambrogio e i miei compagni di pallacanestro nel "Basket Nibionno" e nel "Basket Costamasnaga" perchè sono gli amici di sempre, che rispondono sempre quando li chiami. Ringrazio tutte le band con cui ho suonato su palchi medio alti/medio bassi o inesistenti e quelle che hanno suonato nelle mie auricolari durante questi mesi, hanno reso i pomeriggi in cui lo schermo del computer era nero più piacevoli. Non sono molto bravo con le parole, specialmente quando si tratta di Mara, ma per ringraziare lei nemmeno tutte le parole di questa tesi basterebbero.

Contents

1 Flow batteries

This chapter is meant to be an overview of flow batteries' technologies. Several configuration are analyzed and the comparison with respect to other technologies is done. The theoretical basis of the technology is reported and a brief cost analysis is done.

1.1 History of the technology

Research insitutes and industries have lately increased their interest in the technology of flow batteries. This technology is promising in terms of its capacity to store energy efficiently and for its long lifetime. The first electrochemical device that has the name of "flow battery" was built to be installed on an airship called *La France*.The chemistry was zinc/chlorine, where the chlorine was generated on the airship itself. During the XX'th century the technology was more widely developed and patented. The first patent was got by Walter Kango in 1954 using a battery with titanium clorate. Vanadium batteries where investigated by Pissoort (1933), researchers from NASA (1970's) and Pellegri and Speziante (1978). These pioneers did not succeed in finding a really good solution for the commercial world. Maria-Skyllas-Kazakos did it in 1984. Her research in South New Wales lead to a patent that today is referred as the first all vanadium flow battery. Coming to recent years, much effort has been done in the field of flow batteries. The trends in the research have moved in different directions: some have investigated the possibility to change the redox couple in the battery (Fe-Cr, Zn-Br, Fe-V, V-O), some others have studied the optimization of the cell stacks and the optimal operating point of the cell. All vanadium flow batteries have an advantage from the chemical point of view since the same specie is used for both electrochemical solutions. This fact dramatically increase the life of the battery preventing the permanent contamination of the solutions. Redox flow battery are not the only technology that is nowadays developed as lithium-ion batteries and nickel-cadmium batteries have constantly gained space.

1.2 System description

Vanadium Redox Flow Battery or, more simply, VRFB, are an electrochemical device able to convert an electric current into electrochemical energy of the electrolytes and viceversa.

The name "flow battery" is derived from the fact that the electrolyte is liquid and it is flowed into a cell where a redox reaction occurs.

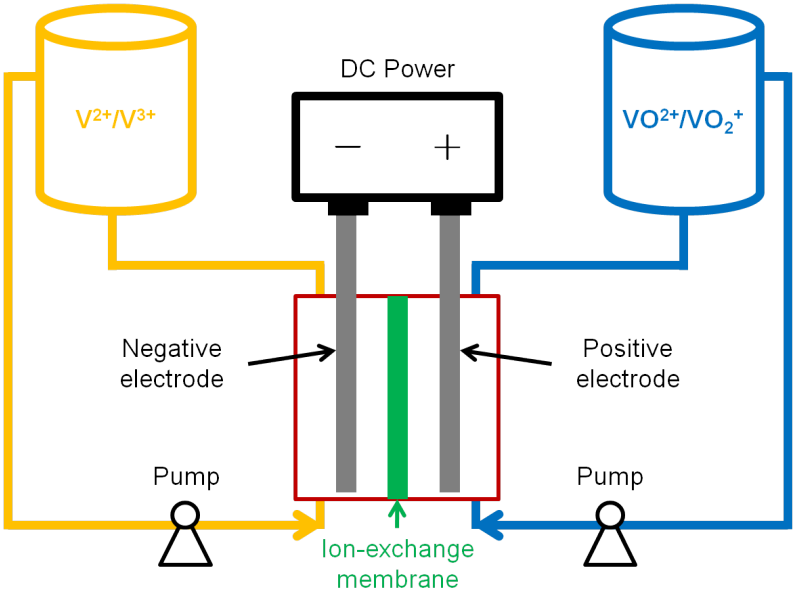

Fig. 1.1: Scheme of a vanadium flow battery

Figure 1.1 shows a scheme of a typical configuration of a flow battery. The main parts of the machine are clearly visible:

- Two tanks for the electrolyte storage,
- Two electrodes for the chemical reaction to take place,
- A membrane to guarantee proton conduction and electrically separate the electrodes,
- The connection with a DC load,
- Pumps for the circulation of the electrolyte solution.

The solutions used in VRFB are usually made of vanadium ions in water and sulphuric acid. Therefore pumps, tubes and valves need to be resistant to acid corrosion. Redox reactions occur at the anodic and the cathodic electrode and release or need electrons depending on the operating condition of the battery. The electric contact between the porous electrode, and the load is guaranteed by a component made of graphite: the flow field. This component has also the scope of distributing the electrolyte upon the porous electrode. The electrolytic solution contains the specie that is reacting and in the batteries analyzed this is vanadium. This transition metal is able to operate both at the anode and at the cathode of the battery since it has 4 different oxidation states and it is easy to distinguish them as they form with water with a distinctive colors.

Two different ionic couples are present in a VRFB:

- The couple of species at the anode is V^{2+}/V^{3+}.

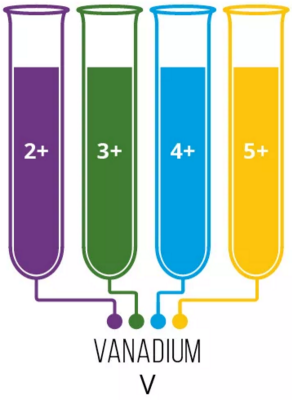

Fig. 1.2: Oxidation states of Vanadium and their colors in aqueous solution.

- The couple of species at the cathode is VO_2^+/VO_2^{++}, that corresponds to the states $+5$ and $+4$ respectively.

A redox reaction occurs in this type of machine and the generic equation can be stated as:

$$aA + bB + ne^- \rightleftharpoons cC + dD \tag{1.1}$$

Coherently the species will give a potential difference according to 1.1 that is the general formulation of Nernst equation.

$$E = E^0 + \frac{RT}{nF} \ln \frac{a_A^a a_B^b}{a_C^c a_D^d} \quad [V] \tag{1.2}$$

This voltage is dependent on the activities of the reactants and the number of electrons involved in the reaction. The term E^0 is called standard potential of equation 1.1. In this work the couple of electrochemical reactions is:

$$V^{2+} \underset{Charge}{\overset{Discharge}{\rightleftharpoons}} V^{3+} + e^- \tag{1.3}$$

$$VO_2{}^+ + 2H^+ + e^- \underset{Charge}{\overset{Discharge}{\rightleftharpoons}} VO^{2+} + H_2O \tag{1.4}$$

Combining 1.3 and 1.4 it is possible to get the complete expression for the battery as follows:

$$V^{2+} + VO_2{}^+ + 2H^+ \underset{Charge}{\overset{Discharge}{\rightleftharpoons}} V^{3+} + VO^{2+} + H_2O \tag{1.5}$$

It is easy to recognize how the presence of the hydrogen in the complete equation will change the pH of the solution during the operation of the machine.

Since the two equation are redox, equation 1.2 is valid for 1.3 and 1.4. One major hypotesis it is stated here and it is infinite dilution of solution that allows to substitute the activity of the species with their concentration. This hypotesis is ubiquitous in the literature regarding VRFB and it is accepted throughout this work. Accordingly it is possible to write:

$$E_A^0 = E_A^{0'} + \frac{RT}{F} \ln\left(\frac{c_{V^{3+}}}{c_{V^{2+}}}\right) \tag{1.6a}$$

$$E_C^0 = E_C^{0'} + \frac{RT}{F} \ln\left(\frac{c_{V^{5+}} \cdot \left(c_{H^+}^C\right)^2}{c_{V^{4+}}}\right) \tag{1.6b}$$

Values for the standard equilibrium potential of each electrode can be found in the literature and the difference between the value at the cathodic electrode and the anodic electrode is called standard potential of the cell and its value is dependent of the redox couples used in the battery.

$$\begin{aligned} E_{Cath}^{0'} &= 1.004 \quad V \\ E_{Anode}^{0'} &= -0.255 \quad V \\ E_{cell}^{0'} &= E_C^{0'} - E_A^{0'} = 1.259 \quad V \end{aligned} \tag{1.7}$$

In real systems the designer has the capability to adjust the voltage connecting several cells in parallel or in series according to his needs building *stacks*. All commercial applications are based on this idea, in this work it will be analyzed just one cell of $25cm^2$. When building *stacks* some particular considerations need to be taken into account and further studies are needed.
Subtracting 1.6a from 1.22b it is possible to get an expression for the voltage across the machine when no current is flowing. This voltage is called "Open Circuit Voltage". It is a very convenient quantity to be measured.

$$OCV_{Cell} = E_{cell}^{0'} + \frac{RT}{F} \ln\left(\frac{c_{V^{2+}} \cdot c_{V^{5+}} \cdot \left(c_{H^+}^C\right)^2}{c_{V^{3+}} \cdot c_{V^{4+}}}\right) \tag{1.8}$$

It is intuitive to understand how the concentration of reactants is someow related to the capability of the battery to be discharged and this concept is formalized in one of the most useful parameters of the VRFB: the State Of Charge. At first it is provided the general formulation:

$$SOC = \frac{c_{V^{2+}} + c_{V^{5+}}}{c_{V^{2+}} + c_{V^{3+}} + c_{V^{4+}} + c_{V^{5+}}} \tag{1.9}$$

This formulation takes into account the possibility that the two tanks do not have the same total concentration of vanadium. This may happen when some vanadium ions pass through the membrane and give rise to the phenomenon of "cross-contamination". This

generates, in other words, an imbalance of capacity between the two tanks. In case of perfect isolation between the two tanks the expression of SOC can be stated as follows:

$$SOC = \frac{c_{V^{2+}}}{c_{V^{2+}} + c_{V^{3+}}} = \frac{c_{V^{5+}}}{c_{V^{5+}} + c_{V^{4+}}} \tag{1.10}$$

Using 1.10 it is possible to rewrite the OCV as a function of the state of charge.This relationship is important as:

- The state of charge can be calculated from a measured OCV.
- The pH of the solutions plays a role in the characterization of the machine.
- When SOC is close to 0 and 1 a small change in its value causes large variations of OCV (see 1.3), while in the central area the relationship is almost linear.

$$OCV_{Cell} = E^{0'}_{cell} + \frac{RT}{F} \ln \left(\frac{SOC^2 \cdot \left(c^C_{H^+}\right)^2}{(1 - SOC)^2} \right) \tag{1.11}$$

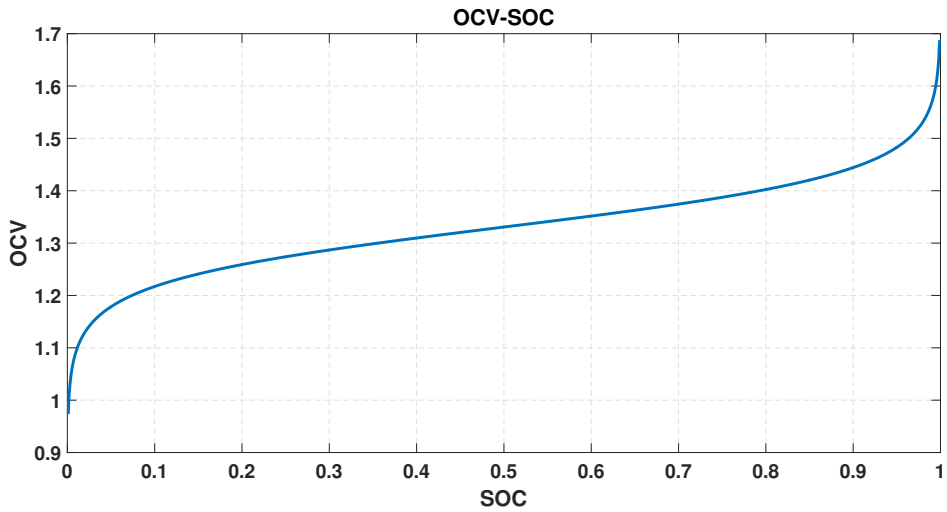

Fig. 1.3: Relationship OCV-SOC

Once the constitutive equations are set, the most common efficiency parameters are defined.

- Charge efficiency (or Coulombic efficiency): it is the ratio between the capacity removed from a battery during discharge compared with the capacity used during charging to restore the original State of Charge. The sources of this loss are related to the parasitic reactions that consume electrons without charging or discharging the battery. Typical values for this technology are around 85% [41]

$$\eta_C = \frac{\int_0^{t_{dis}} I_{dis} dt}{\int_0^{t_{ch}} I_{ch} dt} \tag{1.12}$$

- Voltage effficiency: it is the ratio of the average values of voltage during charge and discharge. It is mainly dependent on ohmic losses, for this reason the higher the current in which one operates the lower the voltage efficiency.

$$\eta_V = \frac{\frac{1}{t_{dis}} \int_0^{t_d} V_{dis}(t)dt}{\frac{1}{t_{ch}} \int_0^{t_c} V_{ch}(t)dt} \tag{1.13}$$

- Energy Efficiency: the product of voltage efficiency and charge efficiency. It is obviously the parameter to be optimized during the operation of an energy storage system.

$$\eta_E = \eta_C \eta_V \tag{1.14}$$

The last part of this brief overview deals with the assumption that are made: the parasitic reactions that occur in reality will not be taken into account. These reaction are hydrogen (1.15) and oxigen (1.16) evolution. In the literature models for these reactions are complicated and the kinetics of the reactions is not very clear. Often [28] these contribution are neglected along with 1.17, which is an "evolution" for vanadium.

$$2H_2O + 2e^- \rightleftharpoons H_2 + 2OH^- \tag{1.15}$$

$$4H_2O \rightleftharpoons O_2 + 4e^- + 4H^+ \tag{1.16}$$

$$VO^{2+} + H_2O \rightleftharpoons HVO_3 + 3H^+ + e^- \tag{1.17}$$

What is more, the contribution of the cross contamination of the vanadium ions through the membrane won't be modelled. Its entity will be discussed more in detail in this work along with its influence on the performance.

1.3 Advantages and disadvantages

Although flow battery are one of the most promising technologies for energy storage, it is important to highlight in this section the main advantages and disadvantages of the technology. The keypoints for the VRFB have to be carefully taken into account when comparing this technology with other energy storage technologies.

- **Indipendence between peak power and energy stored**: these two quantities depend essentially on different parts of the machine. The dimension of the *stack* determines the peak power while the capacity of the battery is related to the dimensions of the tanks and hence the quantity of electrolyte. In this way one could achieve a big storage capacity without over-dimensioning the stack, in case of a

large scale energy storage facility this may turn out to be an important advantage. In conventional technologies such as lithium-ion or lead-acid batteries, the two parameters cannot be divided.

- **Possibility to change the tanks**: it is possible to imagine a configuration in which tanks are istantaneously replaced simply by means of valves. This is an advantage as it allows to follow the need of the load providing istantaneously a new and "charged" battery.

- **Same species in both tanks**: this can be considered an advantage, vanadium is used both at the anode and at the cathode. What may happen, due to the non ideality of the membrane, is that some species migrate from one tank to the other. In case of different chemical species at anode and cathode this would mean an irreversible loss of capacity. In case of VRFB, this phenomenon happens, but since vanadium is used in both sides, the loss of capacity is not definitive. One may shuffle the solutions and go back to the initial state [8]. Furthermore it is possible to leave the battery unused for a long period of time with low loss of charge, due to the fact that electrolytes are stored outside of the battery.

- **Short response time**: the kinetics of the reactions are quick and since there are low inertial effects into the battery VRFB the response time of the system can be in the order of milliseconds. This fact can be extremely useful in a real application.

- **Long life**: electrodes for flow battery are usually made of carbon and do not participate actively to redox reactions, yet providing the active sites for the reactions. There is no exchange of material between the electrode and the electrolyte. Moreover no catalyst is needed and hence a low degradation of the electrode is expected enhancing the life of the battery.

- **Flexibility of operating conditions**: flow battery leave space for a variety of operating condition since one may vary both the flow rate of electrolytes and the potential of the cell. This offers to the designer an additional degree of freedom, the flow rate, with respect to electric quantities in the determination of the operating point.

- **Solution properties**: acid vanadium solutions are not flammable, thing that is not guaranteed for other batteries. The only critic aspect about vanadium is that it is toxic when it is solid (especially in the form of V_2O_5) but this form is not present in the normal condition of working but just when solutions are made.

On the other hand the technology of flow battery has significant drawbacks to be faced and solved. The technology is nowadays in a state of "early commercial" and still is facing

some issues to become in the future years one of the protagonists of the energy storage world.

- **Low specific energy and specific power**: VRFB present significantly lower values of this parameters compared to other technologies, like it is visible in 1.1.This is related mainly to the low cell voltage, the low number of ions involved in the redox reaction and the vanadium solubility in the solutions. In solutions with a molar concentration higher than 2 M vanadium tends to precipitate and it is clear how this is a limiting factor. Also temperature influences vanadium solubility, limiting the range of operability to 5°C to 40°C.

- **Impossibility of operation in mobile applications**: tanks dimensions, temperature conditions force VRFB to be used mostly in stationary applications.

- **High costs**: in section 1.5 this aspect will be fully analyzed but nowadays costs of this system do not allow VRFB to be competitive with most commercial batteries (lithium-ion, lead acid).

- **Shunt current problems**: since the electrolyte has the capability of conducting current, some current may rise into the channels [33]. In a stack operation some small voltage could set between differnent cells, due to local imbalances, giving rise to the shunt current. This phenomenon is a loss of capacity of the machine and has to be avoided properly dimensioning the channels.

1.4 Vanadium Redox Flow Battery as an energy storage technology

During the last years the need for energy storage has grown due to the presence of power generation from non programmable source. Researches have been carried out to compare and contrast different technologies [4] [10] along with their costs [34] [41]. In this work some results are reported in order not to enlighten all the various technologies for energy storage, but to understand how vanadium flow battery could impact the scenario. Different are the types of energy storage depending intrinsically by two factors: the power needed and the time of storage (often expressed in terms of "hours"). As one can see from figure 1.4 storage can be useful for different purposes:

- Guarantee electricity availability in every moment to some special applications (telecommunication and computing), the so called "Uninterruptiblle Power Supply". The technologies for this kind of application have usually a very low capacity (from

seconds to minutes) and a low power. Capacitors, flywheels and batteries are the technologies that are currently used.

- Store energy for trasport and distribution grid support or accumulate in order to deal with energy production from renewable source. For example in some cases it might be needed to store energy during the day and to use it during the night. Powers and times here are higher (in the order of MW and hours respectively). This is the situation in which redox flow battery are expected to work. According to their advantages they can provide the best solution in terms of equivalent hours with respect to the other technologies.
- Store energy for a long period of time and help the grid management in a broader sense. One may think at the possibility to store seasonally water into a dam for understanding the third big area of energy storage. Powers grow significantly along with the equivalent hours of the system.

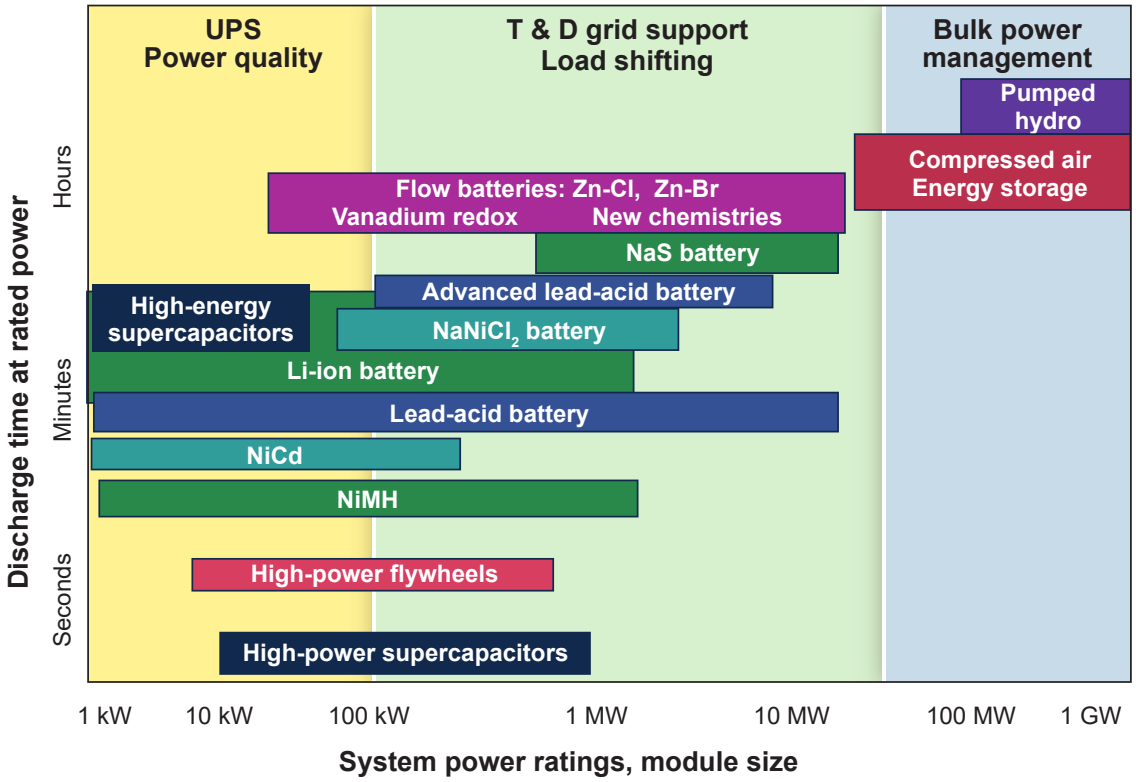

Fig. 1.4: Storage technologies for different needs[10]

Once the position of the technology is set into the scenario of energy storage it is proposed a comparison of the main technologies according to the main technical parameters, as reported in the following tables.

VRFB appear to have an efficiency that is not in line with the most performing technologies but still have a reasonable value. Moreover as mentioned before as a drawback values of power density and energy density are not competitive with the most performing technologies based on electrochemistry (Li-ion). This fact may be a problem for these systems

Technology	Top Power	Top Energy	Energy Density	Response time	η_{round}	Cicle life
	[MW]	[MWh]	[Wh/kg]			x 10 ^ 3
Pumped hydro	3000	10 ^ 4	0.3	min	70-85%	20
Compressed air	300	10 ^ 3	10–30	min	60%	30
Thermal energy storage	20	10 ^ 1	70	min	-	>10
Flywheel energy storage	20	5	11–30	ms	85%	10 ^ 1-10 ^ 2
Advanced lead acid	10 – 40	10 ^ 1	25-50	ms	75-85%	3
Sodium sulfur	34	10 ^ 1	150-120	s	85-90%	4.3-6
Sodium nickel clorine	1	6	95-120	s	85%	3–4
Lithium ion	16	20	100-200	ms	95%	4–8
Electrolyzer/fuel cell	1	>10	800-1300	ms	35-45%	50
VRFB	2–100	6-120	10–50	ms	85%	>13

Tab. 1.1: Characteristics of energy storage technologies 1 [4]

Technology	Capital cost	Capital cost	Capital Cost
	[k$/kW]	[$/kWh]	[$/MWh/cycles]
Pumped hydro	0.4-5.6	10-350	0.5-3
Compressed air	1.7	130-550	4–18
Thermal energy storage	-	5000	500
Flywheel energy storage	2.3	2400	25-200
Advanced lead acid	4.6	130	150
Sodium sulfur	3.5	550	90/130
Sodium nickel clorine	3.5	650	150/200
Lithium ion	3–4	600	150/200
Electrolyzer/fuel cell	17	>10000	200
VRFB	3.2	900	<70

Tab. 1.2: Characteristics of energy storage technologies 2 [4]

but technical studies are expected to increase the value of this parameter. An important advantage of this technology is its capability to guarantee a vaste number of life cycles with respect to other electrochemical energy storage devices and this fact is represented by the capital cost "per cycle" reported in table 1.2. This is a keypoint that could allow VRFB to be a protagonist of the future development of grids and smart grids.

1.5 Cost analysis

As mentioned in the previous section, costs for VRFB are not still competitive with other technologies. Nevertheless intensive studies are lowering the costs of the technology. Many parts of the machine will benefit of this research, especially the materials used in the cell. Despite all this considerations, many are the plants that are nowadays under construction and many more are expected to be installed in the future. In the literature many authors have developed cost models for energy storage technologies [34][10][41] [42]. In this work the main conclusions of [34] and [42] are reported in order to highlight how the costs of the system are divided into the various components of the machine and how the sizing of the machine itself influences the cost composition. In the paper a detailed description of the procedure for cost estimation is provided and the main features of the plant are highlighted. The model takes into account the pressure loss in the system and the losses for the shunt currents. Different chemistries were investigated: V-V in an sulfuric

solution, V-V in a clorine based solution and Fe-V. The second solution is proposed in many articles and seems to be a promising solution as it allows to increase the concentration of vanadium to 2/2.5 M without affecting the precipitation of the species. Cost analysis was performed according to a procedure explained into the details in [34]. The main assumptions can be summarized as follows:

- The power was set at 1MW and the energy was varied from 0.25MWh to 4MWh.
- An iterative procedure to find the minimum capital cost was performed varying three main paramters: the area of the stack, the flow rate and the SOC range. This operating point is not unique varying the ratio between energy and power and the chemistry.

There are some costs that depend from the power of the system and if one wants to lower this cost component the configuration will be a small area of the cells with high operating current as power costs depend essentially from the dimension of the stack. On the other hand, operating at high current density lowers the electrochemical efficiency. In other words the energy costs optimization would require a large cell area operating at low current density. It is clear how these two effects counterbalance and create an optimum. From this consideration an important conclusion can be obtained: the E/P ratio has an influence on the entity of the cost and on the optimal operating point. The entity of the cost is represented in this work reporting a study regarding the levelized cost of electricity for two different chemistries and two different ratio E/P. It is reported the projected trend of cost in the future, as explained in [34] , considering an increase of the volume of production of the parts of the machine.

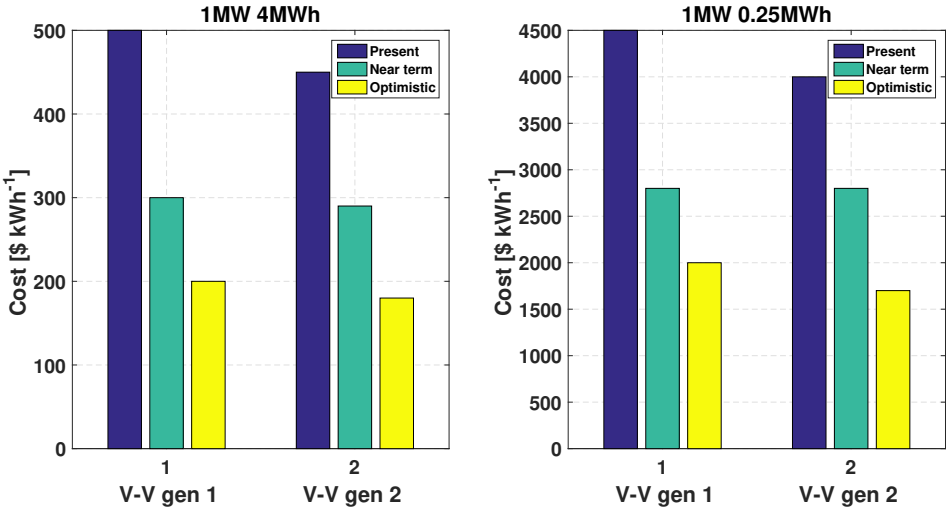

Fig. 1.5: LCOE comparison [34]

The trend is decreasing assuming increasing volumes for the demand as the technology is expected to gain space in the market. What is more the chemistry V-V gen 2 is able to guarantee an improvement of the performance and the related capability to reduce costs.

According to the assumptions made in the paper the total cost is expected to diminish by a factor of 2 in an optimistic scenario. Considering the trend of costs with respect to the ratio E/P it is possible to state how there is a decreasing trend of total with respect to E/P ratio. Important considerations can be withdrawn from figure1.6 where the different cost components are plotted for the "V-V gen 2" chemistry. As the E/P increases energy related costs are more and more important and in the opposite situation power costs dominate. The separator cost dominates (44 %) for E/P = 0.25 followed by the PCS (20 %) while the chemical costs is only 8%. When E/P =4, the chemical costs increase up to 43%. Although the felt electrode adds up just a small part to the costs, an improvement in the electrode properties will bring faster kinetics and hence will increase efficiency. Power density is expected to increase and the stack costs are expected to be lowered. Significant effort is required to lower chemical costs especially for high energy applications.

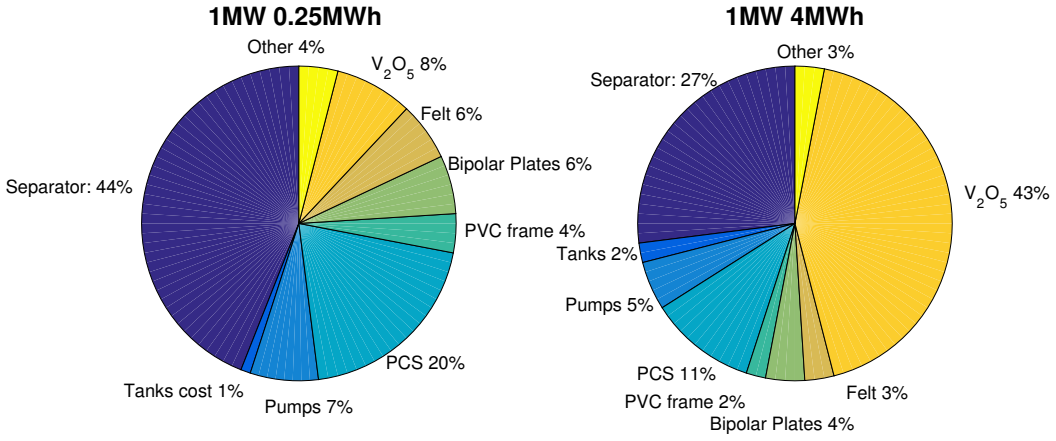

Fig. 1.6: Cost composition comparison between 1MW 0.25MWh and 1MW 4MWh (V-V gen 2) [34]

Another point of view is reported by [42], the author presents a cost analysis for the VRFB considering also an iron chromium battery. In the paper the author models the operation of the battery at a low current density ($0.1Acm^{-2}$) and performs a cost analysis. The base case is a 1MW with 8 hours of capacity and the capacity of the system is changed from 4 h to 12 h. Doing so the values of cost of electricity range from $360\$/kWh$ to almost $200\$/kWh$. These trends are not far from the cost values forecast by [34]. In this section have been analyzed the costs for VRFB and it is showed how nowadays this technology is not able to be a leader in the field of renewable energy storage but there is space for forecasting an improvement of the use of these batteries due to their flexibility and the research.

Year	Power	Energy	Installation	Purpose
	[kW]	[kWh]		
1996	200	800	Kashima Kita electric power	Load leveling
1996	450	900	Tasumi Sub -Station	Peak shaving
2000	200	1600	Kansai electric	Peak shaving
2001	170	1000	Hokkaido wind farm	Turbine stabilization
2001	1500	1500	Semiconductor plant	Emergency&peak shaving
2001	250	500	Eskom power corporation	Emergency&peak shaving
2001	45	90	Cesi Milano	Distributed power systems
2003	250	1000	Huxley Hill Wind Farmon King Island	Wind energy storage
2004	250	2000	Pacific Corp	Voltage support
2005	4000	6000	Hokkaido wind farm	Wind energy storage
2010	18	100	Vierakker	-

Tab. 1.3: Applications of Vanadium batteries

1.6 Existing plants

Many plants exist in the world even though the costs are not fully competitive. In the table 1.3 is reported a brief list of existing plant directly taken from [4]. It is clear how VRFB are a flexible technology and allow a multiple solutions in terms of power and capacity. Furthermore several functions are being investigated, from peak shaving to load leveling down to wind energy storage or voltage support. Among them it is possible to cite the biggest plant, installed in Hokkaido by SEI with the purpose of storing excess wind power. Italy has its own plant based on flow battery at CESI (visible in figure 1.7), with research purposes. The power of the system is 45kW and its capacity is 90kWh. The storage tanks are sized $5m^3$ and can store 4000L. Residential solution exists for smaller powers and capacity: Redflow provides solutions for this kind of purposes [26]

(a) Tanks for CESI plant

(b) Stack for CESI plant

Fig. 1.7: Parts of the CESI Plant

1.7 State of the art for Vanadium Battery

The architecture of real stacks is usually composed by arrays of cells connected in series or in parallel in order to provide the desired voltage. Various studies are present in the literature to understand the behaviour of the system as a stack [22],[25]. Stack architecture (see figure 1.8) may have an influence on the efficiency of the system and the reasons are mainly related to the existence of shunt current into the pipes and the need of a pump to move the reactants through the stack itself. Another consideration has to

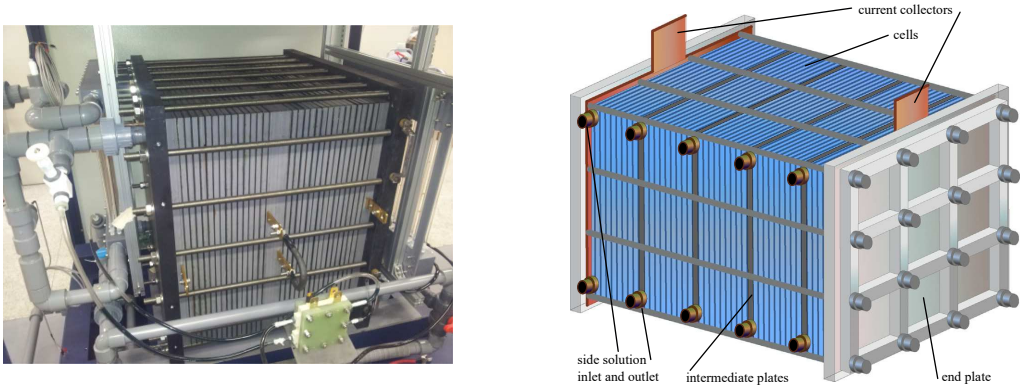

Fig. 1.8: Real stack architecture [22](left), scheme for the real stack (right)

be made: internal imbalances may lead to problems in terms of accelerated degradation of one part and need to be carefully avoided. This involves basically the design of proper piping to bring fresh electrolyte to the cells. In this work stack architecture will not be analyzed as the focus will be more on the performance of the single cell, nonetheless it has to be kept in mind that the architecture of the full stack is important for the performance of a real system. The focus now is driven on the architecture of the single cell, whose part are represented in figure 1.9. Both parts of the cell are symmetric and they are separated by a membrane that allows the protonic exchange. This part is in contact with carbon electrodes on which reaction take place, moreover electric contact is made between this part and the graphite distributors so as to allow electrons' flow. Current collectors allow the external connection with a load or a measurement system and two plastic or steel end plates close the cell and allow the correct value of compression of the parts of the cell. This architecture is very similar to the one of a fuel cell especially in the existance of the MEA (*Membrane Electrode Assembly*). Around the electrodes usually gaskets are placed to avoid excessive compression or damages to these parts.

The membrane is the most critic element of the machine, numerous are its desirable characteristics.

- It has to conduct protons with ease,
- It has to guarantee a low ohmic resistance,
- It has to have a good mechanical an thermal resistance,

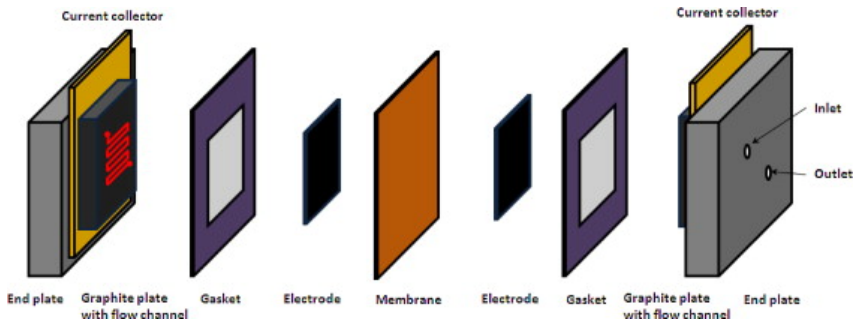

Fig. 1.9: Cell architecture

- It has to avoid vanadium ions crossover.

Usually for VRFB the material for membrane is *Nafion*, a polymeric material called ionomer due to its microscopical structure. Protons on the SO_3H group are able to move between the acid sites of the structure and this fact allows protonic conduction. On the other hand due to its nature electrons cannot pass due to the low conductivity of the membrane. Unfortunately protons are not the only specie able to pass across the membrane and cross contamination takes place: this phenomenon is driven by the difference of concentration across the membrane and the different diffusivities of vanadium between anode and cathode. The result is a flux of vanadium from the anode to the cathode [17]. At the same time water is able to pass through the membrane and this phenonenon is not degratating directly the battery, but it is changing the concentration of the solutions exposing the machine to risks of precipitation of vanadium if solubility limits are passed. Since the membrane is not perfectly impermeable and parasitic reactions take place after a long number of cycles there might be a change in the nature of the solutions. Rebalancing of the solutions is a procedure that allows mixing solutions with different concentrations in order to equate the moles of vanadium in each tank. For this reason there is no irreversible degradation of the solutions. Effort has to be made to control the protonic concentration and particular procedures take place [26]. Researches are also going towards the development of more performing membranes [14].

Electrodes are the chemical core of VRFB and their needs are multiples:

- Allow the trasport of reagents through the pores to the active sites,
- Allow the electron flow in the solid phase and hence have a high electric conductivity,
- Have an high superficial area to maximize the kinetics.

The ideal material should minimize kinetic losses, ohmic losses and mass transport losses. Nowadays the choice for electrode material is usually carbon due to its stability in acid and oxidizing environment and its reasonable cost. Since the activity of vanadium is not maximized in these electrodes some improvement have been made such as thermal treatment or doping. The first improves the hydrofillicity of the electrode and enlarges

the number of functional groups. The second group of techniques deals with a plurality of treatments whose aim can be either increasing the activity of the electrode or increasing the active area. To increase the activity one may use electrochemical oxidation, chemical treatment or doping whereas to enhance the active sites physical deposition or imbibition may help. The last part of the machine is the flow field, whose optimization is basically the aim of this work. The main objective of this part is to deliver reactants to the porous electrode in an uniform way with the lower pressure drop possible. In the following chapters the analysis will be presented. Along with the cell the electrolyte is crucial for the working of the battery. Their cost, as mentioned in 1.5 becomes more and more important especially for energy intensive applications. The electrolyte can be made starting from salts of vanadium sulphate ($VOSO_4$) or from vanadium pentoxide (V_2O_5) which is way far cheaper but significantly more toxic. Detailed information about the procedure for the preparation of the solution can be found in [32]. In the literature many articles deal with an aspect of this machine that might influence its performance: the flow field. It has to be said that in the beginning of the development of the technology of flow batteries the flow field was not used and electrolytes were just injected into the porous electrode. This configuration, called flow through, was common some years ago but than it was abandoned due to its disadvantages: high pressure drop and low performance. The flow field due to its shape is able to deliver the reactants to the porous electrode. One of the most influencing articles on this topic was published by M.M Mench [1] and dealt with the analysis of the improvement of the performance of the machine due to the use of a flow field and a cell architecture similar to the one used in fuel cells. This configuration is very similar to the one shown in 1.9. While the flow through configuration was more and more abandoned, the study of the flow field characteristics' became important in the literature. Several experimental works dealt with the possibility to use several designs for the battery and the first designs were taken from fuel cell technologies whose academical background was bigger. Several studies are available on the flow fields for PEM fuel cells [15] [3]. Much effort was done in this field to use numerical methods to optimize the performance of the flow fields. Results of these analysis are not applicable directly to flow batteries as there are many differences between the technologies both in terms of fluid properties and electrochemical phenomena.

What was taken was the design principle and it is possible to identify some major families of flow field design that are ubiquitous in the literature of PEM fuel cells and are adopted, with some modification, to flow batteries:

- Serpentine design,
- Parallel design,
- Interdigitated design,
- Dotted design.

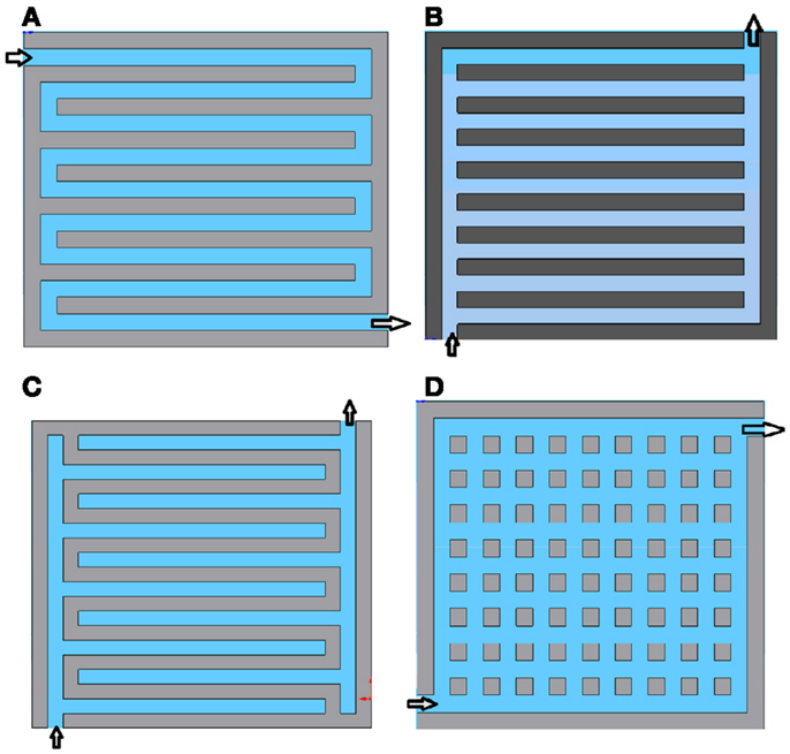

Fig. 1.10: Flow fields design

Dedicated works were proposed for flow batteries and among them it is possible to cite [20] but also [9]. Both of them studied experimentally the performances of the batteries changing the properties of the flow field. It is clear how the flow field actively participates to the losses for mass transport and its shape could influence the performance of the system. On the other hand the flow field introduces a pressure loss to be won by means of a pump. The entity of the pressure drop influences the energy efficiency of the system. Moreover the experimental campaign in [32] showed interesting trends and data about this problem. Particularly it was investigated the impact of two different serpentine flow fields on the performance of the cathodic electrode of a flow battery. Two different electrodes were tested and it was found out that the impact of the flow field on the performance was heavily influenced by the flow field design. Theoretical studies on the flow fields started to be published and some authors modelled just the fluiddynamic behaviour of the cell [6] and [16] and others studied also the electrochemical behaviour [37]. To ease the study of the phenomena several experimental configurations are available and one of these is reported here after.

1.8 Hydrogen Vanadium cell: experimental setup

In MRT Fuel Cell Lab the experimental setup is based mainly on this architecture as well as the experimental data used in the following chapters and reported in [32]. The

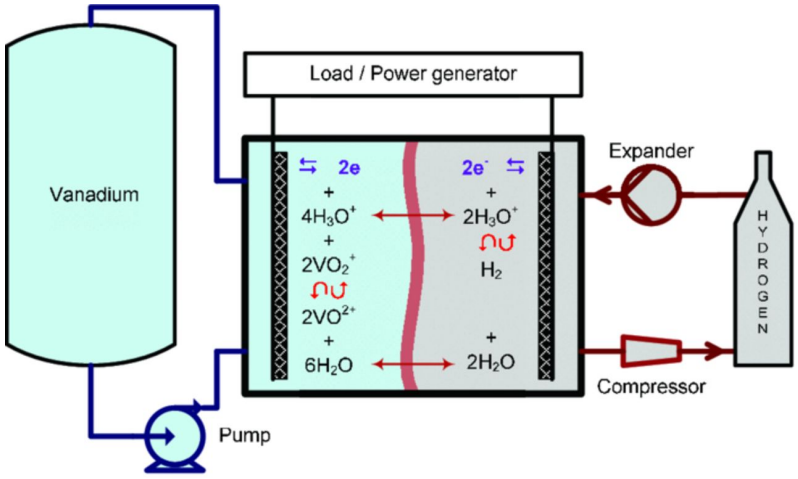

Fig. 1.11: Hydrogen-Vanadium Cell

architecture of the cell is the same as the one depicted in figure 1.9. The membrane is made of *Nafion* and the cathodic electrode is a commercial "Gas Diffusion Layer" that is usually adopted in fuel cells. The anodic electrode is characterized by a platinum charge to act as a catalyst for the reduction of hydrogen. Redox reaction of hydrogen is the anodic reaction. The presence of a catalytic support at the anode increases the kinetic of the reaction which is supposed to be way faster than vanadium oxidation. Furthermore hydrogen redox reaction has $E_0 = 0$ and for this reason the voltage measured across the cell is dependent just on what happens at the cathodic electrode and in the membrane. In a conventional setup for VRFB the voltage accounts both for anodic and cathodic electrode contribution and one measures just the potential difference. It is practically impossible to understand what happens at each electrode.
In case of hydrogen-vanadium cell at the cathodic electrode one may write:

$$VO_2{}^+ + 2H^+ + e^- \underset{Charge}{\overset{Discharge}{\rightleftharpoons}} VO^{2+} + H_2O \tag{1.18}$$

At the anodic electrode:

$$\frac{1}{2}H_2 \underset{Charge}{\overset{Discharge}{\rightleftharpoons}} H^+ + e^- \tag{1.19}$$

Giving for the cell:

$$VO_2{}^+ + H^+ + \frac{1}{2}H_2 \underset{Charge}{\overset{Discharge}{\rightleftharpoons}} VO^{2+} + H_2O \tag{1.20}$$

Accordingly the voltage of the cell can be obtained:

$$\begin{aligned} E_C^{0'} &= 1.004 \quad V \\ E_A^{0'} &= 0 \quad V \\ E_{Cell}^{0'} = E_C^{0'} - E_A^{0'} &= E_C^{0'} = 1.004 \quad V \end{aligned} \tag{1.21}$$

Equilibrium potential for the two sides can be obtained:

$$E_A^0 = E_A^{0'} + \frac{RT}{F} \ln\left(\frac{a_{H^+}}{{a_{H_2}}^{0.5}}\right) \tag{1.22a}$$

$$E_C^0 = E_C^{0'} + \frac{RT}{F} \ln\left(\frac{c_{V^{5+}} \cdot \left(c_{H^+}^C\right)^2}{c_{V^{4+}}}\right) \tag{1.22b}$$

In this work temperature effect will be neglected as the battery usually operate in a range of temperatures that is reasonably small. Activities for protons and gaseous hydrogen are considered one and losses for activation and concentration are considered negligible [36].

$$OCV_{Cell} = E_{Cell}^{0'} + \frac{RT}{F} \ln\left(\frac{c_{V^{5+}} \cdot \left(c_{H^+}^C\right)^2}{c_{V^{4+}}}\right) \tag{1.23}$$

Recalling the definition of *SOC* from 1.10 it is possible to express the open circuit voltage as follows:

$$OCV_{cell} = E_{cell}^{0'} + \frac{RT}{F} \ln\left(\frac{SOC}{(1-SOC)} \cdot \left(c_{H^+}^C\right)^2\right) \tag{1.24}$$

In this formulation one important hypotesis is stated and it is regarding the behaviour of the membrane. What happens in reality is that the membrane has different permeabilities with respect to the species, being of course the proton exchange enhanced. Other species' diffusion happens, even if with low diffusivity. This may turn out in a situation called Gibbs–Donnan equilibrium or Donnan equilibrium. Since the membrane is selectively permeable to charges, an uneven distribution of charged species arises and this fact generates a voltage between the two sides of the membrane called Donnan potential. In a flow battery this effect exists and the Donnan Potential has an influence on the open circuit voltage of the battery and for this reason in the literature models to take into account this effect exist and provide detailed explanation of this phenomena [21],[17]. In this work the influence of the Donnan Potential will not be taken into account for sake of difficulty in modelling correctly the phenomenon and also as it intrests a small area close to the membrane and it is not able to change significantly the behaviour of the coupling between the characteristic of the flow field and the electrode, which is an aim of this work.

1.9 Objectives

The parameters that influence the reaction of the system with respect to the flow field characteristics are many: from the fluiddynamic condition of the flow to the electrochemical properties of the electrode down to the geometrical shape of the channel. The first aim of this work is to understand in which are the parameters that influence the relation between the flow field and the performance of the battery. The second aim of this work is trying to quantify the impact of the parameters on the overall performance. The impact of different families of designs is studied in this work. This comprehension of the problem is intended to be a tool for the design of a new flow field. Since the problem is not related to constitutive equations but to how the geometry impacts on their solution, bidimensional and threedimensional models are implemented to understand the performance of the system and visualize quantities that experimentally would be very difficult or impossible to be measured. The performance of the system is analyzed taking into consideration several operating conditions of the cell and its efficiency. The reference cell in this work will be the Hydrogen-Vanadium cell, explained into the detail in the previous section.

2 Development of a bidimensional model

In this chapter the development of a bidmensional model for the positive electrode of the vanadium redox flow battery is described, the constitutive equations are listed as well as the assumptions made. Results of the fitting procedure of the model for two different electrodes are reported along with the most important quantities of the battery. The limits of this approach are also presented.

2.1 State of the art

Mathematical models for VRFB are available in the literature due to the need to understand its behaviour in a theoretical way. These systems present some characteristics that make them not easy to be studied, since in real systems two main problems have to be solved: electrochemistry and fluid dynamics. The difference among models is mainly related to their capability to understand the various phenomena and the underlying assumptions. The first distinction can be made on the dimensionality of the problem. Having basically a linear domain like the one in figure 2.1 allows showing the variation of the main quantities of the battery, such as reactants' concentrations potentials and current, on a line. This approach limits the computational time and effort and provides a very nimble model to be used in situations where the behaviour of the system may be modeled but the level of detail needed is not too high such as stack design and optimal point of operation problems. Monodimensional models have been developed in $MRT\ Fuel\ Cell\ Lab$ for the

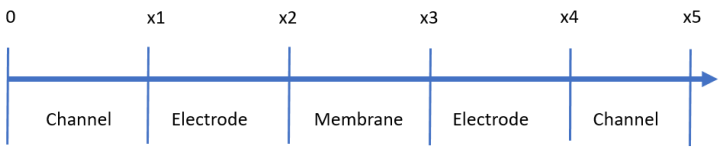

Fig. 2.1: Typical 1D domain

characterization of the behaviour of the system [26],[12] and for the characterization of the charge and discharge curves allowing also the model to be time dependent. It has to be noticed that in these models the fluid dynamic aspect is also monodimensional and the velocity field distribution is not investigated. The capability of a model to be time variant

allows it to be used as a tool for understanding phenomena such as cross-contamination or parasitic reactions. The efficiency of the machine can be obtained by charge and discharge curve, that can be simulated with a time variant monodimensional model. These curves are derived from an experiment in which a fixed current is imposed for a certain time. The charge and discharge curve shows the trends of voltage with respect to the charged or discharged capacity. In this work the approach is different and polarization curves will be shown and compared. In order to get experimentally polarization curves, the state of charge of the solution sent to the battery has to be constant. The configuration that allows this is a two tanks configuration for the cathodic electrode. In this way the solution that has been processed by the battery is not mixed with the original solution, allowing it to stay in the initial state of charge. Polarization curves are significative as they show clearly the transport losses, the ohmic losses and the activation losses. In the literature the most relevant monodimensional models are Vynnycky's[35] and Chen's [7]. Both of them consider the ionomer as perfectly selective for protons, implicitly neglecting cross contamination. In the first fluid dynamics and electrochemistry are not solved together and the use of this model is in the field of stack design and optimization. Chen improves the model including protons activity in the calculation of the open circuit voltage and includes the variation of reactants from the "bulk" concentration to the "surface" concentration. This concept is related with the mass transport phenomena in the electrode and will be explained more into the details in the following chapters.
Among bidmensional models the most influencing examples in the literature are You's [39], Walsh's [29] and Agar's [17]. Agar focuses on cross contamination, his modelling of the battery deals with the problem of the not perfect selectivity of the membrane. All species pass through the membrane except from $SO_4{}^{2-}$ as it is negative and in the membrane there are some fixed negative charges. Despite the fact that fluxes are continous, since the membrane is selective, concentration will have a discontinuity. For sake of simplicity in the model the interface is modeled as a small thickness domain, in which concentration is allowed to vary linearly and create a "discontinuity" in concentration.
Walsh focuses instead on the parasitic reactions and how they can affect the behaviour and life of the battery. Hydrogen and oxygen evolution are taken into account but in this case the cross contamination effect is not taken into account. You provides a simple bidimensional model that focuses more on the constitutive and conservation equations, very useful when one is interested in understanding the basic principles of the electrochemical phenomena. What is more, this model investigates the properties of mass transfer inside the electrode and gives an overlook on their effects. In addition, despite the differences, all models deal *flow-through* configuration. Since this is not the same situation of the experimental setup present in $MRT\ Fuel\ Cell\ Lab$ and from which the experimental data were taken, there was the need to develop a new model according to the needs. This was built by [26] and used by [32] and will be the starting point for this analysis. What is done in this work is using this model to fit the experimental data and to change some of its features to adapt it to the needs of the analysis. The main characteristics in the model presented here are:

- The anodic electrode is not modeled but it is treated as a boundary condition in coherence to the Hydrogen-Vanadium cell.
- The domain is composed by membrane, porous electrode and channel.
- Cross contamination and parasitic reactions are neglected.

The majority of models cited (included the one presented in this chapter) have been solved using *COMSOL Multiphysics* ®. This software has packages for the solutions of electrochemical models, particularly *Tertiary Current Density Distribution* is used for Nernst-Planck equation in electrodes, whereas *Secondary Current Density Distribution* is used for current and potentials in the membrane. This software, having default packages, limits the errors due to boundary conditions and related to the equations. On the other side is not very customizable and, talking about solvers, it may have some undesired convergence problems. For this reason when there will be the need in this work to add the third dimension to the model, *ANSYS Fluent* ® will be chosen as a solver as it allows robust convergence and a full control on the equations.

2.2 Description of the model for the positive electrode

The assumption made in the bidimensional model presented are defined:

- Stationary model: time variant phenomena and boundary conditions are not taken into account.
- Isothermal domain: no temperature variation is taken into account when actually temperature influences the performance. [33]
- Parasitic reactions (equations 1.15,1.16) are neglected.
- Incompressible fluid.
- Isotropic properties for electrode and membrane.
- Electrolyte properties not dependent on the State Of Charge.
- Membrane is permeable just to protons.
- Complete wettability of the membrane.
- Electroneutrality of membrane and solutions.

The geometry of the model takes into account 3 bidimensional domains as visible in figure 2.2 In the experimental setup there are a *Nafion* membrane while as electrode a commercial *Gas Diffusion Layer GDL 10 AA* is used. Geometrical parameters for the model are reported in figure 2.1. From the electrochemical point of view the species that are present in the channels and in the domain are:

$$VO_2{}^+, VO^{2+}, H^+, HSO_4^-, SO_4^{2-}, H_2O \tag{2.1}$$

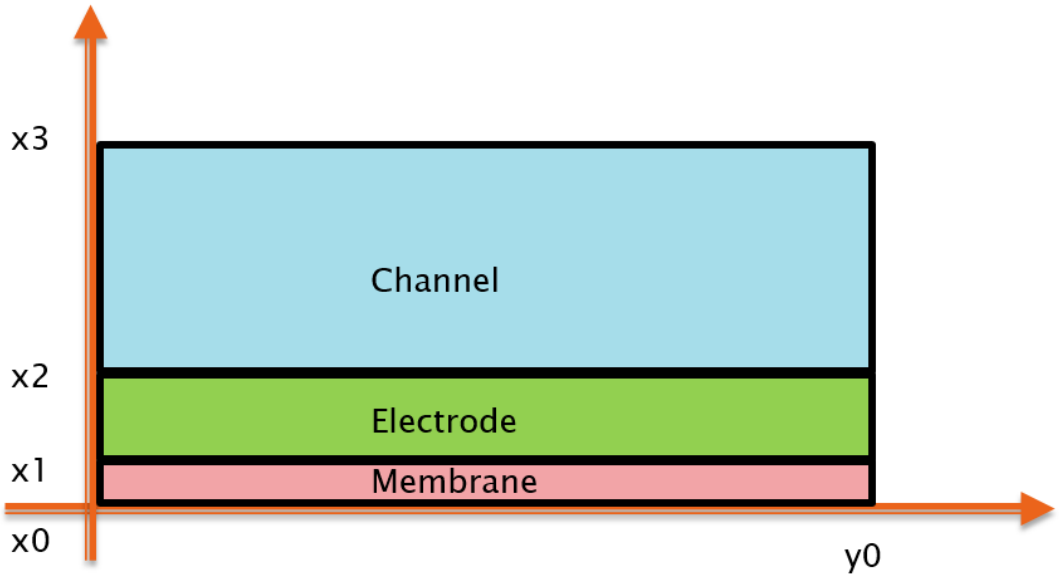

Fig. 2.2: Bidimensional domain

Domain	Dimension
Membrane	125 μm
Electrode compressed	340 μm
Channel	800 μm
Length	5 cm

Tab. 2.1: Dimensions for the 2D domain

The main reaction is:

$$VO_2{}^+ + 2H^+ + e^- \underset{Charge}{\overset{Discharge}{\rightleftharpoons}} VO^{2+} + H_2O \tag{2.2}$$

Moreover dissociation of sulfuric acid is presend and refers to the following reactions:

$$H_2SO_4 \rightleftharpoons HSO_4^- + H^+ \tag{2.3}$$

and

$$HSO_4^- \rightleftharpoons SO_4^{2-} + H^+ \tag{2.4}$$

The modelling of this reaction is done according to [17], neglecting reaction 2.3 as products are favourited and the presence of H_2SO_4 will be negligible. The second step is modeled by a source term according to 2.5, where β and k_d are constants taken from [17].Their values can be found in the table 2.6.

$$R_d = k_d \left(\frac{c_{H^+} - c_{HSO_4^-}}{c_{H^+} + c_{HSO_4^-}} - \beta \right) \qquad \left[\frac{mol}{m^3} \right] \tag{2.5}$$

The constitutive equations for the flow battery's electrochemical model are based on a Butler-Volmer kinetic model, the charge conservation principle and the Nernst-Planck equation.

- Nernst-Planck Equation:

$$\mathbf{N_i} = -D_i^{eff}\nabla c_i - z_i u_i c_i F \nabla \phi_l + \mathbf{u}c_i \qquad \left[\frac{mol}{m^2 s}\right] \tag{2.6}$$

This equation relates the molar areic flux to three components: the diffusion term, due to concentration gradients and due to the diffusivity of species in the mixture, the migrative term, caused by the electrophoretic force acting on ions in an electric field and the convective term caused by the velocity field. The first term depends on the local gradient of concentration and by the effective diffusion of each specie in the mixture. In the literature there are several ways to quantify the effective diffusivity in porous media and in this work Bruggeman correction is chosen. Porosity is defined as the ratio of void space over the total space. The hypotesis of infinite dilution is stated and it allows to consider diffusivity as a scalar.

$$D_i^{eff} = \varepsilon^{3/2} D_i \qquad \left[\frac{m^2}{s}\right] \tag{2.7}$$

The second term depends on the gradient of the liquid phase potential and the coefficient of proportionality for each specie is the product of concentration, charge number, Faraday constant and the mobility. Mobility is calculated using Nernst-Einstein equation.

$$u_i = \frac{D_i^{eff}}{RT} \qquad \left[\frac{mols}{kg}\right] \tag{2.8}$$

The third element is a flux generated by the fact that in the control volume a velocity field exists, it is not easy to determine the entity of this velocity as it means basically understanding the fluiddynamic behaviour of a liquid solution in a porous medium.

- **Butler-Volmer kinetic model**: the kinetic model applied in this work is explained in the details in [19] or in [5] on page 96. It is applicable when the reaction has just one step or one step is much slower than the others and whose velocity can be considered limiting for the overall kinetic process. The expression that is obtained computes a volumetric current source what in this work will be called i_R. For the generic redox one-step:

$$A \underset{Inverse}{\overset{Direct}{\rightleftharpoons}} B + e^- \tag{2.9}$$

$$i_R = k_0 a F \left(c_A^s \cdot e^{\frac{\alpha F \eta^*}{RT}} - c_B^s \cdot e^{\frac{-(1-\alpha) F \eta^*}{RT}} \right) \qquad \left[\frac{A}{m^3}\right] \tag{2.10}$$

Where F, R, T are constants, c_A, c_B are concentrations of species. The magnitude of the source and its sign is determined by two factors: concentrations of species on the surface of the electrode and the overpotentials η^*. Applying this definition to 2.11:

$$VO_2{}^+ + 2H^+ + e^- \overset{Discharge}{\underset{Charge}{\rightleftharpoons}} VO^{2+} + H_2O \tag{2.11}$$

$$i_R = k_0 aF \left(c^s_{V^{4+}} \cdot e^{\frac{\alpha F \eta^*}{RT}} - c^s_{V^{5+}} \cdot e^{\frac{-(1-\alpha)F\eta^*}{RT}} \right) \qquad \left[\frac{A}{m^3}\right] \tag{2.12}$$

The definition of the overpotential comes from the Nernst equation as follows:

$$E^0_C = E^{0'}_C + \frac{RT}{F} \ln \left(\frac{c_{V^{5+}} \cdot \left(c^C_{H^+} \right)^2}{c_{V^{4+}}} \right) \qquad [V] \tag{2.13}$$

$$E^0_C = E^{0'}_C + \frac{RT}{F} \ln \left({c^C_{H^+}}^2 \right) + \frac{RT}{F} \ln \left(\frac{c_{V^{5+}}}{c_{V^{4+}}} \right) [V] \tag{2.14}$$

$$E_{eq} = E^{0'}_C + \frac{RT}{F} \ln \left({c^C_{H^+}}^2 \right) [V] \tag{2.15}$$

$$\eta^* = \phi_s - \phi_l - E_{eq}[V] \tag{2.16}$$

What is done here is basically formulate the kinetics of the reaction using the hydrogen concentration inside the term E_{eq}, the overpotential has the same term inside. Notice how, in the assumptions made in this work, the source will be positive when the solution is in charging mode and negative when the solution is being discharged. The term $k_0\,[m/s]$ is the standard costant for the velocity of the reaction. The higher the value the lower the time to get to the equilibrium. α is the charge transfer coefficient and expresses the symmetry of the energetic barrier between the direct and the reverse reaction. $a\,[m^2/m^3]$ is the active area of the electrode and is a property of the porous medium, it expresses how much surface there is in one cubic meter of the material. In order to complete the Butler-Volmer model the pore model has to be considered. Porous media geometry can be represented by a solid matrix in which there are some cavities. A pore could be defined as a portion of the space that is void and ideally containing a sphere of radius r_p. The place where reaction takes place is on the surface of the carbon, the mechanism through which reagents migrate from the bulk of the pore to the active surface of the electrode may limit the concentration on the active sites and hence limit the current. In steady state the flux of reagents from bulk to surface is equal to the flux generated by the chemical reaction. Consider the behaviour of VO^{2+} during charge, one expects the

concentration to be higher in the bulk condition than on the surfaces, coherently with 2.12.

$$\frac{D}{r_p}(c_{VO^{2+}}^{bulk} - c_{VO^{2+}}^{surface}) = \frac{i_r}{aF} \qquad \left[\frac{mol}{s \cdot m^2}\right] \tag{2.17}$$

Where r_p is the radius of the pore, considered as the mean path for the chemical species and D is the diffusivity of the vanadium species. The opposite phenomenon happens for the VO_2^+ (in charge):

$$-\frac{D}{r_p}(c_{VO_2^+}^{bulk} - c_{VO_2^+}^{surface}) = \frac{i_r}{aF} \qquad \left[\frac{mol}{s \cdot m^2}\right] \tag{2.18}$$

In VRFB modeling the bulk concentration is used in the determination of the overpotential while the surface concentration is used in the Butler-Volmer kinetic expression. Since in numerical models surface concentration can't be calculated explicitly it is more convenient to express 2.12 referring to bulk concentrations. This is possible using 2.17 and 2.18, calculating the superficial concentrations and replacing them in 2.12. The result is:

$$i_r = \frac{k_0 aF}{1 + \frac{r_p k_0}{D} \cdot \left(e^{\frac{\alpha F \eta^*}{RT}} + e^{-\frac{(1-\alpha)F\eta^*}{RT}}\right)} \left(c_{V^{4+}}^b \cdot e^{\frac{\alpha F \eta^*}{RT}} - c_{V^{5+}}^b \cdot e^{-\frac{(1-\alpha)F\eta^*}{RT}}\right) \left[\frac{A}{m^3}\right] \tag{2.19}$$

- **Charge conservation**: considering the electrode and the channel it is possible to distinguish a solid phase and a liquid phase. The amount of current produced or consumed by electrochemical reaction in the liquid phase has to be balanced by an equal charge in the solid phase. A charge conservation equation can be written:

$$\nabla \cdot \mathbf{j_l} = -\nabla \cdot \mathbf{j_s} = i_R \qquad \left[\frac{A}{m^3}\right] \tag{2.20}$$

In the solid phase the current flow can be modelled with Ohm's law, where the conductivity of the porous medium has to be corrected using Bruggeman correction as a function of porosity:

$$\mathbf{j}_s = -\sigma_s^{eff} \nabla \phi_s \qquad \left[\frac{A}{m^2}\right] \tag{2.21}$$

$$\sigma_s^{eff} = (1-\varepsilon)^{3/2} \sigma_s \qquad \left[\frac{S}{m}\right] \tag{2.22}$$

For the liquid phase the Ohm's law is not straightforward as there is the need for keeping into account all the fluxes: summing all the fluxes of ions one gets the

expression for the ionic current. Coherently with 2.20 the divergence of this quantity is equal to the rate i_R.

$$\mathbf{j_l} = F \sum_i z_i(-D_i^{eff} \nabla c_i - z_i u_i c_i F \nabla \phi_l + u c_i) \left[\frac{A}{m^2}\right] \tag{2.23}$$

Nernst-Planck equation is not solved for all the species, as the condition of electroneutrality of the solution is invoked to calculate the concentration of SO_4^- from the linear combination of all other terms. Electroneutrality's mathematical form is:

$$\sum_i z_i c_i = 0 \tag{2.24}$$

Mass sources will act on each specie coherently to the reactions taken into account and the effects of the electrochemical redox process and the acid dissociation are summarized in the following table. Each specie will have its own source and these sources will be defined starting from i_r considering the stoichiometry of the reaction and F.

$$\nabla \cdot \mathbf{N_i} = R_i \qquad \left[\frac{mol}{sm^3}\right] \tag{2.25}$$

Species	Source
VO^+	i_R/F
VO_2^+	$-i_R/F$
H^+	$-2i_R/F - R_d$
HSO_4^-	R_d
SO_4^{2-}	$-R_d$

Tab. 2.2: Source terms for the positive electrode

2.2.1 Membrane Model

The membrane allows the separation of the two electrodes and its modelling is particulary simple if cross contamination effects are neglected: all fluxes are imposed to be zero except the protons' one. $COMSOL$ solves this issue automatically using the *Secundary current density distribution*. In this domain the transport of protons happens using as "carriers" the sulfonic groups present in the structure of the *Nafion* membrane. Modelling the exact phenomenon of transport is very complicated and a simplification is introduced. If the concentration of sulphonic groups is high enough the membrane can be considered a liquid electrolyte [26]. Since no reactions are present in the membrane ($i_r = 0$), mass

conservation forces proton flux and their concentration to be constant along the x-direction.

$$\nabla \cdot \mathbf{N}_{\mathbf{H}^+} = 0 \qquad \left[\frac{mol}{m^3 s}\right] \tag{2.26}$$

Since there is no solid matrix and just one ionic specie, the electrolyte current is expressed by:

$$\mathbf{j_l} = F\mathbf{N}_{\mathbf{H}^+} \qquad \left[\frac{A}{m^2}\right] \tag{2.27}$$

Deriving the expression current is proved to be constant:

$$\nabla \cdot \mathbf{j_l} = \nabla \cdot \mathbf{N}_{\mathbf{H}^+} = 0 \tag{2.28}$$

Since proton concentration has to be a constant, recalling the Nernst-Plank equation, it is possible to state that the current is defined by the properties of the membrane and proton concentration.

$$\mathbf{j_l} = \frac{F^2}{RT} z_i^2 D_{H^+}^{eff} c_{H^+} \nabla \phi_l \qquad \left[\frac{A}{m^2}\right] \tag{2.29}$$

Based upon this idea it is possible to define a pseudo-conductivity of the membrane and model the phenomenon as governed by Ohm's law.

$$\mathbf{j_l} = -\sigma_m \nabla \phi_l \qquad \left[\frac{A}{m^2}\right] \tag{2.30}$$

$$\sigma_m = \frac{F^2}{RT} z_i^2 D_{H^+}^{eff} c_{H^+} \qquad \left[\frac{S}{m}\right] \tag{2.31}$$

It is neglected the influence of other species permeability in the membrane as it is difficult to be carefully modelled. Donnan potential does not influence the membrane behaviour.

2.2.2 Fluid dynamic modelling

COMSOL Multiphysics ® has a package specifically designed for the calculation of fluid flow in a porous medium using the Brinkmann equations. These relations are an extension of Darcy's law and take into account the dissipation of kinetic energy due to viscous stresses, like Navier-Stokes equations. In the porous medium Brinkmann equations are solved while the channel's flow field is solved with Navier-Stokes' equations. Mass and momentum conservation are modelled as follows (under the hypotesis of incompressible fluid):

$$\rho \nabla \cdot \mathbf{u} = 0 \tag{2.32}$$

$$\nabla \cdot \left[-p\mathbf{I} + \frac{\mu}{\varepsilon}\left(\nabla \mathbf{u} + (\nabla \mathbf{u})^T\right) - \frac{2\mu}{3\varepsilon}(\nabla \cdot \mathbf{u})\mathbf{I}\right] - \left(\frac{\mu}{\kappa} + \beta_F |\mathbf{u}|\right)\mathbf{u} + \mathbf{F} = 0 \tag{2.33}$$

One can notice on the right part of 3.3 the existance of two momentum "sinks": the Darcy resistance and the Forchheimer term. Darcy term is dependent on viscosity of the liquid, permeability of the porous medium and scales linearly with velocity, while the importance of the Forchheimer terms becomes more and more important at high velocities as it scales with the square of the velocity. The last term F is needed to take into account the effect of external forces, such as gravity and is not taken into account. The viscosity has been taken from[37] and the porosity of the material is taken from manufacturer [26]. Notice how in this formulation of the momentum equation the terms of viscous dissipation depend actively from porosity: $\mu\left(\nabla\mathbf{u}+(\nabla\mathbf{u})^T\right)-\frac{2}{3}\mu\left(\nabla\cdot\mathbf{u}\right)\mathbf{I}$ are multiplied by the factor $1/\varepsilon$. The solver will automatically distinguish wheather to use 3.3 or Navier-Stokes momentum balance considering both porosity and permeability of the considered domain. Permeability and porosity of the channel are considered equal to one.

Tab. 2.3: Constants for fluiddynamic modelling

Property	Value
Density $[kg\cdot m^{-3}]$	1350
Viscosity $[Pa\cdot s]$	0.005
Porosity [-]	0.88
Porosity of the compressed electrode [-]	0.8588
Permeability $[m^2]$	40e-11

2.2.3 Boundary conditions and numerical details

In this section boundary conditions and numerical details will be explained as their choice determines the strategy of solving the constitutive equations. For the fluid dynamic part the boundary conditions are straightforward and consist of a condition on the velocity at the inlet of the channel and a pressure reference at the outlet of the channel. The condition in the solver assumes fully developed flow at the inlet and imposes a parabolic distribution of velocity according to:

$$L_{ch}\int_0^{L_{ch}} v dx = V_{avg}L_{ch}^2 \qquad \left[\frac{m^3}{s}\right] \tag{2.34}$$

where V_{avg} is computed from the volumetric flow rate desired and imposed by the user.

Tab. 2.4: Boundary condition fluiddynamic part

Condition	Equation
Inlet (Laminar flow)	$L_{entr}\nabla_t\cdot\left[-p\mathbf{I}+\mu\left(\nabla_t\mathbf{u}+(\nabla_t\mathbf{u})^T\right)\right]=-p_{entr}\mathbf{n}$
Outlet (pressure reference)	$p_{out}=0$

The condition for the electrochemical modelling are more complicated as both fluxes of species and potentials need to be imposed. Considering the same geometry as 2.2 boundary conditions are reported in 2.5. It is crucial to understand the strategy regarding

Tab. 2.5: Boundary condition for 2D model

Condition	Position
No flux : $-\mathbf{n}\cdot\mathbf{i_l}=0$, $-\mathbf{n}\cdot\mathbf{i_l}=0$	$x=x_3$
No flux : $-\mathbf{n}\cdot\mathbf{i_l}=0$, $-\mathbf{n}\cdot\mathbf{i_l}=0$	$y=0$, $y=H$
Impermeable wall: $-\mathbf{n}\cdot\mathbf{N_i}=0$	$x=x_3$
Impermeable wall: $-\mathbf{n}\cdot\mathbf{N_i}=0$	$y=0$ and $y=H$ for $x_1<x<x_2$
Fluid inlet : $c_i=c_{0,i}$	$y=0$ for $x_1<x<x_2$
Outflow : $-\mathbf{n}\cdot D_i\nabla c_i=0$	$y=H$ for $x_1<x<x_2$
Liquid Potential : $\phi_\mathbf{l}=0$	$x=0$
Solid Potential: $\phi_\mathbf{s}=\phi_{user}$	$x=x_2$
Continuity of current: $-\mathbf{n}\cdot\mathbf{i_{l,mem}}=-\mathbf{n}\cdot\mathbf{i_{l,por}}$	$x=x_1$
Continuity of potential: $\phi_{\mathbf{l,mem}}=\phi_{\mathbf{l,por}}$	$x=x_1$

boundary conditions and particularly the last 4 are very important. The condition on the liquid potential in $x=0$ is basically able to exclude all the phenomena at the anode, coherently with the hypotesis made in this work. On the other hand the last two conditions express the way to control the model in a potentiostatic way. In order to make the model working under these hypotesis, a value for the solid potential is imposed at the interface between electrode and channel.The solver is able to calculate both solid and liquid current but continuity of the electrolyte current between the porous medium and in the membrane has to be imposed. This is necessary as in the first domain current is calculated from the flux of all species and in the second the current is related to the flux of protons only. This is not the only way of closing the system of equation as a galvanostatic model may be possible. The main assumption in this second case would have been:

- Continuity of electrolyte current and liquid potential at the interface x_1
- Electrolyte (liquid) potential null at $x=0$
- Solid current specific flux is imposed at $x=x_2$.

The convergence of the model has been investigated in both cases and it is proved that the second way is more stable than the first. Nonetheless, due to the characteristic of the model, galvanostatic control means imposing a specific flux $[A/m^2]$ in $x=x_2$. The solution in this way provides a uniform distribution of the current on the interface between the channel and the porous electrode allowing the voltage to distribute freely. What happens in reality is different from this situation and the current will have a significant distribution in the cell, implicitely neglected by a galvanostatic model controlled by the flux. When an experimental setup allows galvanostatic control it means that it is possible to impose the volumetric integral value of the current and not its flux. For these reasons the first strategy is adopted and a voltage-controlled model is built.

The models have been run using "*COMSOL with MATLAB* ®", a link that allows better customizability of the software. Solving fluiddynamics and electrochemistry together has proved to be numerically problematic on this platform. To solve this issue it was chosen to solve the velocity field first, solve electrochemistry consequentely with the results of the fluiddynamic study as initial value for the flow field and in the end a third coupled solver was performed, using as starting values the results from the first two steps. Meshing of the domain was performed trough the built-in mesher of *COMSOL* and presents 7560 quadrilateral cells. A detail of the domain close to the inlet can be seen in 2.3: close to interfaces, where the gradients are expected to be higher, cell dimension decreases. The same principle is applied along the y-direction, allowing the central part of the domain having lower accuracy in the discretization.

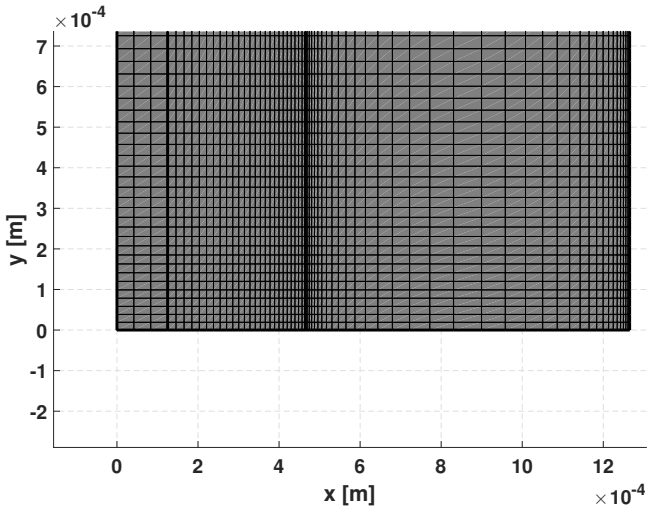

Fig. 2.3: Detail of the mesh for the GDL10AA cell

2.2.4 Model calibration for GDL 10 AA electrode

In order to validate the model a calibration procedure has been made using the experimental data in [32]. The experimentals chosen were held on $Sigracet\ GDL\ 10AA$ with single channel flow field as they were the ones with the highest repetibility. Repetibility is a fundamental requirement when dealing with calibration as it may weaken the theoretical results. Dealing with VRFB one main source of uncertainty is affecting the state of charge of the battery, calculated from the measured OCV. Tanks actually present stratification and the OCV may change during the operation of the battery since different solution may enter the cell. What is more at high currents the measurement uncertainity grows significantly due to the limits of the instruments and due to the weight of the non perfect steady flow of the pump. The experimental points are expected to be affected by some low yet existing measurement error. Parameters that have been fitted are: permeability, mean pore radius and velocity of the reaction. In order to increase the validity of the fitting it has been chosen to validate the model not just on one curve but on two different operating conditions and the choice was to use two different values of flow rate: $20\ ml\ min^{-1}$ and $10\ ml\ min^{-1}$. A long effort has been made trying to develop an iterative procedure whose aim was to increase the procedure's automation, but the complexity of the relations and the computational time did not let the procedure to become fully automatic. Consequentely

Tab. 2.6: Parameters used in the simulations

Parameter	Value	Unit	Origin
$D_{V^{4+}}$	$3.9 \cdot 10^{-10}$	$m^2\ s^{-1}$	[17]
$D_{V^{5+}}$	$3.9 \cdot 10^{-10}$	$m^2\ s^{-1}$	[17]
D_{H^+}	$9.312 \cdot 10^{-9}$	$m^2\ s^{-1}$	[17]
$D_{HSO_4^-}$	$1.33 \cdot 10^{-9}$	$m^2\ s^{-1}$	[17]
$D_{SO_4^{2-}}$	$1.065 \cdot 10^{-9}$	$m^2\ s^{-1}$	[17]
T	295	K	-
F	96485.3365	$C\ mol^{-1}$	-
R	8.314472	$J\ mol^{-1}\ K^{-1}$	-
Q_1	$3.45 \cdot 10^{-7}$	$m^3\ s^{-1}$	-
v_1	0.53906	$m\ s^{-1}$	-
Q_2	$1.76 \cdot 10^{-7}$	$m^3\ s^{-1}$	-
v_2	0.2700	$m\ s^{-1}$	-
ρ_{sol}	1350	$kg\ m^{-3}$	[17]
μ_{sol}	0.005	$Pa\ s$	[17]
α	0.5	-	Assumed
ϵ	0.8588	-	[30]
a	$3.5 \cdot 10^4$	m^{-1}	[12]
K	$40 \cdot 10^{-11}$	m^2	Fitted
r_p	$32 \cdot 10^{-6}$	m	Fitted
k_0	$1.8e-6$	m/s	Fitted

the fitting procedure has brought to the data visible in figure 2.4. The availability of such

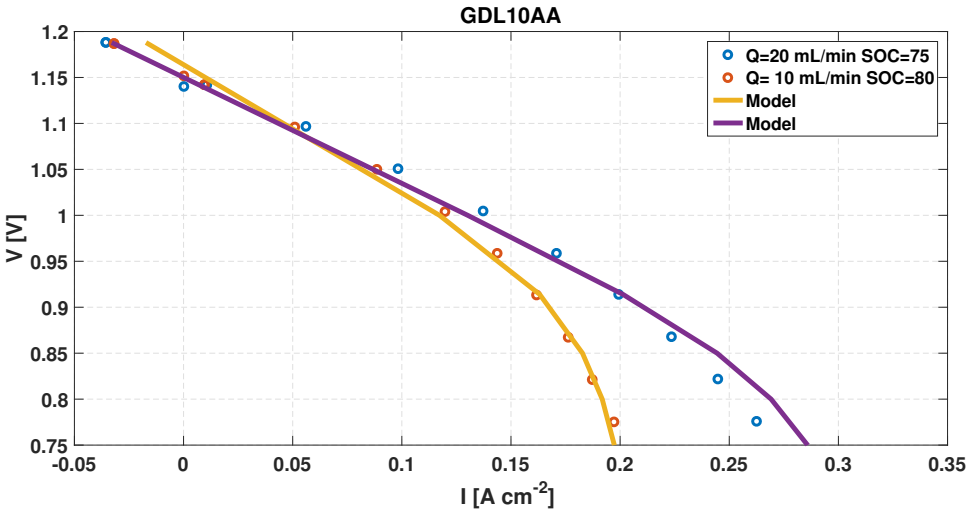

Fig. 2.4: Fitting of the performance$Sigracet\ GDL\ 10AA$

model is important from the scientific point of view as it allows the visualization of the variation of the main quantities of interest along 2 directions, extending the utility of a monodimensional model. In this work the main results will be presented for the 2D analysis. Several condition are chosen as significative for the working of the system, some points are chosen from 2.4. The results are plotted on lines or using contours and arrows, the lines are horizontal lines that start from $x = 0$ and finish in $x = x_3$. The values of the y-coordinate are reported into the legends. Black vertical lines distinguish the domains. Two main conditions are shown:

- Discharge condition: the working condition chosen is $V = 0.75V$, the average of the current is proved to be $0.3\ A\ cm^{-2}$, the flow rate is $20\ mL\ min^{-1}$, the state of charge is $SOC = 0.77$
- Charge condition: the working condition chosen is $V = 1.3\ V$, the average of the current is proved to be $-0.09A\ cm^{-2}$, the flow rate is $20\ mL\ min^{-1}$, the state of charge is $SOC = 0.77$.

Concentration trends (shown in figure 2.5 and 2.6) and mass sources depend significantly on the concentration and on the charging/discharging condition. The direction of the reaction is determined by the value of the voltage, if it is higher than the OCV there will be charge, under it discharge. Considering the specie V_4 during discharge, moving from the channel to the membrane the concentration has an increase as the reaction during this phase produces this specie. Similarly moving from the inlet to the outlet the concentration tends to increase. Since the reaction is symmetric, opposite consideration can be stated for V_5. The profile has a trend that is not regular in the x direction due to the fact that the vanadium redox is not the only one reaction present, acid dissociation changes locally the presence of protons changing the slope of concentration with respect to x. In the channel the model does not see any change in the concentration and this not

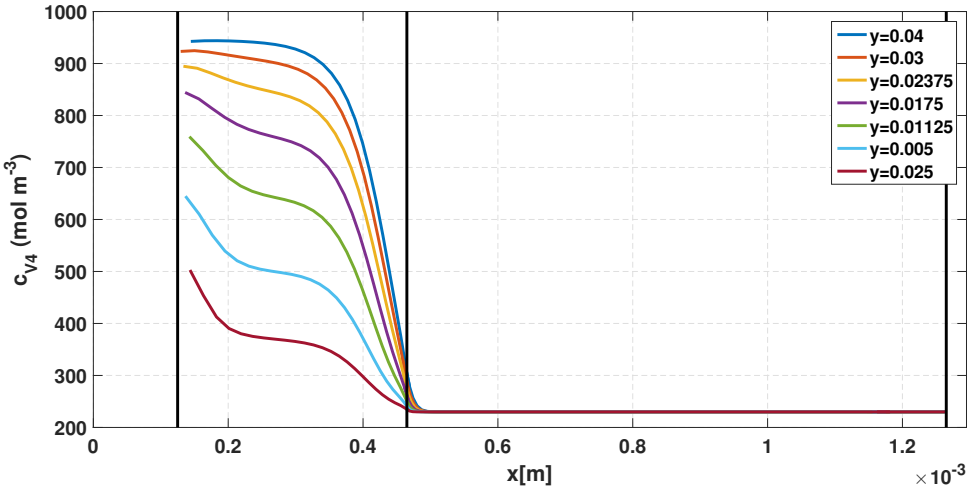

Fig. 2.5: V_4 concentration during discharge condition

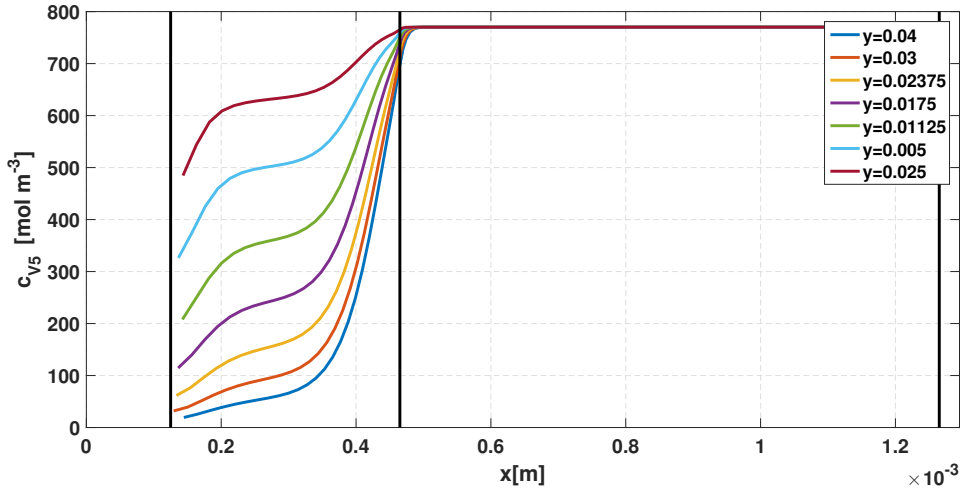

Fig. 2.6: V_5 concentration during discharge condition

likely to be a correct interpretation of the reality, since the concentration is virtually no changing, the state of charge of the battery is virtually costant in the channel. A possible explanation of this fact may be the fact that the current exchanged is not enough to change also the composition of the "undisturbed" channel. The kinetic of the equation 2.9 is determined by 2.11 and it is composed by concentration and overpotentials reported in 2.8 . Overpotential are negatives as well as the rate as discharge condition is examined. The trend of the overpotential along x is almost constant, while the area of the cell that has the highest rate is close to the inlet. It is intresting to notice how the rate is not constant along the horizontal coordinate and has a significant increase (2-3 times the average value) close to the interface between the channel and the porous medium. This area is interested with the highest reaction rate as it is the area with the highest concentration difference between reactants and a significant velocity component. Liquid current is not uniform throughout the cell length as it is not fixed in the model that is potentiostatic. The

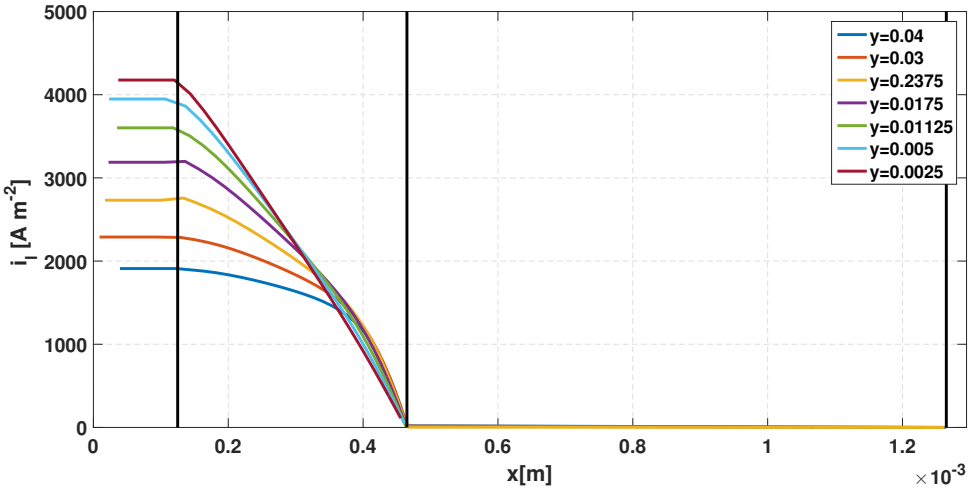

Fig. 2.7: Electrolyte current in discharge

area weighted average on the interface between membrane and porous medium of this distribution gives the value of the average operating current density. Regarding potentials,

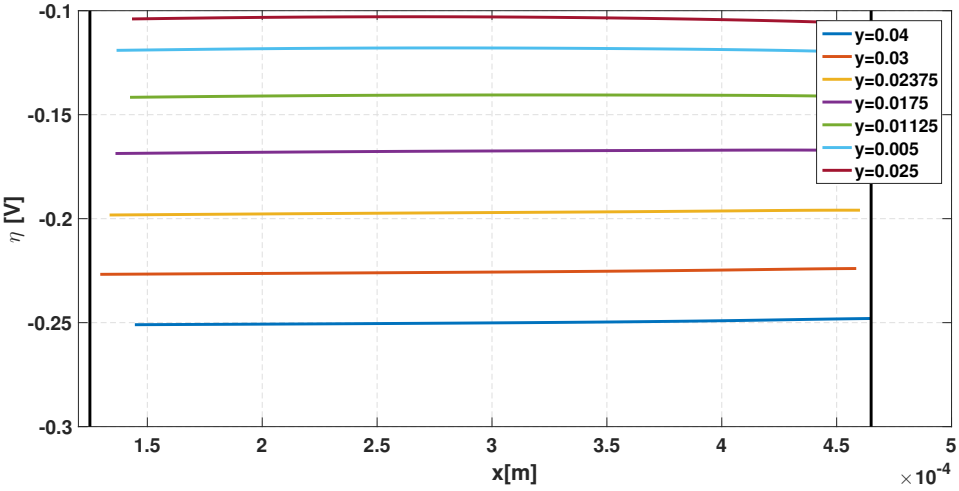

Fig. 2.8: Cathodic overpotential during discharge

the distribution resembles the presence of sources as stated in the constitutive equations. The variation of solid potential is smaller (few mV) with respect to the electrolyte one, being the conductivity of the solid matrix much larger than the liquid electrolyte's one. The values of the distribution depend on the operating condition, the higher the current the higher the variability of potential values. The link to what happens during charge can be made directly from these quantities as they are the responsible for the current generation processes. Solid potential changes concavity while the liquid one has a more complex behaviour due to the presence of a concentration term. Overpotentials and rate change sign to become positive and concentration trends invert. Since the state of charge of the battery is higher than 0.5, the charge reaction will not be as enhanced as the discharge one and current densities during this phase are expected to be lower. The

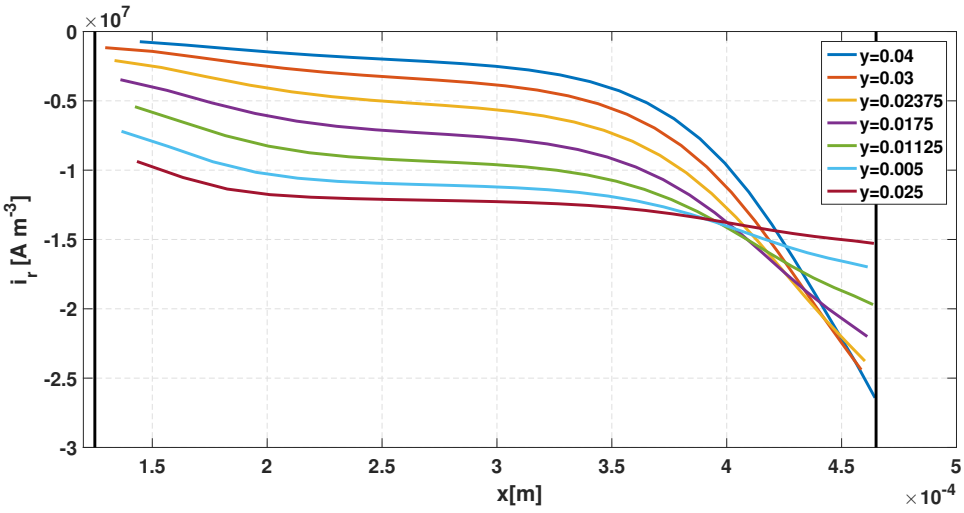

Fig. 2.9: Cathodic overpotential during discharge

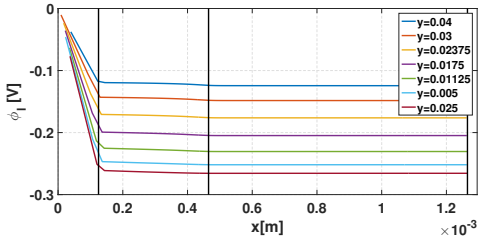

(a) Liquid potential Discharge

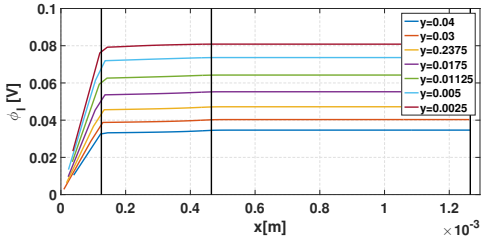

(b) Liquid potential Charge

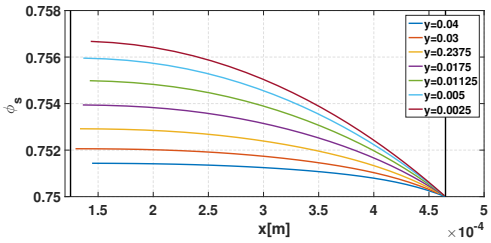

(c) Solid potential Discharge

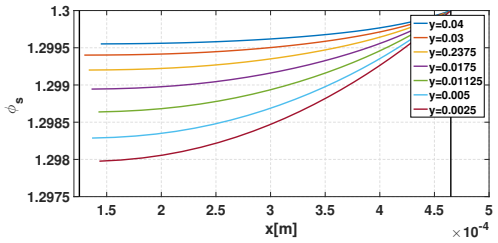

(d) Solid potential Charge

Fig. 2.10: Potentials' behaviour during charge and discharge condition

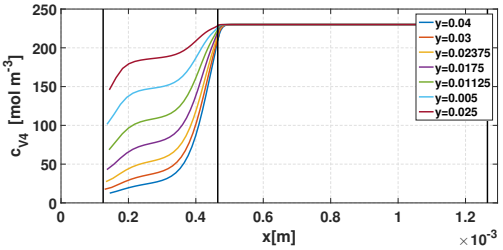

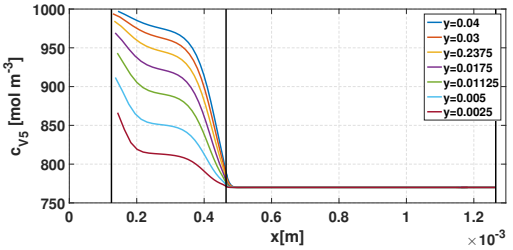

Fig. 2.11: Concentration of V_4 (left) and V_5(right) during charge

imbalance of concentration penalizes the charge reaction, limiting the possibility of the battery to be charged. As a last result of this preliminar analysis it is presented the fluid dynamic behaviour in the domain. In figure 2.12 is reported the velocity in the domain.

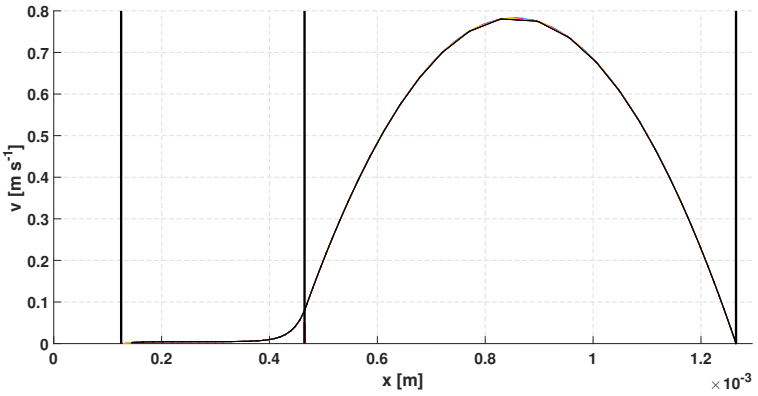

Fig. 2.12: Velocity magnitude

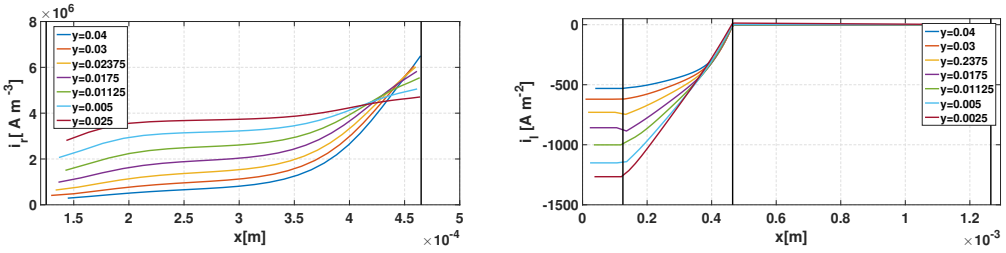

Fig. 2.13: Reaction rate (left) and current density (right) during charge

No evident variation is visible along the y-direction and all profiles are practically equal. The interface between channel and porous medium sees an area in which the velocity penetrates into the porous medium and another in which the velocity is almost constant. The values of the velocity in both these sections are small (few percentages and less than 1 percent respectively) when compared to the value of the mean velocity in the channel. It is not difficult to think that the fluiddynamic behaviour influences the electrochemical behaviour of the cell and if one looks at figure 2.5 realizes that in the area where the velocity components are higher the concentration gradient is higher as well as the reaction rate. What is difficult is to understand how one phenomenon influences the other and in which measure this area is important with respect to the whole cell. This model does not see any variability of the velocity field with respect to the y-direction in fact in 2.12 all profiles are reported even if equal. In order to enlighten the nature of the transport phenomena it is performed an analysis of the species fluxes. Migrative, diffusive and convective components are separated and for each direction ratios were defined. For example a ratio could be defined as:

$$R_{i,x} = \frac{|\dot{N}_{i,migr,x}|}{|\dot{N}_{i,conv,x}| + |\dot{N}_{i,migr,x}| + |\dot{N}_{i,diff,x}|} \tag{2.35}$$

$$R1_{i,y} = \frac{|\dot{N}_{i,migr,y}|}{|\dot{N}_{i,conv,y}| + |\dot{N}_{i,migr,y}| + |\dot{N}_{i,diff,y}|} \tag{2.36}$$

$$R_{i,xy} = \frac{|\dot{N}_{i,tot,x}|}{|\dot{N}_{i,tot,y}|} \tag{2.37}$$

This approach can be used also in the y-direction and it is able to understand the behaviour of each species locally in the domain. It is calculated the ratio for each specie of the y-component of the flux with respect to the x-component of the flux. This analysis gave just qualitative results but one interesting fact emerged. For all species, considering y-direction, convection is the major contribution accounting for more than 95 percent of the total flux in all operating condition. For all species, the x-component flux is not dominated by convection which is comparable with diffusion and migration and the three contribution are of the same order of magnitude. Particularly considering a region close to $y = 0.25$ one may state that diffusion plays the major role, like figure 2.14 testifies. In the figure the contours show the magnitude of the ratios calculated according to 2.35 in a discharge condition for VO^{-2}. In the x-direction, close to the channel diffusion has a major contribution while close to the membrane migration is more important.

The arrows in the figure show the direction of the total migrative and diffusive flux and do not have any quantitative purpose. Diffusive flux for VO^{-2} is directed from the membrane to the channel as well as the migrative term. Nonetheless for all species the magnitude of the total flux in the x direction was negligible with respect to the total flux in the y-direction. Figure 2.15 shows how the total flux in the y direction is 3 orders of magnitude larger than the flux in the x direction. For this reason it was possible to state that convection plays an important role in delivering the reactants to the porous medium and acts in a major way along y-direction, but is also possible to state how the phenomena are very complex and no definitive and global conclusion can be stated for all working conditions.

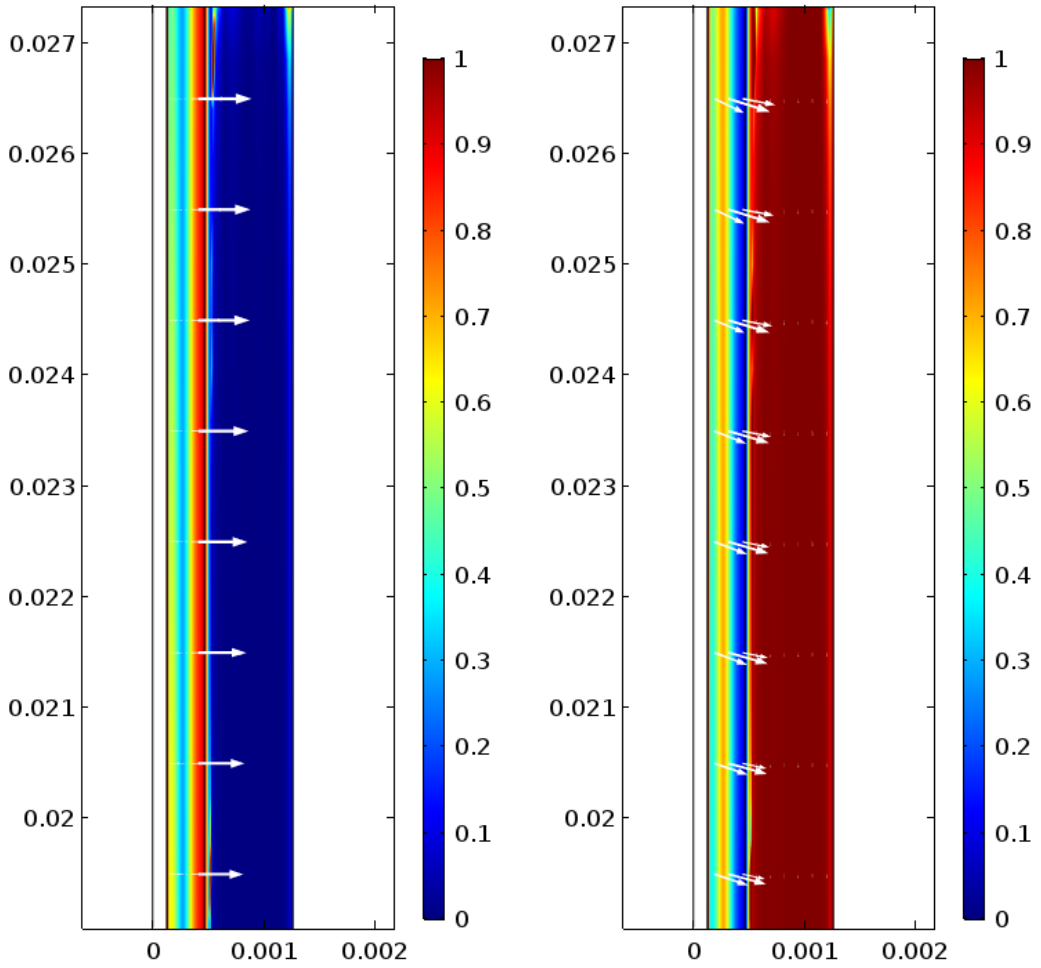

(a) Ratio of the migrative x-flux to the total x-flux for VO^{2+}

(b) Ratio of the diffusive x-flux to the total x-flux for VO^{2+}

Fig. 2.14: Results of the fluxes analysis

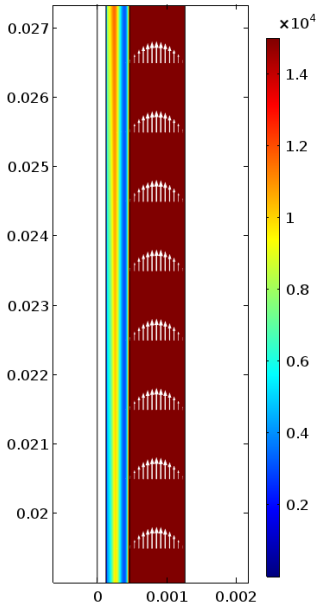

Fig. 2.15: Ratio of the total flux in y direction with respect to x direction for VO^{2+}

2.3 Model calibration for Sigracell GFD 4.6 EA electrode

In several literature's experimental and modellistic studies often the electrode used is not a $Sigracet\ GDL\ 10AA$ electrode but is a thicker electrode made of carbon felt. The properties of this material make it suitable for applications in the field of flow batteries and many are the examples in the literature. Experimental data were available in [32] regarding the performance of a "$Sigracell\ 4.6\ EA$". The electrode is more than 10 times thicker than the previous electrode: its initial thickness is 4.6 mm while in the model it is assumed a compression of 25 percent. As stated in the preface and by the most influencing

Tab. 2.7: Parameters used in the simulations

Parameter	Value	Unit	Origin
L_c	$0.8 \cdot 10^{-3}$	m	-
L_m	$3.45 \cdot 10^{-3}$	m	-
L_e	$125 \cdot 10^{-6}$	m	-
H_{cell}	$5 \cdot 10^{-2}$	m	-

authors in this field [2], the behaviour of the cell is determined by its architecture. This electrode has some differences both in terms of size and properties with respect to the fuel cell derived electrode. The reason why it was used widely in the flow battery systems was related to the flow through configuration, that, due to its feeding approach, needed larger electrodes to work with reasonable pressure drops at high flow rates. The porosity is higher for this electrode while permeability is not known but it is assumed to be of the same order of magnitude of the previous electrode's one. The higher thickness influences both diffusion losses and ohmic losses. A longer path for the species to diffuse into the electrode implies a higher loss. The behaviour of this electrode is different from the others also in the way it reacts to changes of operating conditions such as the flow rate. Particularly the performance of the "Sigracell" electrode is less influenced by the flow rate change. A calibration of the bidimensional model in order to enlight the main parameters of the new electrode has been performed and the results reported in table 2.8.

Unfortunately with low flow rate ($10\ mL\ min^{-1}$.) the model exibits some convergence issues and for this reason it is chosen to fit it on two flow rates: $20\ mL\ min^{-1}$ and $40\ mL\ min^{-1}$. The overall quality of the fitting procedure decreases but the $20\ mL\ min^{-1}$ curve was well fitted. It has to be noticed that also the second curve fitted had a different SOC condition and this complicated the procedure. Changing few parameters it is difficult to get a good fitting procedure but an improvement could be achieved working also with the parameter α. This fitting procedure anyway is not the main aim of the work and therefore is not performed. The equations are exactly the same of the previous section and the only difference was regarding the geometry of the cell as one can see in 2.16. Spatial

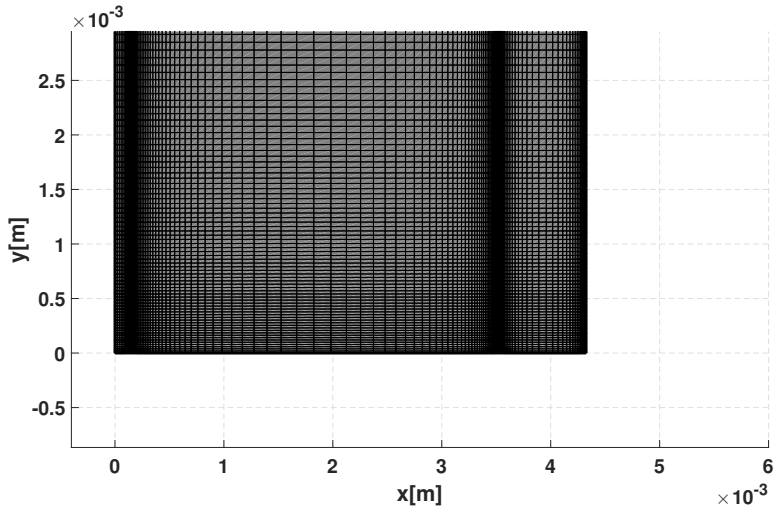

Fig. 2.16: Detail close to the inlet of the mesh for the Sigracell electrode

accuracy was increased with respect to the previous case as the model had some problems of convergence.

Tab. 2.8: Parameters used in the simulations

Parameter	Value	Unit	Origin
ϵ	0.89	$-$	[32]
a	$2.8 \cdot 10^{3}$	m^{-1}	Fitted
K	$40 \cdot 10^{-11}$	m^{2}	Fitted
r_p	$70 \cdot 10^{-6}$	m	Fitted
k_0	$1.5e-6$	m/s	Fitted

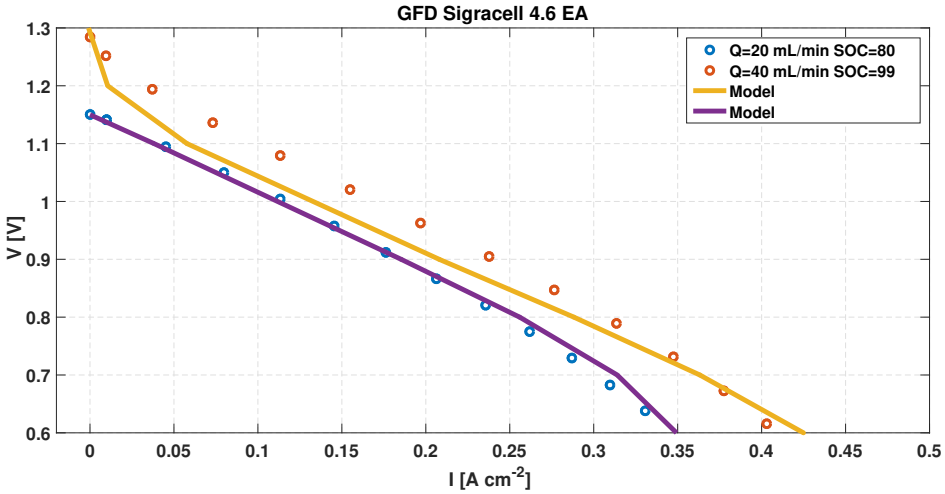

Fig. 2.17: Fit of the model with Sigracell electrode

Understanding the behaviour of this electrode is not simple as its volume is big with respect to the channel and its properties are not precisely known. Since the overall current density

is more or less the same of the thinner electrode but the volume is approximately ten times something has to be dramatically different in the two electrodes. The fit was done allowing permeability to be slightly lower than the other electrode, keeping almost the same value for the kinetic rate but lowering the active area and increasing the pore diameter. This attempt is emphatizing the worse performance of the felt electrode regarding its capability to diffuse efficiently electrolytes. Trends of major quantities in the model are reported in a condition of discharge where the flow rate is $20\ ml\ min^{-1}$, the state of charge is 0.77 and the voltage is 0.71 in order to get a current density of approximately $0.3\ A\ cm^{-2}$.

- The area in which the influence of the channel flow-field is present is very low compared to the overall area. The velocity field distributes in a way that leaves the vaste majority of the electrode with practically still fluid.
- Reaction rate in this case distributes in a more uniform way and reaches values that are two orders of magnitude lower than the previous electrode.
- Uniformity of the reaction rate causes also smoother concentration gradients as visible in 2.19.

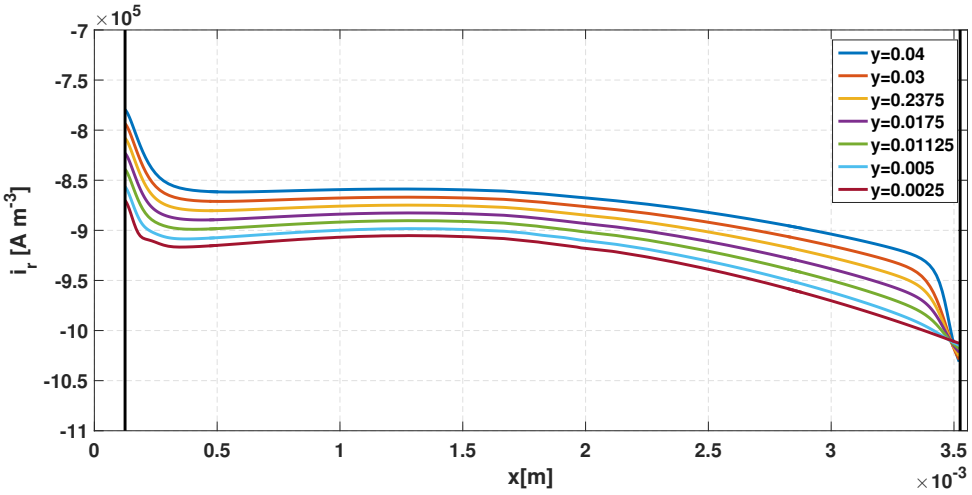

Fig. 2.18: Reaction rate for the "$Sigracell\ 4.6\ EA$ electrode

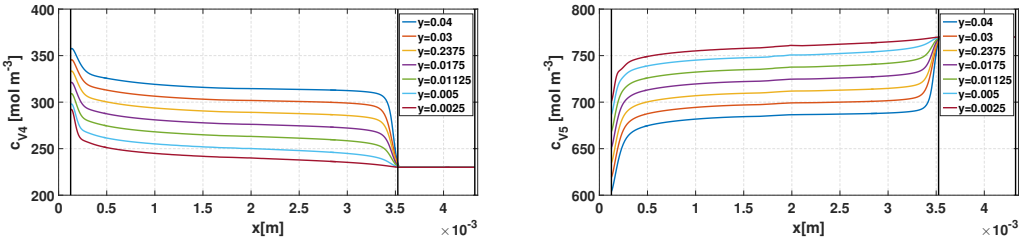

Fig. 2.19: Concentration trends for "$Sigracell\ 4.6\ EA$ electrode

The lower generation term influences also the trend of the electrolyte current which is found to be almost linear with respect to the x coordinate. Potentials trends are different from the previous electrode as the variability along the y-direction of both solid and liquid potential is much smaller than in the previous case. On the other hand, especially

considering the solid potential along the x direction, the variability is much higher than in the previous case (10 times more). Fluxes' analysis is carried out also for this electrode, hoping to find a correlation between the mass transport phenomena and the performance. The situation is complicated by the larger thickness of the electrode and for this electrode convection migration and diffusion cannot be efficiently separated in their contribution in the domain. The only thing that can be withdrawn is that y-direction convection is again the most important contribution among the phenomena regulating cell operation. The graphical representation of this phenomenon was poor as in some zones of the domain numerical errors changed the values of the electrode to values that are not significant and for this reason graphs are not shown.

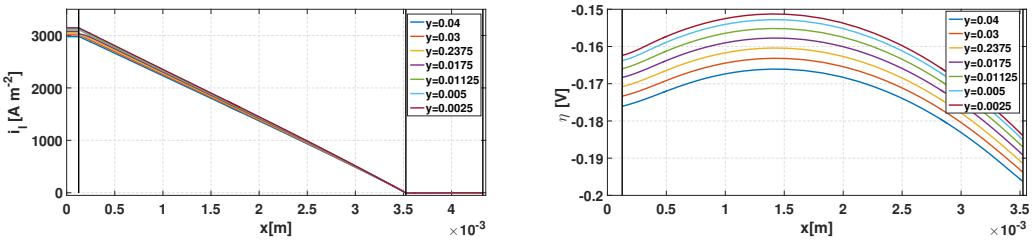

Fig. 2.20: Current density (left) and overpotent(right) during discharge

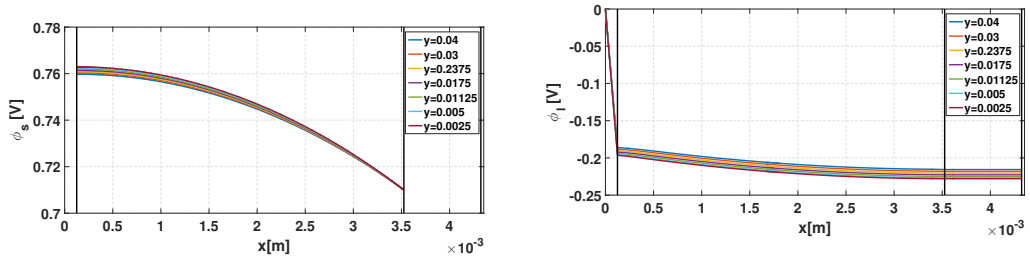

Fig. 2.21: Solid (left) and liquid (right) potential in discharge

2.4 Limits of a bidimensional model

Understanding the phenomena that occur in a bidimensional model is important to have a sensibility on trends but it also introduces a simplification of the domain that is not coherent with a real cell. The first thing is that this model assumes that along the z-direction, the cell behaviour is exactly the same of the one shown in this chapter, as if the cell it was made of multiple but identical slices. This is not true as the flow field changes the properties along this direction. What is more, imposing potential at the interface between channel and electrode is not correct as in reality potential values are continuous at the interface between the rib and the porous electrode. Considering the data in [32], the same electrode (the $Sigracet\ GDL\ 10AA$) exhibit different performance with respect to the flow field (see figure 2.22 used as showed in 2.23.

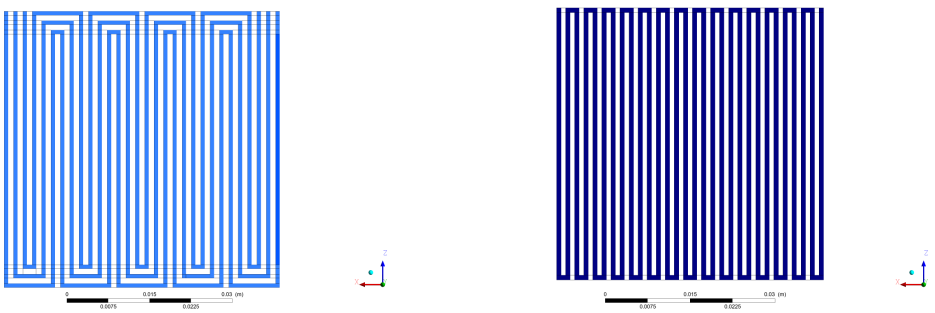

(a) Multiple Serpentine **(b)** Single Serpentine

Fig. 2.22: Different flow fields

It is clear how threedimensional effects are present and need to be characterized by a more detailed analysis.

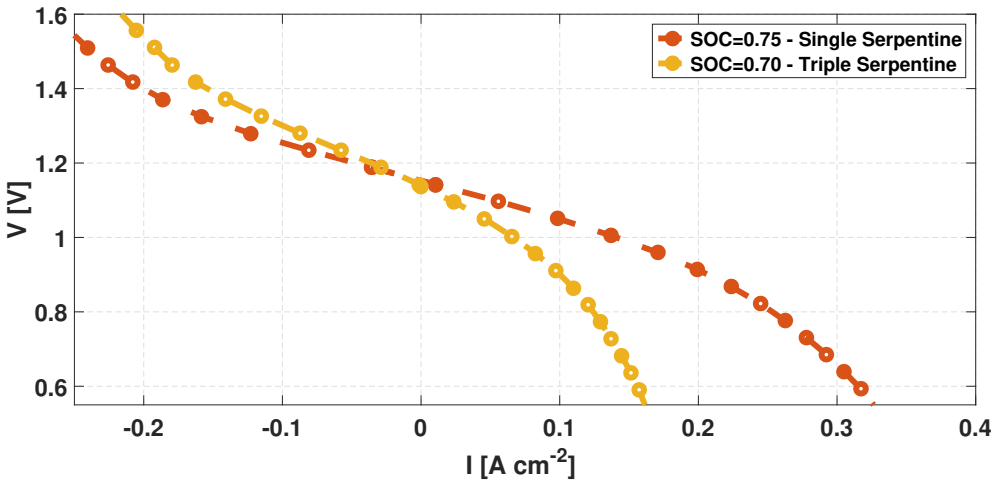

Fig. 2.23: Difference of performance of GDL electrode with 2 different flow fields.

Even though the state of charge of the two curves is not exactly the same, the variability of the curves is way larger than the difference caused by such a small difference of the state of charge. The flow field characteristics are playing a role: the addition of the third dimension to the model is needed.

3 Development of a three dimensional model

In this chapter the development of a threedimensional model for the cathode of a VRFB is presented. The comparison between experimental results from [32] and model is performed for a $Sigracet\ 10\ AA$. Trends of major quantities are shown and in order to verify the solidity of the numerical model a sensitivity analysis with respect to the major parameters and a mesh independence test are performed.

3.1 State of the art

In the literature several authors proposed threedimensional models that exhibit differences regarding their characteristics. Many are the purposes of the modelling of these batteries and consequently the possible configurations one may simulate. The main examples are cited:

- Xu and Zhao [37] proposed a threedimensional model for the full cell and pointed out the differences of performance related to the flow fields.
- Yin and Tang [38] proposed a 3D model for an interdigitated flow field with two different designs. Their focus was on the how to build the inlet, whether to use a single-inlet configuration or a multi-inlet one. Simulations were structured in the model are to study the distributions of fluid pressure, electric potential, current density and overpotential during operation of VRFB cell.

Particularly important for this work is [37] as it uses a threedimensional model to understand the fluid dynamic behaviour of a flow battery for the flow field design. It is basically the same purposes presented in this work but in the paper a full cell is modelled. Other important differences from the model presented are the dimensions of channels and electrode and the molarity of the inlet solution. It has to be reported that in the literature there are also models that do not solve the electrochemical part of the cell, limiting their action just to the fluid dynamic behaviour and the characterization of the relation between the flow regime and the pressure loss. Among them the most influencing are the works of the following authors:

- Bordolin presented fluid dynamic studies [6] aiming at understanding the best configuration in terms of pressure loss.
- Jyothi [16] proposed a paper specifically devoted to the analysis of the flow regimes and the "under the rib" fluxes.

All considerations presented in this chapter are devoted to the analysis of a battery with an active area of $25\ cm^{-2}$. The extrapolation of the results in order to quantify the impact of the parameter on a bigger cell or a smaller one is not straightforward and dedicated studies are needed even if it is not part of this work. In the literature one important paper is present [18] and it is related to the fluid dynamic study of both a $25\ cm^{-2}$ and a $200\ cm^{-2}$ cell with several flow field configurations. This study is very important as it gives an insight on how the features of an interdigitated and a serpentine flow field, such as the dimension of the channel and the rib size influence the behaviour of a large cell. Some detailed informations about how the conclusion one gets for a cell size can be applied to a case with a different area. The results presented are able to quantify the dependence of pressure loss on cell size and design, demonstrating that the details of the digits that distribute the flow between individual channels and the inlet and outlet position have a major impact on pressure losses in larger cells.

3.2 Constitutive equations

The equations used in the model are conceptually the same previously used in the bidimensional model although the solver chosen was not COMSOL but *ANSYS Fluent* ®. This choice required coding since there was not such a model in the Fluent's libraries. Actually templates for chemical reactions are present in the commercial code, allowing also the use of a Butler-Volmer kinetic model. It has been tried to adapt to the need of the user this template but its scarce customizability worth the coding of a new model. The fluid dynamic part of the model is given to the *ANSYS Fluent* ®'s template for porous media. The electrochemical part of the model is written by the user and is explained in 3.2.2.

3.2.1 Fluid dynamic modelling

In this work flow through porous medium has been modelled using the default template in *ANSYS Fluent* ®. The study of flow through porous media is explained into the details in [23]. Considering a volume of porous medium the porosity is defined as the ratio of the fluid volume over the total volume:

$$\epsilon = \frac{v_{void}}{v_{tot}} \tag{3.1}$$

A distinction is made between an average taken with respect to a volume element *V* of the medium (incorporating both solid and fluid material) and one taken with respect to a volume element consisting of fluid only. The first quantity has been given various names, by different authors, such as seepage velocity, filtration velocity, superficial velocity, Darcy velocity, and volumetric flux density. This is not the only choice and taking an average of the fluid velocity over a volume of fluid one gets the intrinsic average velocity called also physical velocity. The link between them is straightforward:

$$V_{physical} = \frac{V_{superficial}}{\epsilon} \left[\frac{m}{s}\right] \tag{3.2}$$

The porous media model incorporates an empirically determined flow resistance in a region of your model defined as "porous". In essence, the porous media model adds a momentum sink in the momentum equations. Consequently, the following assumptions and limitations should be readily recognized:

- Since the volume blockage that is physically present is not represented in the model, by default ANSYS Fluent ®uses and reports a superficial velocity inside the porous medium, based on the volumetric flow rate, to ensure continuity of the velocity vectors across the porous medium interface. This superficial velocity formulation does not take porosity into account when calculating the convection and diffusion terms of the transport equations.
- The superficial velocity porous formulation generally gives good representations of the bulk pressure loss through a porous region. However, since the superficial velocity values within a porous region remain the same as those outside the porous region, it cannot predict the velocity increase in porous zones and therefore limits the accuracy of the model.

For these reasons in this work it is preferred to model fluid flow according to a physical velocity formulation when solving continuity and momentum equations since the values of the velocity in the porous medium are important for our purposes.

$$\nabla \cdot \left[-p\mathbf{I} + \frac{\mu}{\varepsilon}\left(\nabla\mathbf{u} + (\nabla\mathbf{u})^T\right) - \frac{2\mu}{3\varepsilon}(\nabla\cdot\mathbf{u})\mathbf{I}\right] - \left(\frac{\mu}{\kappa} + \beta_F|\mathbf{u}|\right)\mathbf{u} = 0 \tag{3.3}$$

This formulation of the momentum equation adds two momentum sinks, one proportional to velocity and the other proportional to the square of the velocity. The determination of the coefficient of the Forcheimer is hard and it is difficult to find adequate literature. What is more, according to literature models [37], the Darcy term is sufficient to model the pressure drop through the electrode: velocities values are limited in the porous medium (the order of magnitude is not larger than $10^{-1}\ m\ s^{-1}$ in all working conditions). As a proof, it has been performed a check in the model using the ratio of the pressure drop due to the Darcy term and the Forcheimer term computed with a value for the proportionality coefficient equal to the one used in $COMSOL$. In the range of flow rates analyzed (from

$10\ to$ to $60\ mL\ min^{-1}$) the value of this ratio was never below 30, justifying the choice of neglecting the Forcheimer term. Permeability values are crucial for the correct modelling of the battery and their value is determined by the properties of the electrode and by its compression. For simplicity the medium is treated as isotropic. This fact is not guaranteed in the reality as the electrode might not be homogeneous and behave differently according to the direction taken into account. Particularly, for this kind of application, it is not strange to forecast a different behaviour of the electrode between the in-plane direction and the through-plane direction but, since in the literature few detailed studies are present, the medium is treated as isotropic. Many authors calculate permeability from the mean fiber diameter and the porosity from the Kozeny-Karman relation:

$$K = \frac{{d_f}^2 \epsilon^3}{K_{KC}(1-\epsilon)} \qquad [m^2] \tag{3.4}$$

Where K_{kc} is the Kozeny Karman constant, usually 180.

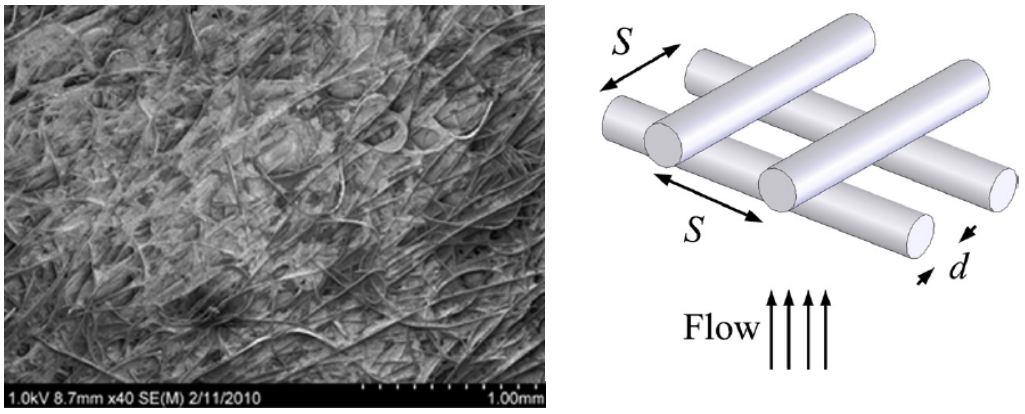

Fig. 3.1: Fibers orientation model

Since the datasheet for the Sigracet 10 AA electrode does not provide directly the value of permeability, the value for this parameter is taken from an article[24]. In this work an experimental setup for the determination of a through plane permeability of commercial gas diffusion layers is presented, the effect of compression is examined and a theoretical model is proposed. M. Bahrami explained how permeability can be seen as proportional to 3 terms:

$$K = f(\epsilon, \delta_c^2, \tau) \tag{3.5}$$

where ϵ is the porosity, τ is the tortuosity factor and δ_c is a geometrical parameter dependent on the geometric orientation of fibers. Supposing a structure of planar fibers like shown in figure 3.1 δ_c is equal to half of the space between fibers. Details of both the numerical correlations and the theoretical approach can be found in [24]. Furthermore porosity and permeability have to be corrected to take into account mechanical compres-

sion. In porous media compression does not change the shape of the fibres but reduces the void space. A correction for porosity follows from its definition in 3.1.

$$\frac{t_1}{t_0} = \frac{1-\epsilon_0}{1-\epsilon 1} \tag{3.6}$$

Similarly permeability decreases increasing compression and to quantify this trend a correlation has been used:

$$\frac{K}{K_{uncomp}} = 1.6\frac{t}{t_{uncomp}} - 0.6 \tag{3.7}$$

The value for permeability was found therefore to be $K = 1.75e^{-11}\ m^2$, notice how this value is one order of magnitude lower than the value used in the bidimensional model. This is reasonable considering the geometry of the 2D model: the pressure gradient is expected to be mainly distributed along the channel direction and it is not supposed to have a component that is pushing the fluid actively into the porous medium. For this reason, in order to have an effective access of the reagents to the electrode a lowered value for permeability is required. Regarding the fluid dynamic condition, the model of the flow is laminar. This choice is coherent with the velocity values present in the flow fields and with the literature. To check the validity of this hypothesis Reynolds number based on the equivalent diameter of the channel is calculated and reported for the highest flow rate considered. The velocity chosen to calculate Reynolds is the maximum in the channel and for the highest flow rate presented in the work ($100\ mL\ min^{-1}$) the value of the adimensional group is around 600. Since the values are well below the transition Reynolds number the choice of laminar flow is justified.

3.2.2 Electrochemical modelling

Electrochemical modelling is done considering the vanadium redox reaction 2.11 but not the acid dissociation for sake of convergence reasons. The implementation of the model involved the introduction of two additional transport equation respectively for solid potential and liquid potential. A significant difference is present between the 3D model and the 2D one regarding the modelling of the membrane. $COMSOL$ solved the flux of protons through the membrane according to what stated in chapter 2. In the 3D approach it is difficult to model carefully a semipermeable membrane between two fluid domains, as it is done in $COMSOL$, for this reason some assumptions have been made:

- The membrane domain is set as a still fluid domain.
- The interface between membrane and porous medium stops all species.

In order to model effectively the membrane presence, a conductivity of $\sigma_m = 2\frac{S}{m}$ with respect to the scalar ϕ_l is introduced in the membrane domain. The value has been chosen

from the value of the the pseudo-conductivity (see 2.30) assumed by the membrane in the bidimensional model. In this way the proton flux is not physically present, but its influence on the liquid potential and hence on the current generation is modelled. Current values will be calculated and shown using the volume integral of the reaction rate, invoking the charge conservation principle. The exact solution procedure would involve a dedicated numerical method to virtually link the fluxes of protons from one side to the other of the membrane wall. This is probably possible but it would require a more detailed work in terms of coding and it would be an improvement of the existing situation.

3.2.3 Boundary conditions

Boundary conditions are set to create a stationary voltage controlled model. At the inlet mass fraction are imposed from the value of the state of charge and the molarity of the acid solution and expressed according to [26]. The link between concentration and mass fraction is the following:

$$X_i = \frac{C_i M M_i}{\rho 1000} \qquad \left[\frac{kg_i}{kg_{tot}}\right] \tag{3.8}$$

The equations that link molarities and state of charge to the concentration of the solutions are reported according to [26].

$$c_{VO^{2+}} = (1 - SOC)M_{van} \qquad c_{VO_2^+} = SOCM_{van} \qquad \left[\frac{mol}{m^3}\right] \tag{3.9}$$

$$c_{H^+} = M_{acid} - M_{van} + M_{van}SOC \qquad \left[\frac{mol}{m^3}\right] \tag{3.10}$$

$$c_{HSO_4^-} = M_{acid} + M_{van} \qquad \left[\frac{mol}{m^3}\right] \tag{3.11}$$

Velocity is also imposed at the inlet to control the flow rate. For sake of simplicity an uniform distribution is imposed whose value is derived from the volumetric flow rate. For the serpentine channel a velocity of $0.53\ m\ s^{-1}$ gives $20\ mL\ min^{-1}$. At the outlet pressure is set at a null value to create a pressure reference. On the ribs between the channels a value of the solid potential is fixed, while at the interface of the membrane where the anode should be the liquid potential is set to zero. This is conceptually the same approach presented in chapter 2 even if the existence of a rib area is important as it allows to set the solid potential on its surface. The interface conditions are stated as follows:

- Membrane-electrode interface: in this zone continuity of liquid potential is imposed. Fluxes of all species are set to zero according to what stated in the membrane modelling part.

- Electrode-channel interface: regarding velocity the boundary condition is imposed automatically by the solver when coupling the flow fields of the porous electrode and the channel.

All other zones in the domain are treated as walls.

3.2.4 Domain and meshing

Meshing is performed using "GAMBIT" as the software allows a very precise control on the meshing quality of the domain. The software offers the possibility of using quadrilateral cells to discretize the domain and the user has the capability of choosing the accuracy in each direction. Since the geometries in this work are characterized mainly by regular shapes, the choice for the mesh is to use quadrilateral cells. The portion of the domain in which velocity gradients are expected to be higher are meshed with higher accuracy, as well as the porous electrode domain since in this area there are more equations to be solved. The advantages of this meshing software count also its capability to store the commands of the user in a file, called "journal", which can be run multiple times, allowing doing some minor change in the geometry but giving full and instantaneous control on the mesh quantities. The different parts of the domain are shown and the geometric characteristics are: the area of the cell is $25\ cm^2$, the channel has a side of $0.8\ mm$ and the rib size is also $0.8\ mm$. Notice how the inlet and the outlet are on the same side of the domain. A dedicated procedure is implemented to build the polarization curve. Each point is calculated increasing progressively the under relaxation factors for the constitutive equations.

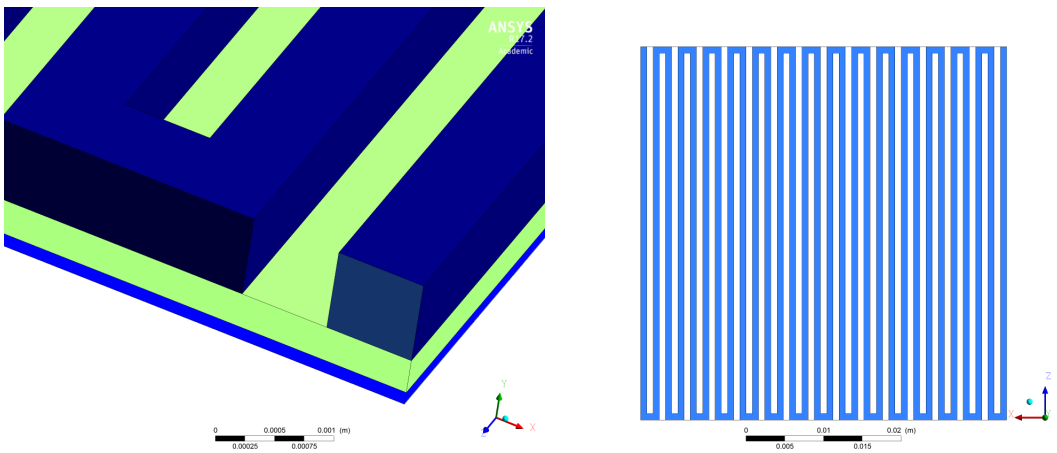

(a) Detail of the 3D model **(b)** Serpentine geometry

Fig. 3.2: Domain of the model

3.3 Performance of the cell

Parameters for the fitting of the model are the same of table 2.6 except for permeability that was lowered to the value of $K = 1.75e{-}11m^2$. The performance is analyzed through polarization curve just during the phase of discharge for sake of convenience due to the long computational time needed by the simulations: each point to reach convergence needed 3000 iterations that is nearly 30 minutes of calculation on a 16 cores cluster. To get a polarization curve two hours are needed. The trend of real curves (see 3.3) is not perfectly the same of the models but it is reasonable since no dedicated fitting procedure has been performed directly on this model. The variability of the performance with respect to the flow rate is forecast by the model even if at low flow rate there is underestimation of the performance. These differences have to be kept into consideration when dealing with reasonings.

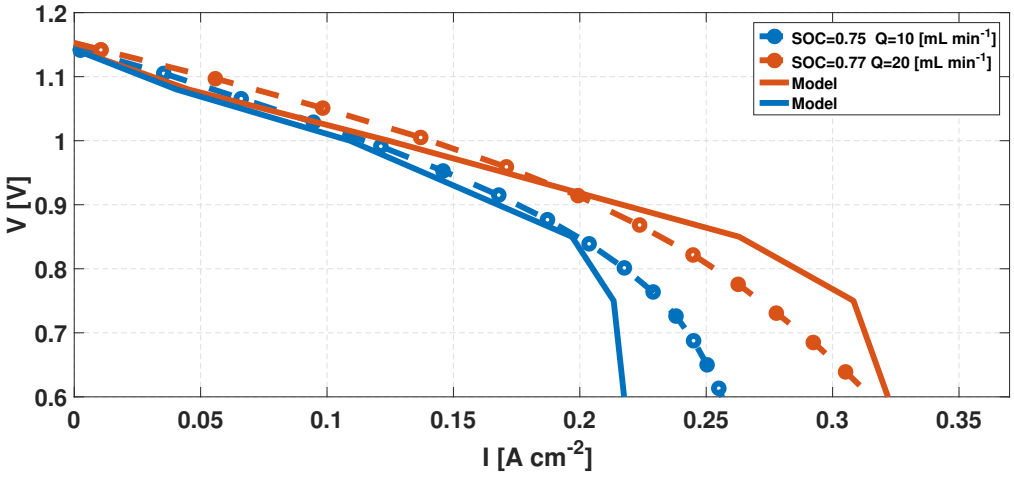

Fig. 3.3: Comparison of the performance of the real cell with the model for *Sigracet 10 AA* electrode

Coding a new model required much effort and during the first attempts mono dimensional trends have been very useful to understand if the constitutive equation were written correctly and if the model was coherent with the 2D one. To show liquid and solid potential y-direction lines are chosen at the center of a channel at the center of the cell $x = 0.0247m$. Various lines are chosen and their position along the z-direction are shown in the legends. The z-direction is along the channels the y-direction is from the membrane to the channels while the x-direction is from the inlet to the outlet. The working condition of the battery chosen is a discharge one with $20\ mL\ min^{-1}$, a state of charge of 0.77 and a potential $V = 0.75\ V$. This gives a current density of approximately $I = 0.3A\ cm^{-2}$. One may say that the trends of liquid and solid potential are in line with the bidimensional model. On one side this is true as concavities and trends with respect to the y-direction are coherent with the 2D-model.

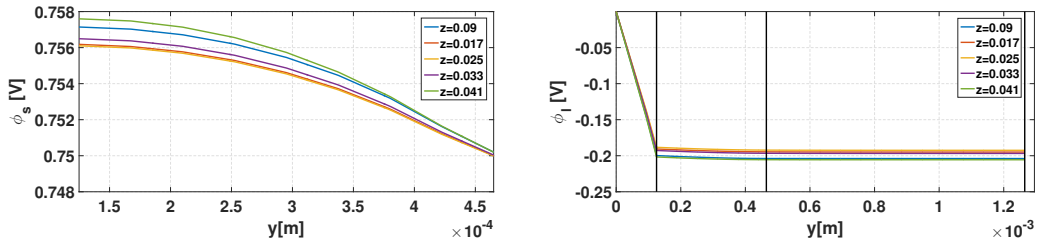

(a) Solid potential **(b)** Liquid potential

Fig. 3.4: Trends of potentials on y-direction lines

On the other side, if the $COMSOL$ model forecast a monotonic growth of the potential with respect to the longitudinal direction of the channel, the threedimensional model shows that there is not such growth in this direction. The initial part and the final part of the channel behave differently from the center of the cell and it is a sign that threedimensional effects are influencing the cell behaviour. The main advantage of having a full 3D model is to have information about the quantities in planes or in volumes that consider the whole cell. In order to have a first insight in the cell the state of charge is shown using contours in a plane that is at half height of the porous electrode. The inlet is in the top-right corner while the outlet is in the top-left corner.

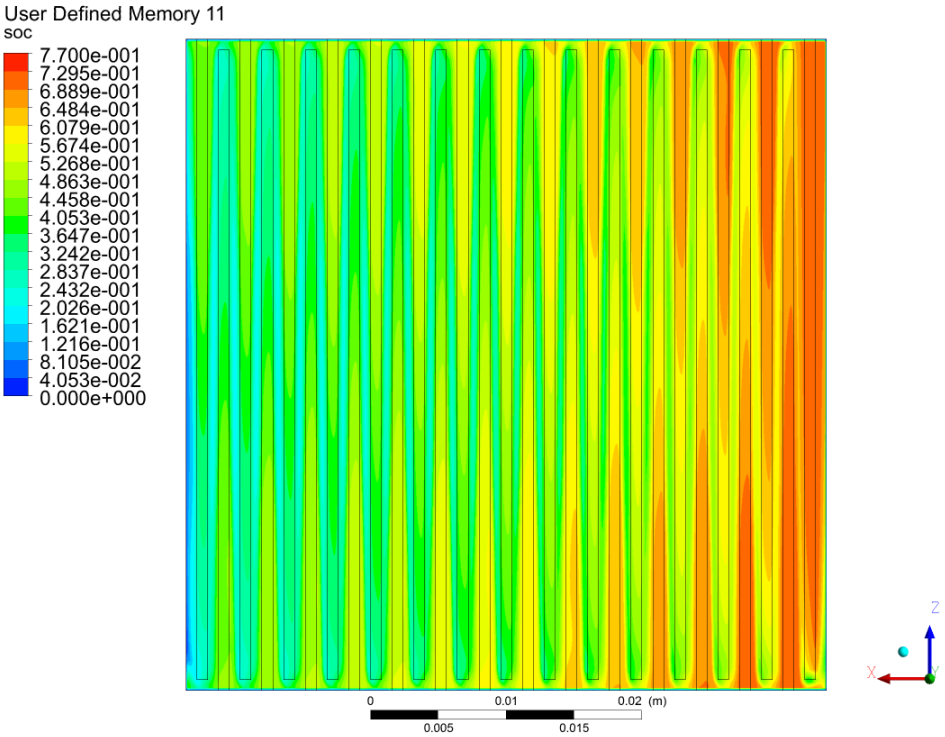

Fig. 3.5: State of charge on a plane at half the height of the electrode

Showing the trend of SOC is particularly wise as it allows to visualize the concentration of both the vanadium species in the domain. Several information can be withdrawn from figure 3.5: the first thing is related to the behaviour of the state of charge along the area of the cell, from the beginning to the end of the cell the state of charge decreases and this is coherent with a discharge condition. What is more, there is a very marked disuniformity when moving from under one channel to a zone under the following one. These zones have a slightly higher state of charge with respect to the nearby zones and are located under the beginning of a rib. What is more at the center of the cell it seems like there is an area of the cell in which the state of charge varies smoothly. Some explanations to the trends of the state of charge are provided by the reaction rate. This quantity is influenced by both concentration and potentials' distributions. Figure 3.6 testifies how there are some zones under the rib where the rate is much higher than in the adjacent one. The order of magnitude of the reaction rate is comparable with the values of chapter 2.

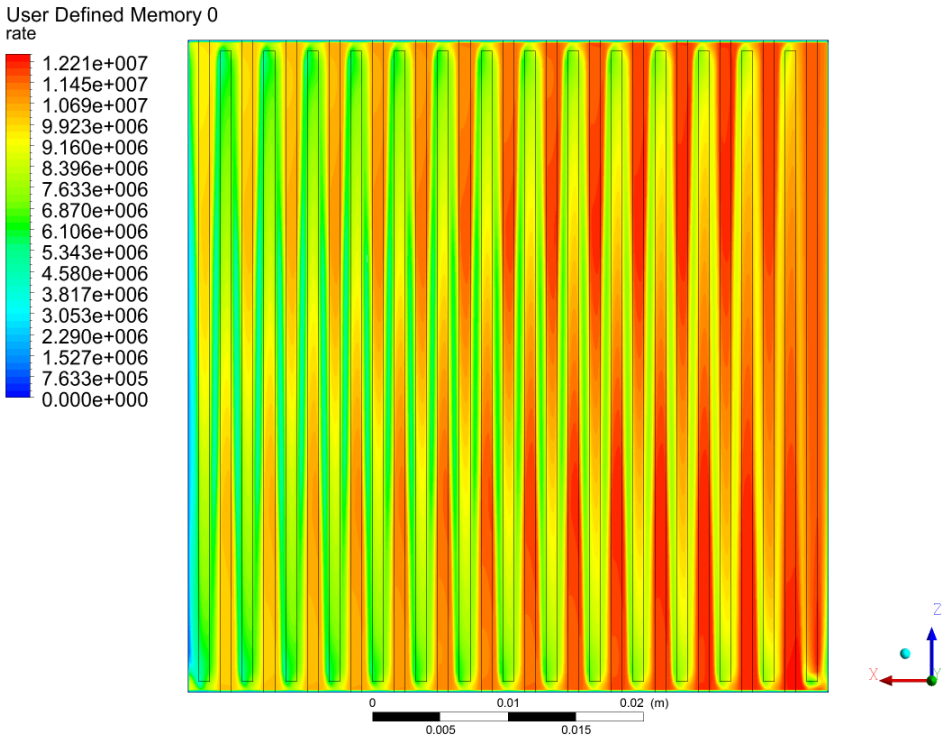

Fig. 3.6: Reaction rate on a plane at half the height of the electrode

A detail of the variation along the y direction of the reaction rate is shown in the next figure and it is visible how some zones, corresponding to the zones that are under the rib, experience a higher rate.

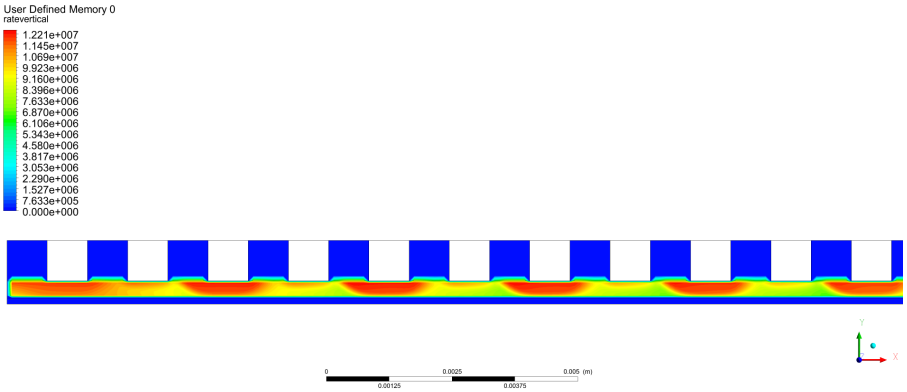

Fig. 3.7: Reaction rate on a XY plane at $Z = 5\ mm$ from the inlet

Since electrochemical quantities vary in such way one may ask how the fluid dynamic flow field is shaped in the porous medium and the answer is shown in figure 3.8. The quantity reported is the velocity in the porous medium on a plane at half of the height of the electrode. What is clear is that the fluid is very slow in the porous medium and the magnitude of velocity is not higher than 5 percent of the channel velocity and this gives values for the velocity in the order of $0.02\ m\ s^{-1}$. It has been calculated also the same variable on a XZ plane very close to the channel interface and the value of velocity did not reach 10 percent of the velocity in the channel. Another interesting fact is that there is higher velocity in certain zones of the domain that are under the rib. A better visualization

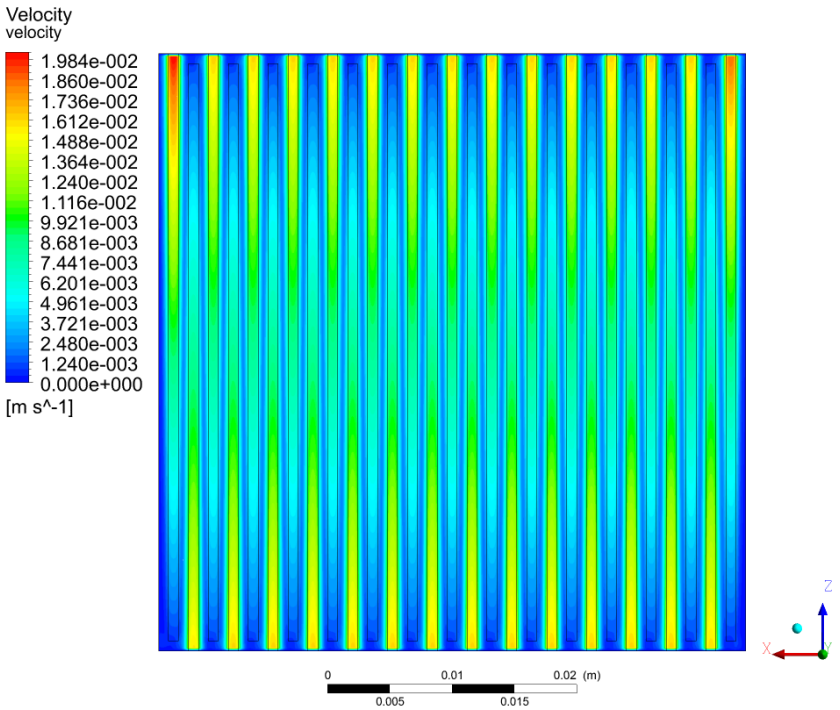

Fig. 3.8: Velocity distribution on a plane at half the height of the electrode

is done using 3.9, where the ratio of the local velocity to the velocity in the channel is proposed. The quantity is shown on three x-directed lines, the first line is in the higher part of figure 3.8 at a distance of $5\ mm$ from the inlet, the second is in the center of the cell, while the last is in the lower part of figure 3.8.

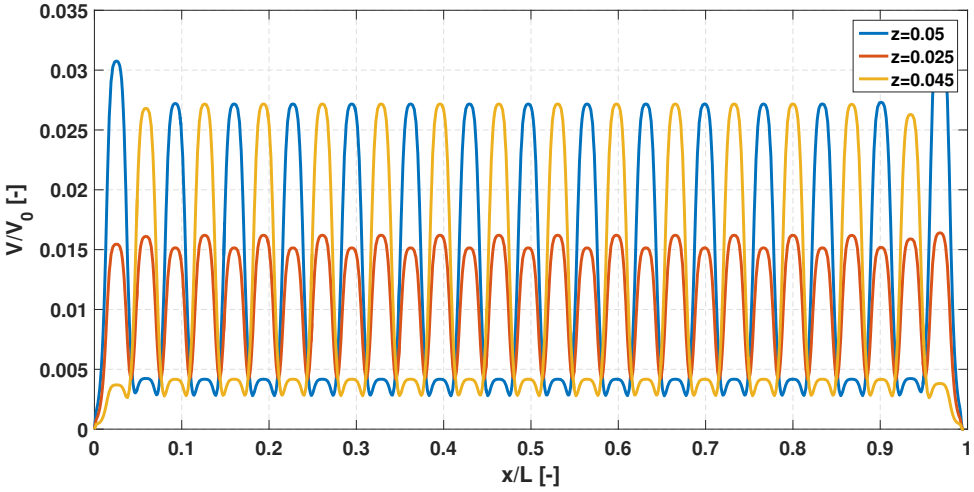

Fig. 3.9: Under the rib fluxes on a plane at half the height of the electrode

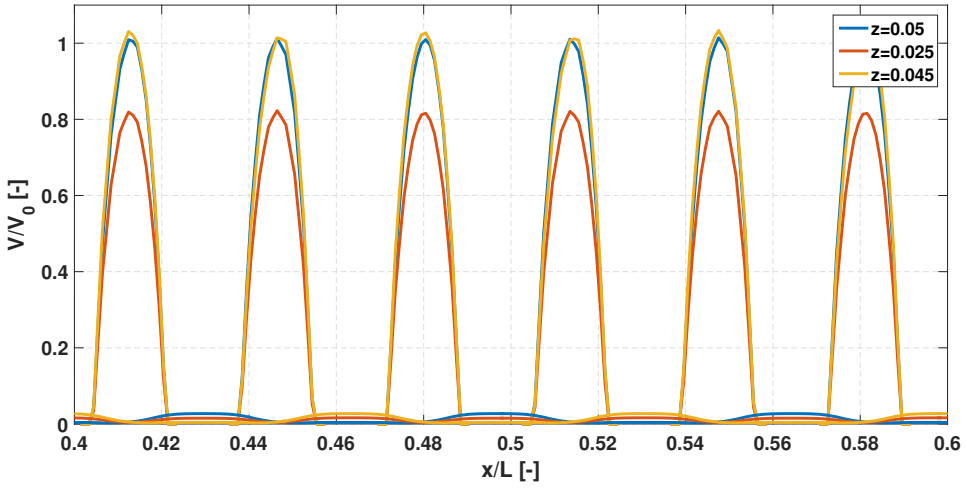

Fig. 3.10: Under the rib fluxes and channel elocity on a plane at half the height of the electrode

The entity of the scaled velocity is below 5 percent and its values are lower in the center of the cell (red curve) than in the initial and final part. Considering the phenomenon along the z-direction, due to the geometry of the cell the under the rib fluxes will be not in the same position along the x-direction and this is testified by the difference of the yellow and the blue line. What is more inlet and outlet influence the fluxes in a region close to them, as seen by the blue curve. This variability anyway is not peculiar of the porous electrode but also the channel velocity experiences such decrease in the central part of the cell, while

close to the curves the fluid accelerates as testified by figure 3.10. This figure compares the scaled velocity for a plane at mid height of the channel and one at mid height of the porous medium, the domain chosen is the central part of the cell in the x-direction. Under the rib fluxes are well known in the literature [16] and arise from the fact that the flow is forced to go through the minimum resistance path. Close to the curve part of fluid passes under the rib as the pressure drop associated to the electrode is much smaller than the pressure drop associated with the length of the channel and a curve. What happens is that the pressure drop in the porous electrode is mainly linear with velocity while the pressure drop in the channel and particularly in the curve is proved to scale quadratically with velocity. For a given flow rate and hence for a given velocity in the channel the entity of the pressure drop will depend effectively on the geometry of the channel and its length. For this reason fluxes under the rib will be influenced themselves by the channel's dimension and shape. The serpentine design has elevated velocity along the edges of the flow field, particularly over the lands where the high pressure drop of the switchbacks forces the electrolyte to jump over the lands and through the electrode material to reach the outlet. This can be seen also in figure 3.7 where the distribution of the reaction rate is concentrated in the zones mentioned. When the cell is operating in a lower state of charge, what happens is that some zones will be more influenced by mass transport problems as the concentration of the reactants might be an issue in the porous electrode, limiting the current generation process. A graphical interpretation of under the rib fluxes is present in 3.12. The role of these fluxes is very important as they bring fresh electrolyte under a zone, the rib, where the potential is fixed. These two conditions push the reaction rate to higher values and convert the vanadium with higher volumetric rate. Wide studies in the literature show their existence [16] although few studies examine their effective influence on the local current generation. According to the knowledge of the writer, not much effort has been done to couple locally the performance of the cell and its fluid dynamic behaviour and no cases in the literature analyze such trends. For this reason the graphs 3.11 and figures 3.9 and 3.10 represent a tiny innovation to the approach of this problem regarding flow batteries. In figures 3.11, reaction rate, state of charge and overpotential are shown on the left axis while on the right axis the scaled velocity is shown. The inlet is corresponding to x/L equal to zero and the outlet is one. From the beginning to the outlet of the cell state of charge decreases but in the zones where the velocity is higher also the state of charge increases. The reaction rate is higher for the under the rib zones but the overpotential has a lower absolute value. What happens in this zone is that the absolute value of the volumetric rate 5.6 is pushed to higher values not by the overpotential but by the higher concentration of reactants brought in this position by the under the rib flux from a fresh solution. The overpotential is a measure of the electrochemical loss in the battery: going from the inlet to the outlet the absolute value of η^* decreases as, since the state of charge of the battery is decreasing, the losses to convert reactants increase.

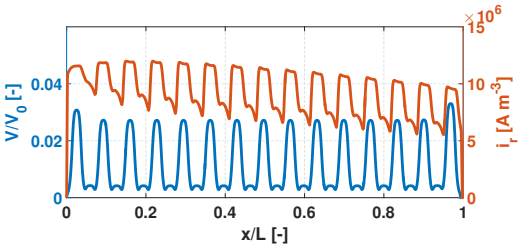

(a) Reaction rate on the right axis, scaled velocity on the left axis

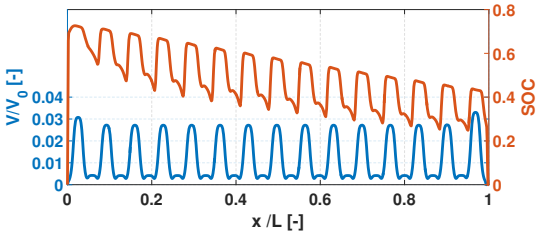

(b) State of charge on the right axis, scaled velocity on the left axis

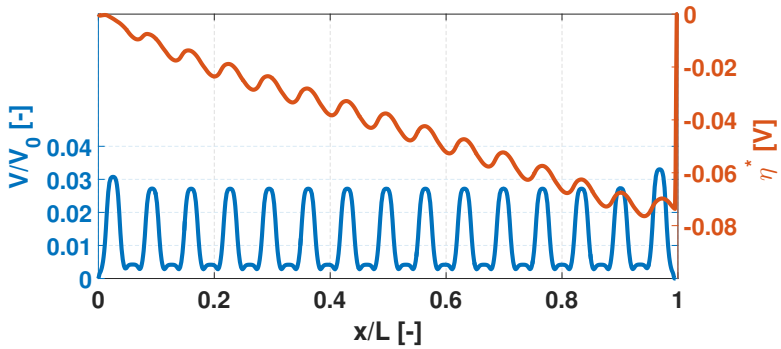

(c) Overpotential on the right axis, scaled velocity on the left axis

Fig. 3.11: Fluid dynamic and electrochemical quantities comparison

To end this analysis a visualization of the under the rib fluxes is reported along with the values for the reaction rate. The distribution of the two quantities is important according to what stated in this chapter to locally characterize the mass transport phenomena and the electrochemical performance.

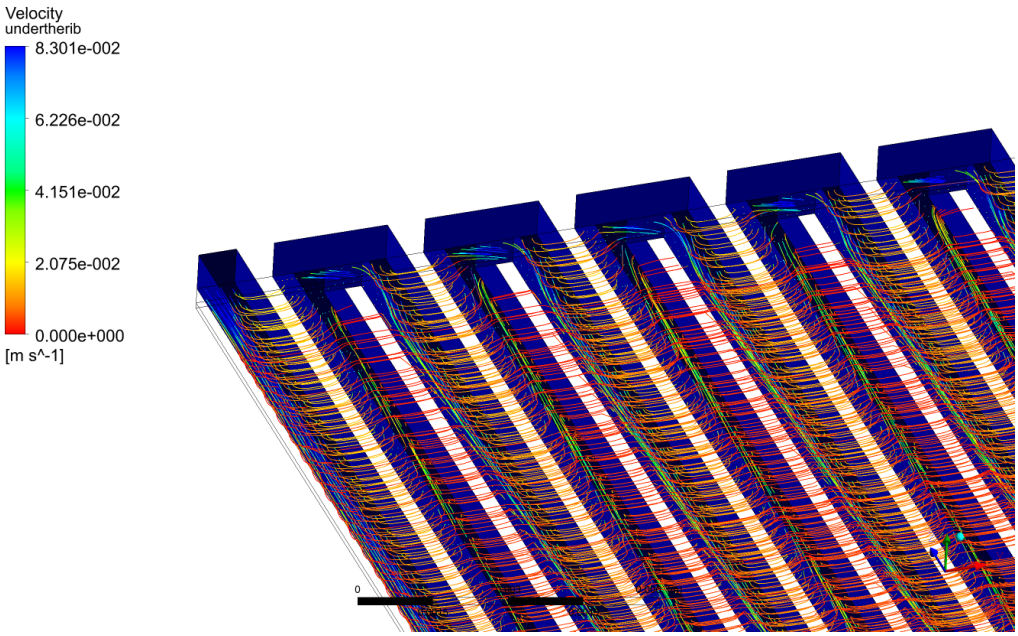

Fig. 3.12: Under the rib fluxes on the half-height plane for serpentine flow

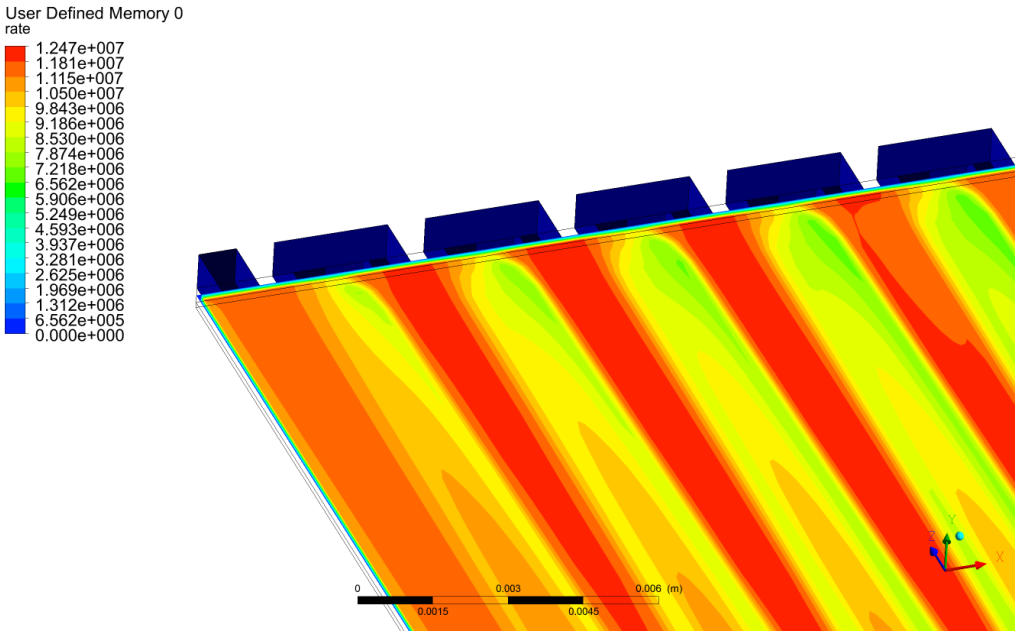

Fig. 3.13: Reaction rate on the half-height plane for serpentine flow

3.3.1 Sensitivity analysis

The results of the model are influenced by the choice of the phenomena to be modelled, the way in which them are modelled and the parameters used. If the first two are fixed in this part of the work, a sensitivity analysis is carried out to understand how much influence there is and which are the parameters whose effect is more marked. In the sensitivity analysis presented all parameters have been increased and decreased by 30 percent. It is useful to rewrite equation 2.19.

$$i_r = \frac{k_0 a F}{1 + \frac{r_p k_0}{D} \cdot \left(e^{\frac{\alpha F \eta^*}{RT}} + e^{-\frac{(1-\alpha) F \eta^*}{RT}} \right)} \left(c^b_{V^{4+}} \cdot e^{\frac{\alpha F \eta^*}{RT}} - c^b_{V^{5+}} \cdot e^{-\frac{(1-\alpha) F \eta^*}{RT}} \right) \left[\frac{A}{m^3} \right] \quad (3.12)$$

It is possible to quantify the impact of each parameter. Velocity of reaction has a limited impact on the performance of the battery at least in the range of variability analyzed: a possible interpretation may be the fact that increasing the speed of reaction the reactants are converted with more ease. On the other hand the reaction becomes more and more concentrated inside the pore, increasing locally the mass transport. Anyway this trend might be different out of the limits of the sensitivity analysis, the value of the velocity or reaction is stated in many articles about electrochemistry, though its value is not determined with high precision as it is influenced by the properties of the electrode and the nature chemical reactants themselves. Active area is a more straightforward parameter and changes the performance more linearly. Its influence is present both at low and high current densities, coherently with 5.6. Permeability's impact on the performance is reported and it is clear how, in order to see a more marked effect of the parameter, it has to vary more

than 30 percent. Nonetheless increasing permeability the effective movement of reactants in the porous medium is enhanced and this causes an improvement of the performance. The radius of the pore changes dramatically the performances at high current densities. Its influence has to be considered remembering that in this work the difference between bulk and surface concentration is determined by a diffusive resistance D/r_p. The mechanism through which reagents move from bulk to surface changes the generation term in a very heavy way and this is testified by the variability of the polarization curve with respect to a variation of the radius of the pore. In this work the effect of mass transport is modelled by a diffusive resistance between bulk and surface. When taking into account just diffusion a smaller pore implies a higher diffusive resistance and penalizes the performance and the same consideration can be done in the opposite way. In the study of porous media the value of the mean pore radius is very detailed and deals with techniques such as imaging or complex numerical simulations. This value is meant to be a mean dimension of the radius of the spheres that can approximate dimensions of pores. It is clear that assuming that just one number is able to model the mass transport in an eterogeneous medium such as an porous electrode is forced, anyway this techniques proves to be effective in introducing a loss for mass transport in the polarization curves. One has to remember that these parameters are affected by an intrinsic uncertainty and even if for some of them the order of magnitude might be known, their variability in their order of magnitude may affect the performance in a very heavy way. Other limitations are related to the infinite dilution model used and the fact that the anodic electrode is not modelled.

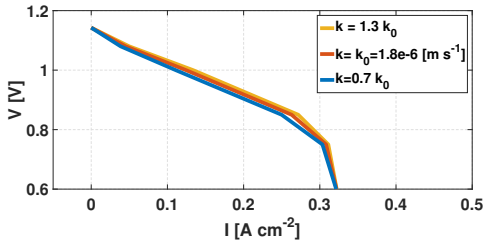

(a) Sensitivity to the velocity of reaction

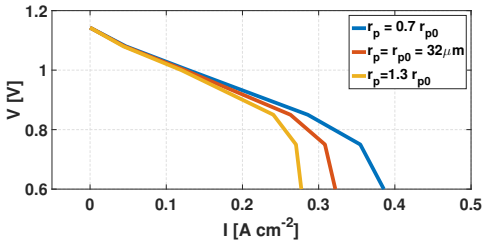

(b) Sensitivity to the pore radius

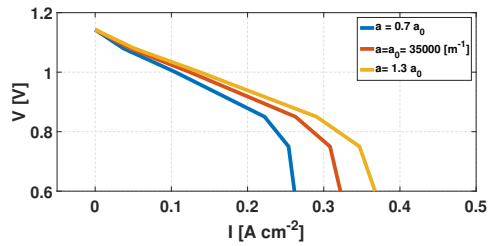

(c) Sensitivity to the active area

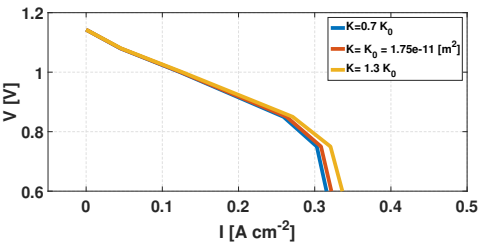

(d) Sensitivity to the permeability

Fig. 3.14: Sensitivity analysis

3.4 Comparison between triple and single serpentine

The model presented in this chapter is able to predict a difference between the single serpentine and the triple serpentine. Regarding the triple serpentine the area of the cell is kept at 25 cm^{-2} while the size of the channels in the case of triple serpentine is $L_c = 0.8\ mm$ while the rib size is kept to $L_{rib} = 0.7\ mm$. Meshing has been done also in this case using $GAMBIT$ and the spatial discretization was similar to the one used for the single serpentine. The numerical entity of the difference in current density was not exactly the same of the experimental values but it has to be kept in mind that parameters' influence is large. The triple serpentine is adopted as a modification of the single one and for a given flow rate the triple flow field has a velocity component in the channel which is lowered since its inlet area is larger. In the case examined the ratio of the inlet areas was approximately 2.6. The lower velocity component influences on one side the capability of the flow field of delivering reactants effectively to the porous medium and on the other side the pressure loss values of channels and curves. This flow field design has been proposed as a serpentine channel with lower pressure drop. Due to its nature two adjacent channels have more or less the same pressure level and therefore the "under the rib" mechanism is not enhanced. Other zones, where the three channels actually switchback, have a significant pressure difference with respect to the adjacent channel. In figures it is shown the trend of the local velocity in the porous medium. Both figures have the same limits that are zero and show differences: the single serpentine has higher velocity components and the number of spots interested by the under the rib fluxes is much higher than in the case of triple serpentine. The modified flow field has just 9 spots interested by heavy under the rib fluxes whose magnitude anyway is lower than the single serpentine one. These two phenomena combine and the performance of the single serpentine is proved to be higher both numerically and experimentally.

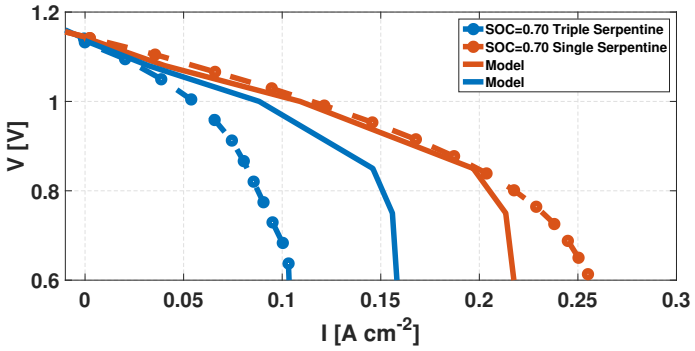

Fig. 3.15: Comparison of the performance of single and triple serpentine for a flow rate of $10\ mL\ min^{-1}$

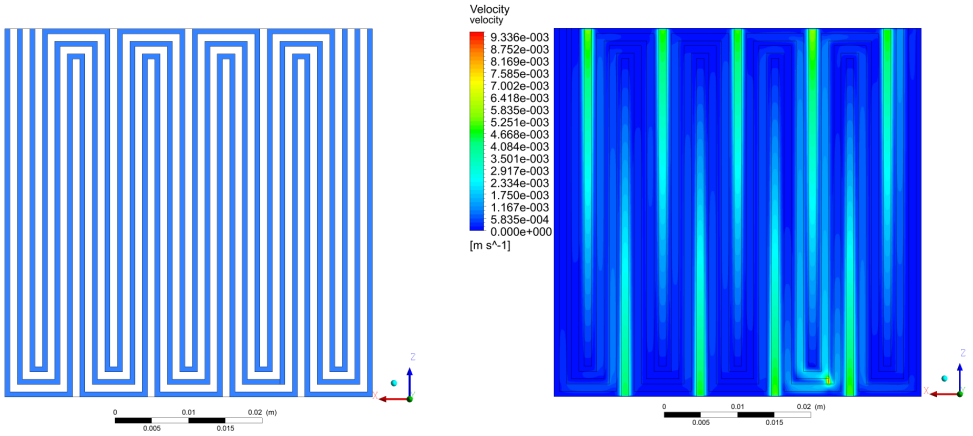

(a) Geometry triple

(b) Velocity components in porous medium

Fig. 3.16: Triple serpentine

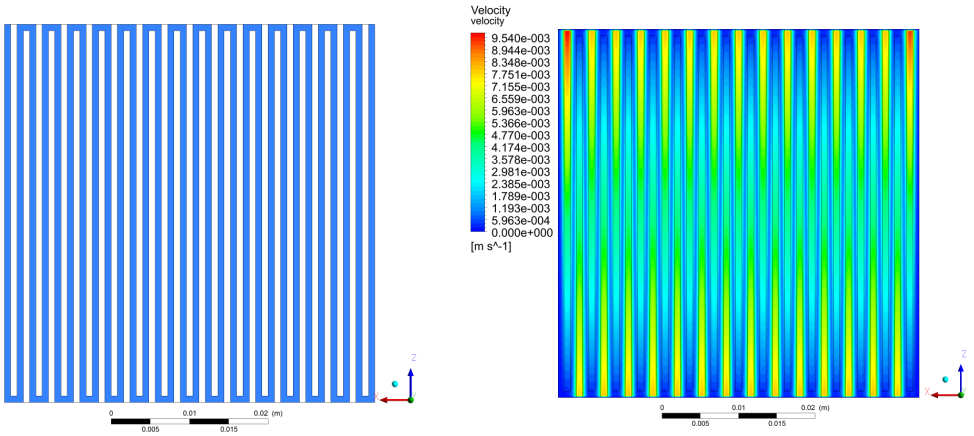

(a) Geometry of the single serpentine

(b) Velocity components in porous medium

Fig. 3.17: Single serpentine

3.5 Grid convergence study

In order to evaluate the validity of the spatial discretization chosen and determine the independence of the solution from it, a grid independence study has been performed. A non accurate spatial discretization may worsen the quality of the numerical solution and give wrong results. In figure 3.18 one can see the accuracy of the mesh used in this

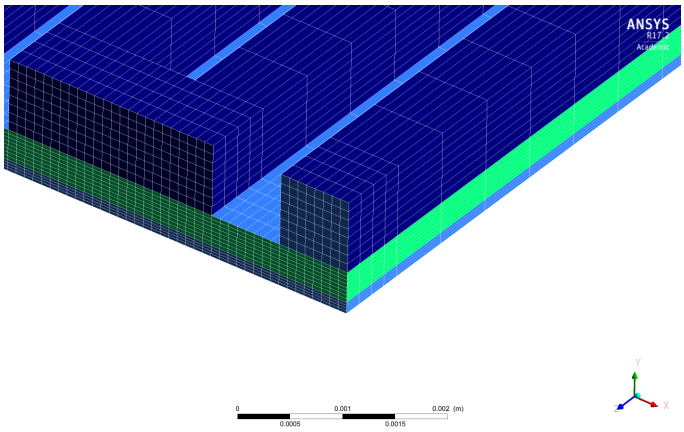

Fig. 3.18: Detail of the mesh

work. Close to the switchbacks the accuracy increases while in the middle of the cell, where velocity gradients and electrochemical quantities are expected to vary less, the mesh is a bit coarser. To perform the mesh independence study two additional meshes are built coarsening or refining the spatial discretization in every direction by a factor of 2. Respectively meshes consisted of around 149000, 630000 and 4154000 cells. The operating condition simulated is $V = 0.75\ V$ with a nominal flow rate of $20\ mL\ min^{-1}$. This choice is done as in this condition large values of current occur and it is of interest for the operation of the battery. The following variables are chosen:

- Volume integral of the reaction rate in the electrode domain,
- Pressure drop of the cell computed as the difference between pressure at the inlet and at the outlet,
- Average value of the overpotential in the electrode domain.

it is possible to state that the chosen meshes are in an asymptotic area of the graph and therefore the solution guarantees a small error with respect to the ideal exact solution. In order to get a measure of this error the calculation of the *Grid Convergence Index* has been performed according to the procedure explained in [11]. Calculations for pressure, current and overpotential are reported.

$$GCI_{12} = \frac{F_s \left| \frac{f_2 - f_1}{f_2} \right|}{r^p - 1} \tag{3.13}$$

$$GCI_{23} = \frac{F_s \left| \frac{f_3 - f_2}{f_3} \right|}{r^p - 1} \tag{3.14}$$

$$p = \frac{ln \frac{f_3 - f_2}{f_2 - f_1}}{ln(r)} \tag{3.15}$$

Numeric indexes 1,2,3 stand for coarse, base case and fine respectively, r is the refinement ratio, f are the values for the considered quantity and F_s is the security factor chosen to be 1.25. The main results of this analysis are reported and the the errors are low which is an index of the fact that solution is mesh independent. The exact value, given by an extremely fine mesh can be extrapolated using 3.16.

$$f^* = f_2 + \frac{(f_3 - f_2) r^p}{r^p - 1} \tag{3.16}$$

Quantity	Exact theoretical value	GCI23
Pressure drop [Pa]	84787	0.4 (0.002%)
Current [A]	6.966	0.01 (0.1 %)
Overpotential [V]	-0.0682	0.00054 (0.79 %)

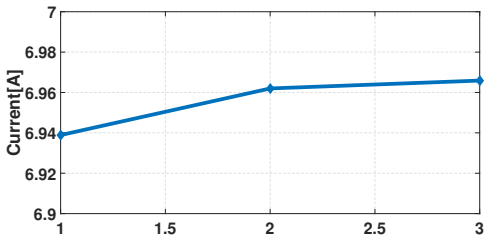

(a) Variation of the volume integral of the current in the electrode

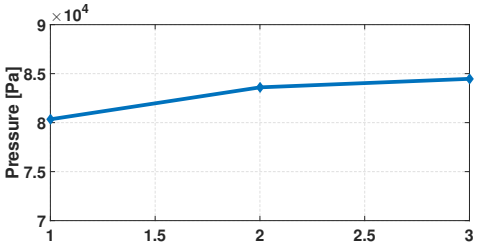

(b) Variation of the values of the pressure drop of the cell

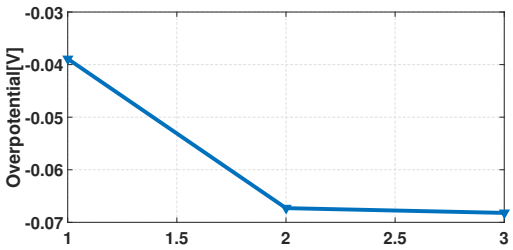

Fig. 3.20: Variation of the values of the average of the overpotential in the electrode

4 Influence of flow field design

In this chapter several geometries are analyzed using a threedimensional model with a "$Sigracet\ GDL\ 10\ AA$" electrode. A sensitivity analysis is performed for the serpentine flow field considering both the pressure loss and the performance changing the number of the channels. The parallel flow field is also presented. The model results are compared with the data of the literature and experimentals in order to understand up to which point the forecast is reliable. The model is used as a tool for the design of a novel component and as a measure of the performance of the flow fields that will be tested in the experimental campaign in chapter 5. To end the numerical part of this work a comparative analysis is presented along with a critical approach.

4.1 Sensitivity of serpentine geometry

The influence of the position of the inlet with respect to the outlet has been analyzed and the main result is that the most efficient configuration is placing inlet and outlet on two opposite vertexes of the cell. This basically fixes the pressure values in the two points and will drive the pressure gradient to cross diagonally the cell. If inlet and outlet would be on the same side the pressure gradient would be maximum across that side and the some fluid may be influenced by this fact. The area close to the side of inlet and outlet might experience a different situation with respect to the other. For this reason the simulations presented in this chapter have the inlet and the outlet placed oppositely even though the numerical entity of the change is small. At this point it is interesting to understand how geometrical parameters may change the performance of a cell for a given flow rate as it is a measure of the phenomena of mass transport in the cell. The geometric characterization of the serpentine flow field is done using two parameters: the number of digits and the ratio between the channel side and the rib. In this work the effect of the dimension of the channel is taken into account while the ratio between channel side and rib is kept to one. Having decided the squared shape of the flow field and the ratio of channel and rib all geometrical parameters of the flow field can be written as a function of the channel side dimension. This enabled the development of a script that in the software $GAMBIT$ semi-automatically changed the geometries. Particularly for the serpentine number the digits has to be an odd number and the analysis has been performed using the configuration reported in the following table.

Number of Digits	31	29	27	25	23	21	19	17	15
Channel size [mm]	0.82	0.88	0.94	1.02	1.11	1.22	1.35	1.52	1.72

Tab. 4.1: Geometrical parameters for the sensitivity analysis

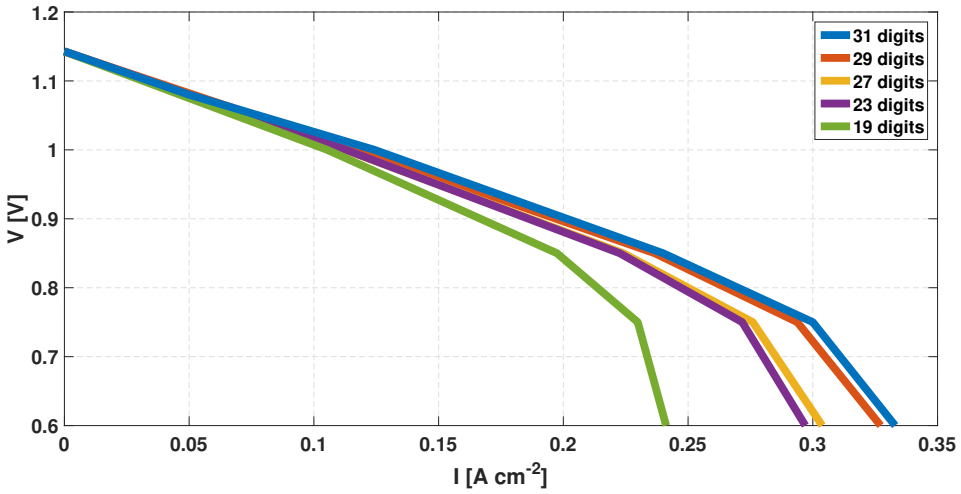

Fig. 4.1: Sensitivity for the channel geometry with a flow rate of $20\ ml\ min^{-1}$

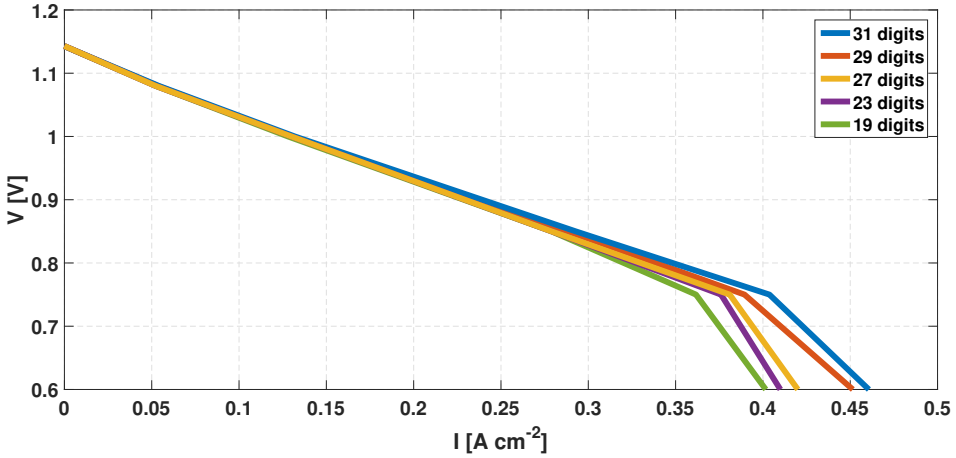

Fig. 4.2: Sensitivity for the channel geometry with a flow rate of $60\ ml\ min^{-1}$

From the analysis of the polarization curves it is possible to see that the influence of the channel is marked at high current while its influence decreases as the current decreases, as expected. The trend presented is monotonic with respect to the dimension of the channel: the bigger the channel the lower the performance. This is mainly related to two facts: the first is that comparing different channel sizes at the same flow rate means comparing different velocities in the channel; the second fact is that the higher the number of digits the higher the number of switchbacks and hence the higher the under the rib

fluxes. Different velocities will give rise to different pressure drop distributions and this is clearly influencing the performance according to the analysis in chapter 3. What is more, the same analysis has been performed for a higher flow rate. Feeding more solution to the cell improves its performance, therefore all curves move to the right in the current density-voltage plane, the differences among the flow fields consequently become smoother and smoother giving rise to a lower variability of the performance. This is caused by the larger amount of reactants fed to the cell, the mass transport problems is less limiting and its influence is more marked when one goes under $0.6V$, an area not analyzed in this work. For these system the capability to work with the flow rate which is variable is actually another degree of freedom that enlarges the flexibility of this system. The increase of the flow rate, on the other side, increases the pressure loss introduced by the cell as shown by figure 4.3.

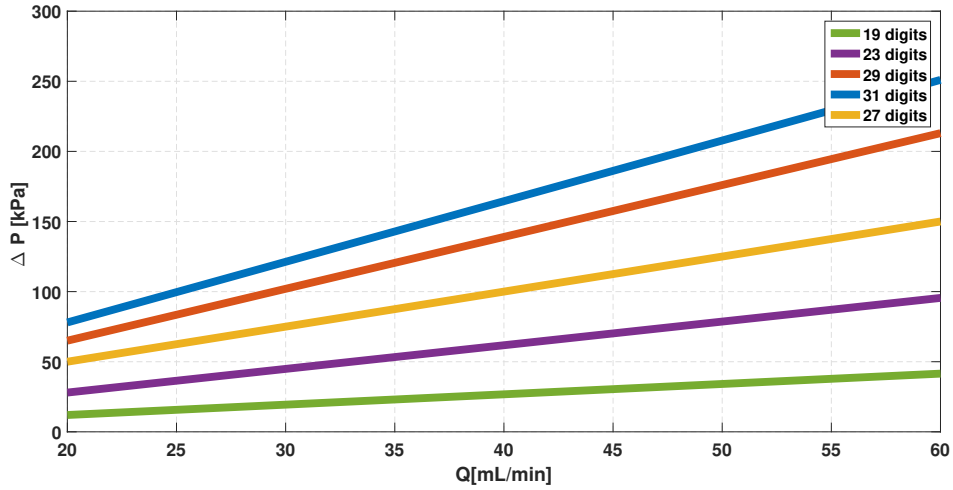

Fig. 4.3: Pressure drop across the cell for the serpentine flow field

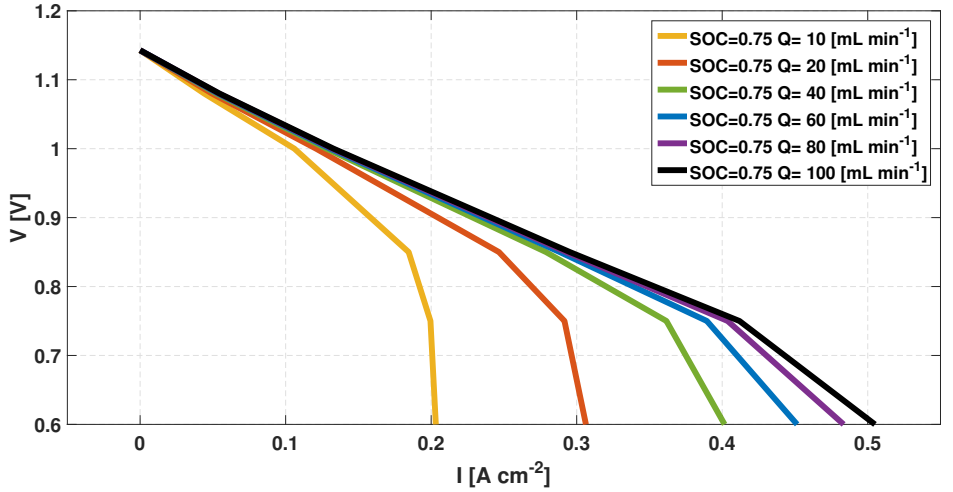

Fig. 4.4: Effect on the flow rate on the performance of a serpentine channel with 25 digits.

In the cases examined the pressure losses are in the order of tens of kPa for the $20\ ml\ min^{-1}$ case and in the order of hundreds for the $60\ ml\ min^{-1}$, considering the cell is just $25\ cm^{-2}$ one can say that the pressure drop is marked for the high flow rate. The variability of the pressure drop with the channel size is more marked at high flow rate. The effect of this aspect will be fully analyzed in the end of this chapter along with its impact on the energy efficiency of the system. As a last result of this analysis, it is presented in figure 4.4 the characteristic of the serpentine that will be analyzed in chapter 5 and that has been tested in *MRT Fuel Cell Lab*. Both channel and rib dimension are set to $1\ mm$ giving a cell with 25 digits.

In an area with low current density (below $0.1 A cm^{-2}$), the difference in the performance caused by the change in the flow rate is very small. In this area, called kinetic, the working condition is dominated by the kinetic of the reaction and mass transport problems are not present. Working with a low operating current means working with large excess of reactants from the chemical point of view. When the reactants distribution becomes important, at high current densities, the flow rate influences the performances and the higher the flow rate the higher the performance. Considering what stated in the previous chapter, the influence of the flow rate changes the pressure and velocity distribution of the whole cell. Some major trends can be identified:

- The higher the flow rate the higher the pressure drop associated to the channels and the curves, therefore the higher the under the rib mechanism.
- The improvement of the performance of the machine is decreasing while flow rates are reaching high values.
- Considering the same current density, the lower the flow rate the higher variation of SOC between the inlet and the outlet and therefore the higher the area of the cell working in limiting conditions.

The influence of the flow rate is an important phenomenon to be fully understood and its control may change the performance of a real system and its capability to operate in accordance to the need of the load. On the other side, the possibility to change the flow rate and hence the characteristic curve of the machine is a tool during the phase of the system design and extents the field of operation for these machines, being actively an additional degree of freedom.

4.2 Parallel geometry

Since the pressure drop introduced by the serpentine channel is high, several authors proposed the use of a parallel geometry like shown in figure 4.5. This geometry is proposed in several studies about fuel cells and flow batteries.

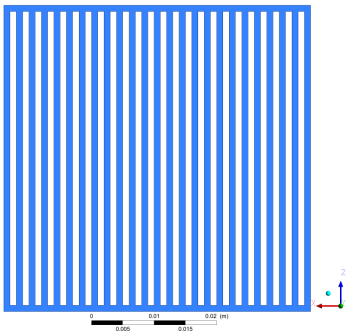

Fig. 4.5: Parallel flow field

The inlet and the outlet are connected by a number of digits placed perpendicularly with respect to the feeding channel. Due to this configuration the pressure drop is expected to be significantly lower than the serpentine's one. In this work it has not been analyzed for this geometry the effect of channel size and rib dimension. A case with a squared channel is presented with a rib dimension of $1mm$ and a channel to rib ratio of one. The number of channels is therefore 25.

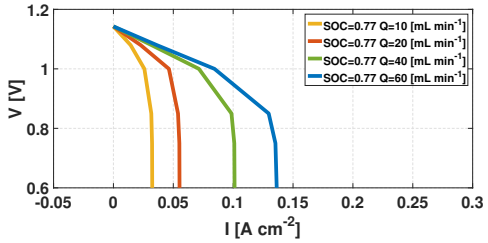

(a) Parallel flow field performance

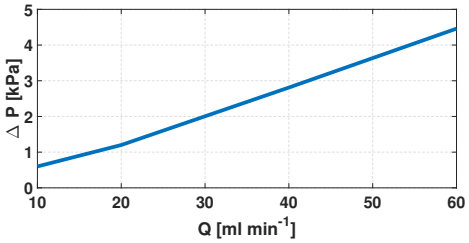

(b) Pressure drop for parallel flow field

Figures 4.6a and 4.6b show how this flow field is able to minimize the pressure drop but it is not able to guarantee a proper distribution of reactants inside the porous medium. The shape of the polarization curve is peculiar: it is possible to identify a sudden drop in the voltage at a certain value of current and this is typical of situations in which the mass transport phenomena are a limiting factor. An observation can be done on the velocity components in the channels: since they are in parallel the fluid will divide in all channels giving a much lower velocity component in each channel. In order to have a first approximation of the value of the velocity one may say that it is equal to:

$$V_{ch} = \frac{V_0 A_{in}}{N_{ch} A_{ch}} \qquad \left[\frac{m}{s}\right] \tag{4.1}$$

This equation gives a very rough estimation of the velocity as it does not take into account the porous medium presence and it has to be treated as a upper limit for the value of the velocity. Threedimensional effects take place and enhance the flow in the first and in the last digits as testified by the figure 4.7a where the ratio between the velocity in the central

point of the channel and the velocity giving the flow rate is reported. One may notice how this behaviour is very marked close to the inlet which is placed on the left. The comparison of the velocity both in the channel and in the porous medium is performed and reported. The channel velocity is much lower than V_0 but, the central digits have a lower velocity than the ones on the edges; the horizontal line is the measure ideal velocity calculated according to 4.1. The under the rib fluxes (in figure 4.7b) experience the influence of the inlet and this is visible on the blue line, while the outlet changes the shape of the yellow line. The channel velocity does not change moving along the channel in the z-direction while the flow in the porous medium is influenced by the presence of the outlet.

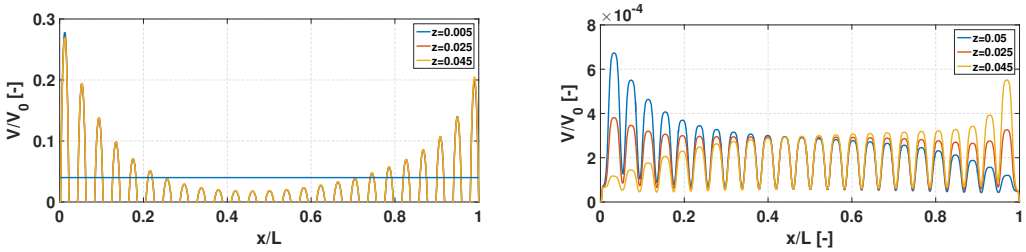

(a) Velocity in the channels **(b)** Velocity in porous medium

Fig. 4.7: Velocity field for parallel geometry

The velocity in the porous medium is shown on the contour in 4.8 and in order to appreciate a variability the color scale has to be set to a value that cuts the velocity values close to the inlet as its influence on the flow field in the porous medium is very present.

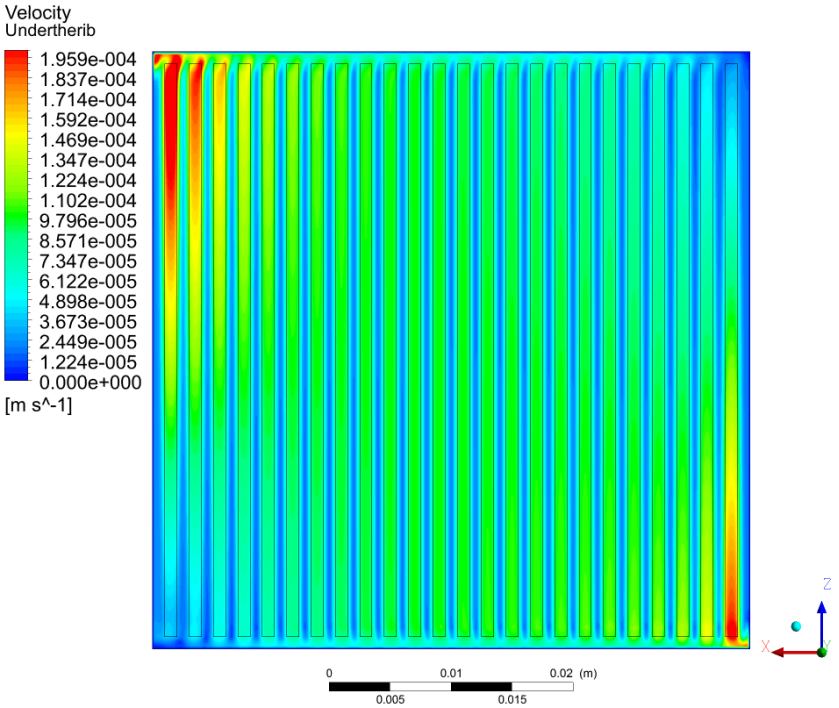

Fig. 4.8: Velocity on a plane at half height of porous medium

Figure 4.9 shows the trend of SOC, reaction rate and overpotential on horizontal lines at the middle height of the porous medium at a distance of $5\ mm$ from the inlet. Their behaviour is shown in relation with the velocity values in the porous medium. The situation of this flow field is different from many point of views from what is said for the serpentine one. The state of charge does not vary with respect to the x-direction while it happens with the serpentine flow field. The values of this quantity are anyway much lower than in case of the other flow field and this is a measure of how the reactants are not able to move through the electrode. Where the velocity values are higher the local state of charge increases but it is enough to give enough reactants to the electrochemical reaction in all the domain: the reaction rate trend has spots in which it is null. The values of overpotential are everywhere one order of magnitude larger than in case of the serpentine flow field and this is a measure of how the problems of mass transport generate an electrochemical loss. This analysis' aim is to give quantitative insights on how a mass transfer limiting situation can be quantified using local variables. The parallel flow field will not be used in the test facility due to its low performance. This is in line with the result got experimentally by [9] and for this reason the model seems to perform in a reasonable way.

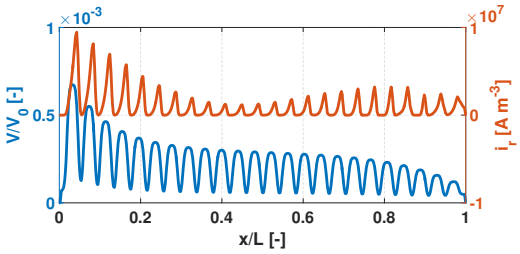

(a) Reaction rate on the right axis, scaled velocity on the left axis

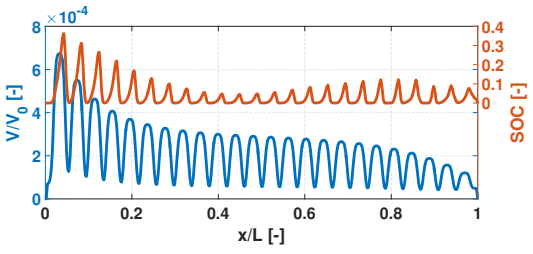

(b) State of charge on the right axis, scaled velocity on the left axis

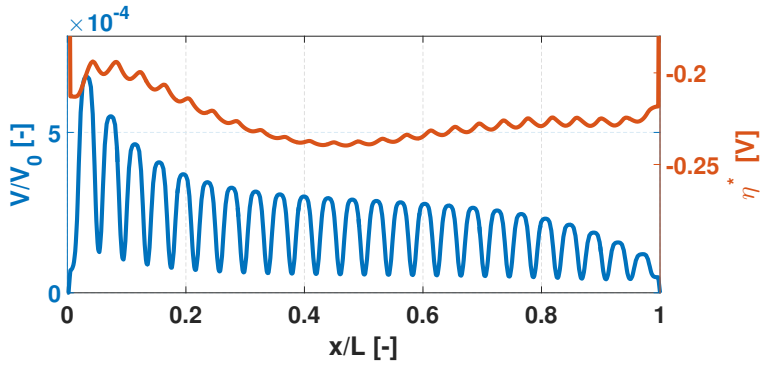

(c) Overpotential on the right axis, scaled velocity on the left axis

Fig. 4.9: Fluid dynamic and electrochemical quantities comparison on a line at $5\ mm$ from the inlet at half height of the porous medium

4.3 Interdigitated geometry

The analysis of the interdigitated geometry is important as it is proposed in the literature as an innovative component for vanadium redox flow batteries several studies focus on its properties [13] [9], [37]. The configuration is different from the others as there are two sides of the flow field as one can see from figure 4.10. The main characteristic of this flow field is that all the fluid is forced to pass under the rib to reach the outlet. For this reason some channels will deliver the solution to the electrode and others will take the reacted solution to the outlet. The first will be called feeding channels while the others will be called discharge ones. In the field of fuel cells this geometry is not likely to be used as, in case of gaseous reactants, the pressure drop caused by this flow field is higher than the one of the serpentine. The situation in case of liquid reactants is not the same and simulations are performed in this chapter to clarify this aspect. Regarding the geometrical configuration, a first channel is used as a distributor for the solution to effectively move in the channels. In order to evaluate the performance of this geometry with respect to the channel dimension a sensitivity analysis is presented similarly to what has been done for the single serpentine flow field. In this case the flow field has an even number of digits and the sensitivity analysis is performed according to the following dimensions:

Number of Digits	30	28	26	24	22	18	14
Channel size [mm]	0.85	0.91	0.098	1.06	1.16	1.43	1.85

Tab. 4.2: Geometric parameters

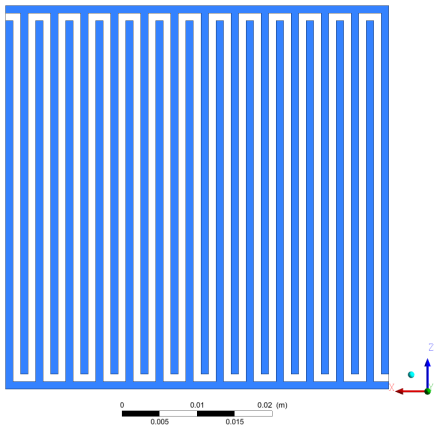

Fig. 4.10: Geometry for the 26 digits interdigitated flow field

The comparison of polarization curves with a flow rate of $20\ mL\ min^{-1}$ and $60\ mL\ min^{-1}$ are performed and it is reported the case for low flow rate.

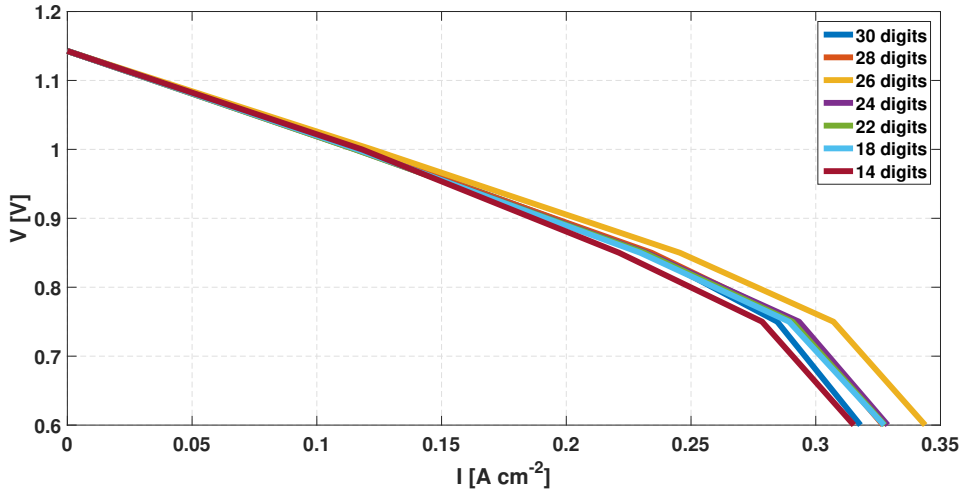

Fig. 4.11: Sensitivity analysis for the channel size for a flow rate of $20\ mL\ min^{-1}$

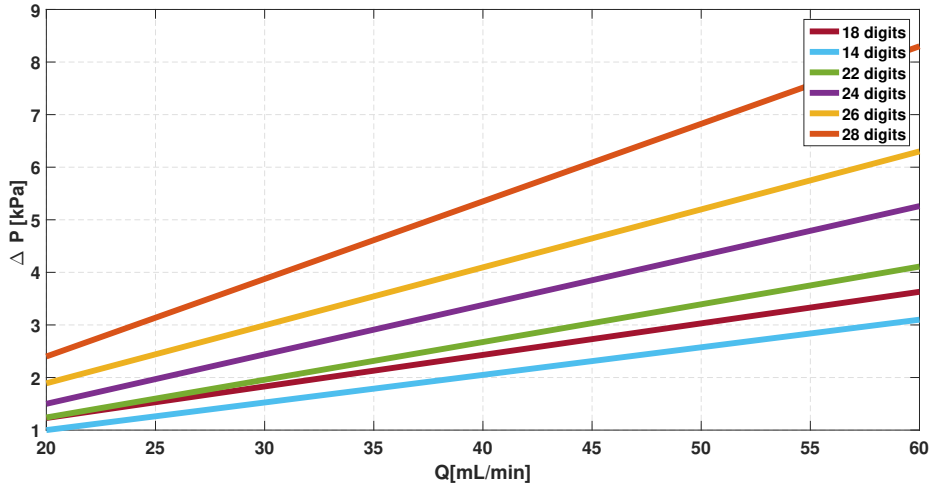

Fig. 4.12: Pressure drop of the interdigitated flow field

At low flow rate the differences in the performance are more marked than when considered at high flow rate. Contrarily to what happened for the serpentine, in this case there is a number of digits that maximizes the performance and it is found to be 13, corresponding to a channel size of $0.98\ mm$. At high flow rate the situation is basically the same and the same optimum is found, the graph is not reported but essentially the same conclusion of the low flow rate analysis can be considered. The reason why the trend is not monotonic has been investigated and it is found out that the different cells behave in a different way due to the different flow distribution. What is observed is that an uneven distribution of velocity among the digits occurs when they are too small. The central digits experience a much lower velocity than the ones close to the cell's edges. The pressure drop associated with the central digits is proved to be higher than the one of the extreme ones due to the existence of harsh curves that the fluid has to do. The lower the number of digits the

higher the uniformity of the velocity between them. The overall pressure drop associated to this flow field is much lower than the serpentine one as it is shown in 4.12, this is an interesting feature of this flow field that will be fully analyzed in a comparative study. This results are coherent with [13]. In order to confirm the results of this chapter a flow field with 26 digits is chosen giving a channel side dimension of $1\ mm$; this geometry is realized and tested in the experimental facility in $MRT\ Fuel\ Cell\ Lab$. Coherently with what presented in this work so far trends of the major quantities are reported to enlighten the main characteristics of this flow field. The condition chosen has a flow rate of $20\ ml\ min^{-1}$, the state of charge is 0.77 and the voltage is $V\ =\ 0.75\ V$, that results in a current density slightly higher than $0.3\ A\ cm^{-2}$. The plane on which the quantities are shown is an XZ plane at mid height of the porous electrode. The state of charge of the battery is proved to have a smooth variation along the z-direction and this is due to the fact that the channels effectively bring fresh solution along the whole length of the cell. A significant variation is present in the x-direction and particularly some zones in the center of the cell experience a very low state of charge. An important insight is also given by the contour of the state of charge on a XY plane at $5\ mm$ from the inlet. The state of charge changes heavily from a zone under the feeding channels, in which it is maximum, to a zone under the channel bringing the electrolyte to the outlet. In this zone the state of charge is proven to be very low as the solution has already reacted in the porous medium. The link between state of

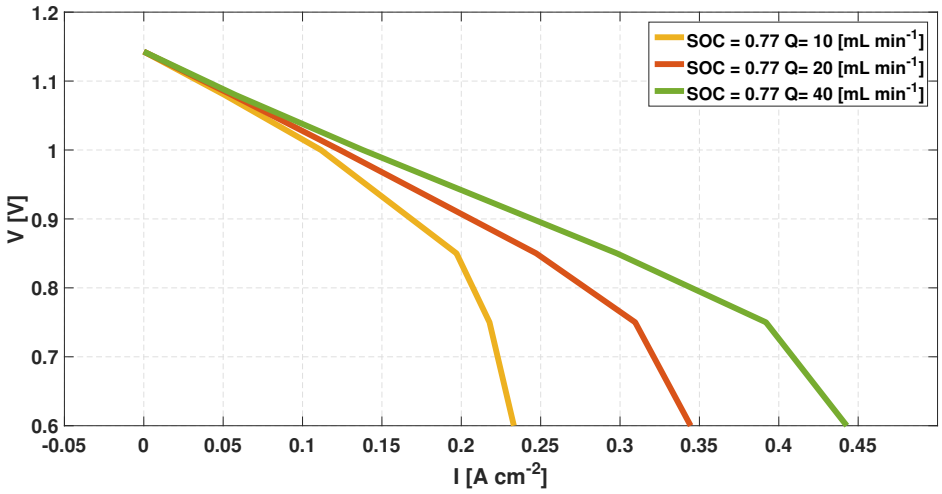

Fig. 4.13: Performance of the interdigitated flow field

charge and electrochemical rate is done at first using this contours and the two trends are actually coherent to the consideration stated. When showing rate with the same scale of the serpentine in figure 3.6, one notices how the values of the reaction rate are much higher than the other flow field's one and this is testified by the higher number of red spots. The higher reaction rate is under the feeding channels, or better, immediately under the rib close these channels,while it is lower under the discharge channels.

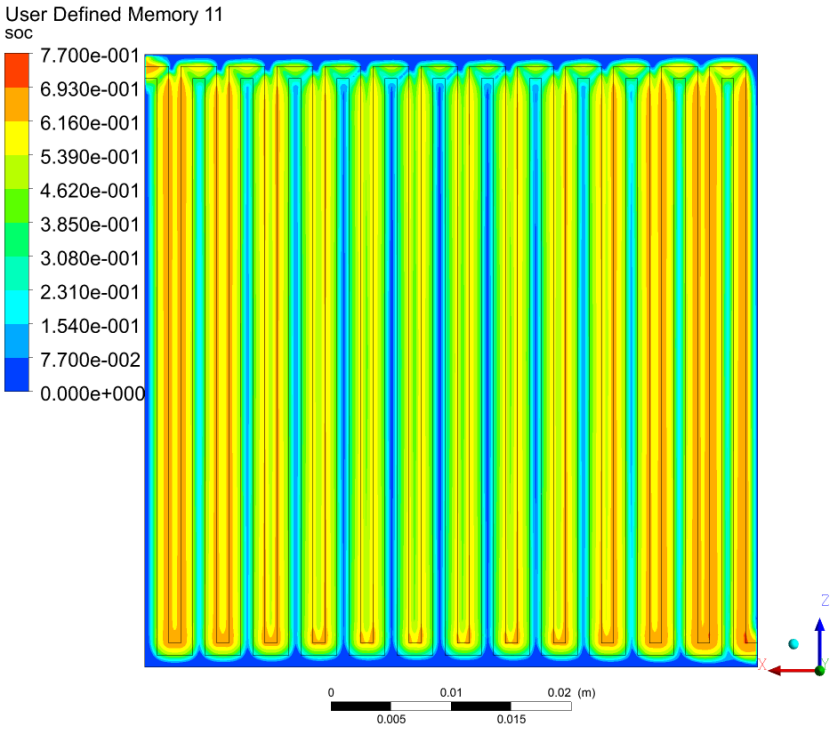

Fig. 4.14: State of charge for the half height plane for the interdigitated flow field

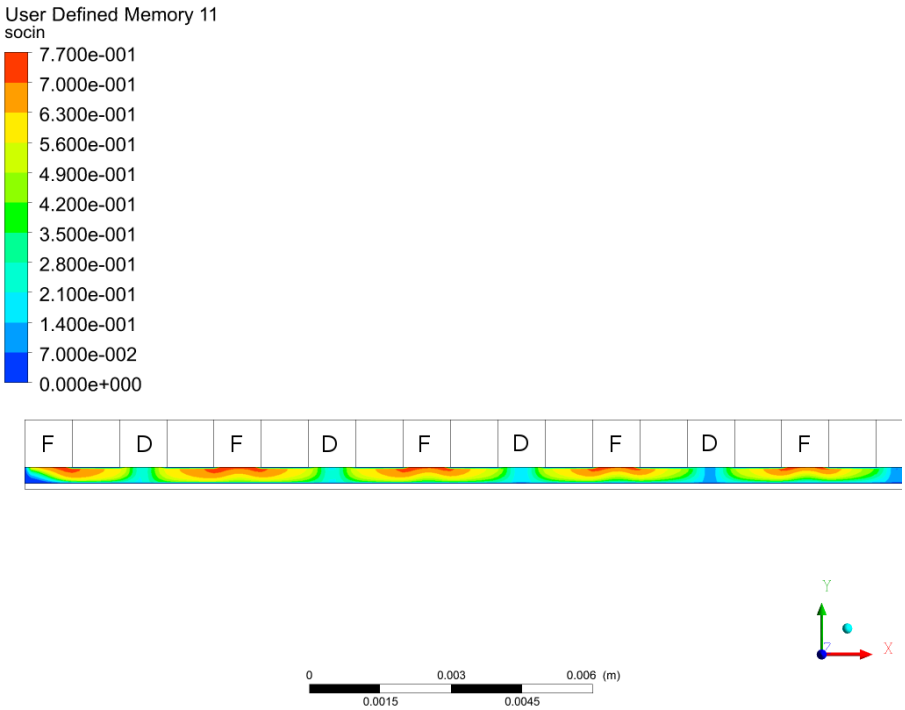

Fig. 4.15: State of charge on a XY plane at $5\ mm$ from the inlet (F stands for feeding, D for discharge)

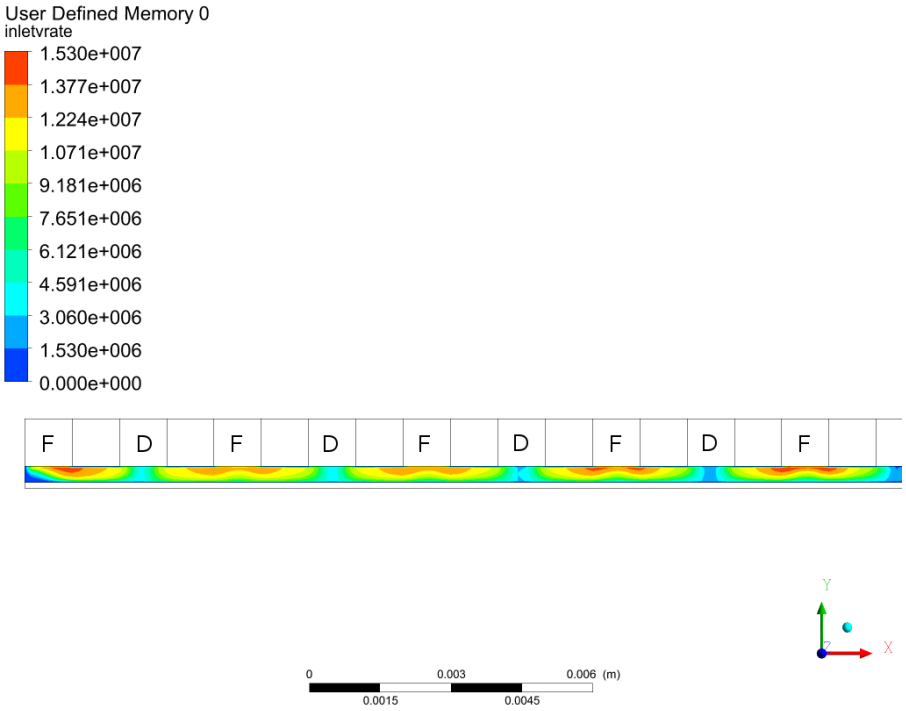

Fig. 4.16: Reaction rate on a XY plane at 5 mm from the inlet (F stands for feeding, D for discharge)

As one may notice from figure 4.14, the interdigitated flow field is able to deliver the solution to the porous medium with more or less the same state of charge of the inlet and this is able to push the kinetic of the reaction towards higher values. On the other side the trends of velocity in the channels reveal a sort of uneven distribution as it is possible to see from figure 4.18 and the central digits experience a flow with lower velocity component.

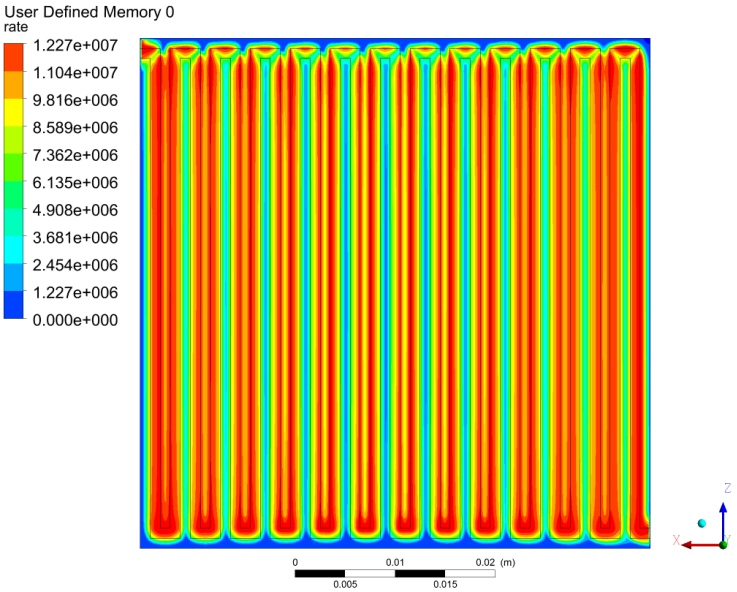

Fig. 4.17: Reaction rate on the half height plane for the interdigitated flow field

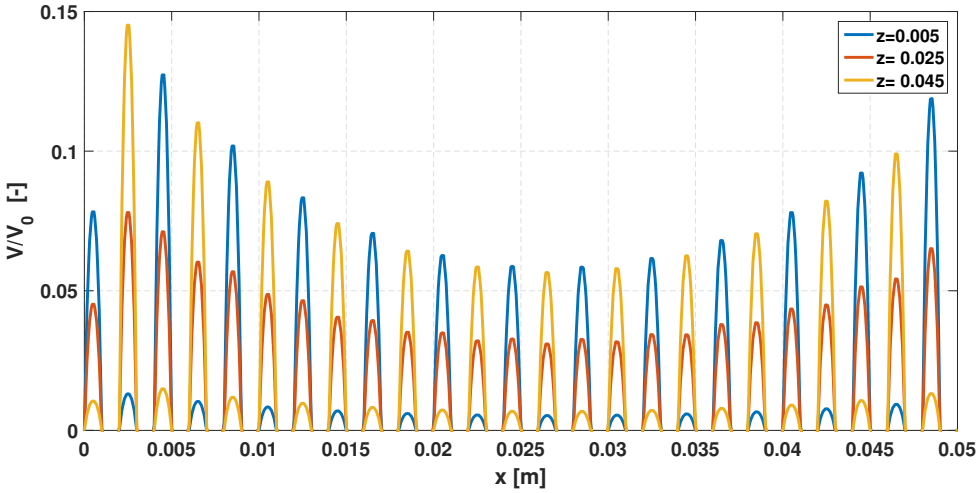

Fig. 4.18: Scaled velocity at the center of the channel for interdigitated flow field

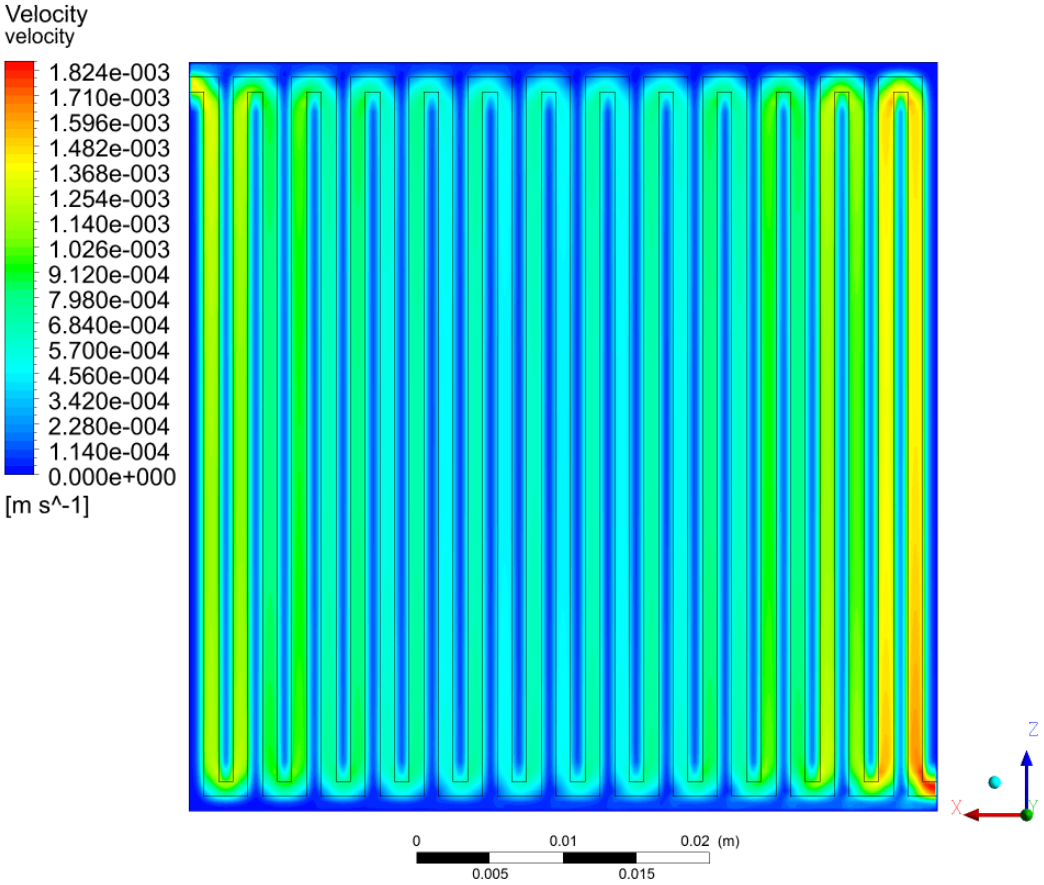

Fig. 4.19: Velocity components in porous medium on a plane at half height for the interdigitated flow field

Close to the inlet,represented on the left of figure 4.18 and in the higher left corner for figure 4.19, just the feeding channels will have a significant velocity component while

the others will not have it. Close to the outlet the situation reverses and the the trend of the blue and yellow line resemble the change in the flow path. In the middle of the cell both feeding and discharge channels will experience the same velocity component. The central digits do not receive a high flow rate from the distribution channel. The mechanism through which reactants move from channel to channel is forced to be under the rib. The shape of the under the rib fluxes testifies how they are distributed between the feeding and the discharge channels. What is more the central part of the machine has considerably lower velocity components, coherently to what visible in 4.18 in which the velocity of the channels is reported. The relation between the fluid dynamic condition and the electrochemical quantities is shown for a x-directed line at half height of the porous electrode, coherently with what has been performed for the parallel and serpentine flow field. The shape of the reaction rate and the state of charge resembles the velocity distribution: the lower peaks of reaction rate and state of charge are related to the zones under the discharge channels, that have a low velocity component.The value of the state of charge of the solution in this zone is very low. Both curves present a small V-shaped zone where the reaction rate is significantly lower than in the immediate nearby. This is corresponding to the zone under the feeding channels, where the concentration of reactants decreases due to the reaction occurred in the space between the channel and the plane on which the quantities are shown. Overpotential values are smaller in absolute value where the fluxes under the rib effectively bring the solution to the active sites expressing that the increase of concentration lowers the electrochemical loss. As a last

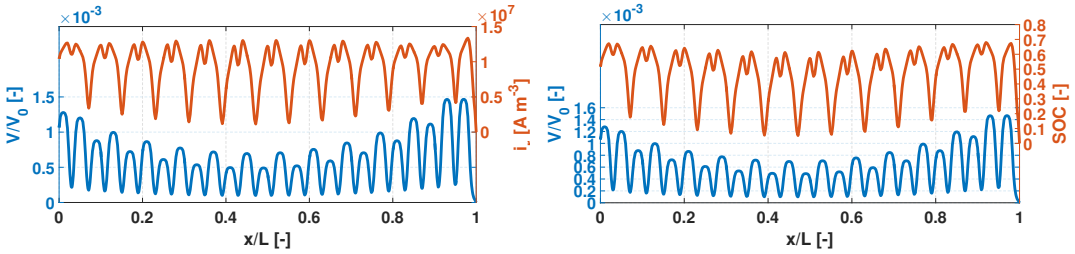

(a) Reaction rate on the right axis, scaled velocity on the left axis

(b) State of charge on the right axis, scaled velocity on the left axis

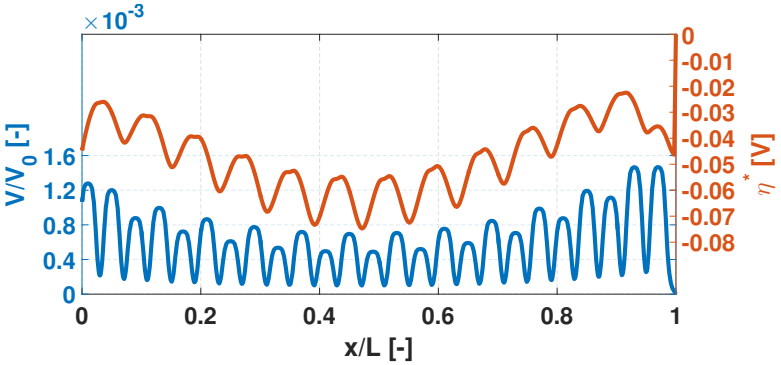

(c) Overpotential on the right axis, scaled velocity on the left axis

result streamlines from the interface between the channel and the porous medium are

reported along with the value of reaction rate in order to further clarify the link between fluid dynamic quantities and electrochemical ones on the same plane used in 4.14.

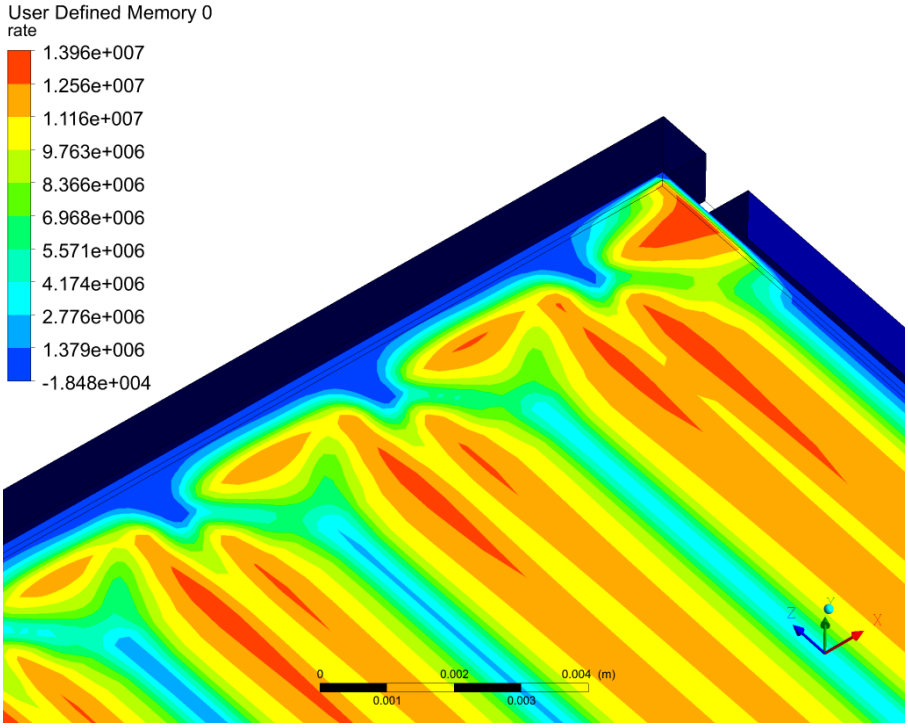

Fig. 4.21: Reaction rate in porous medium

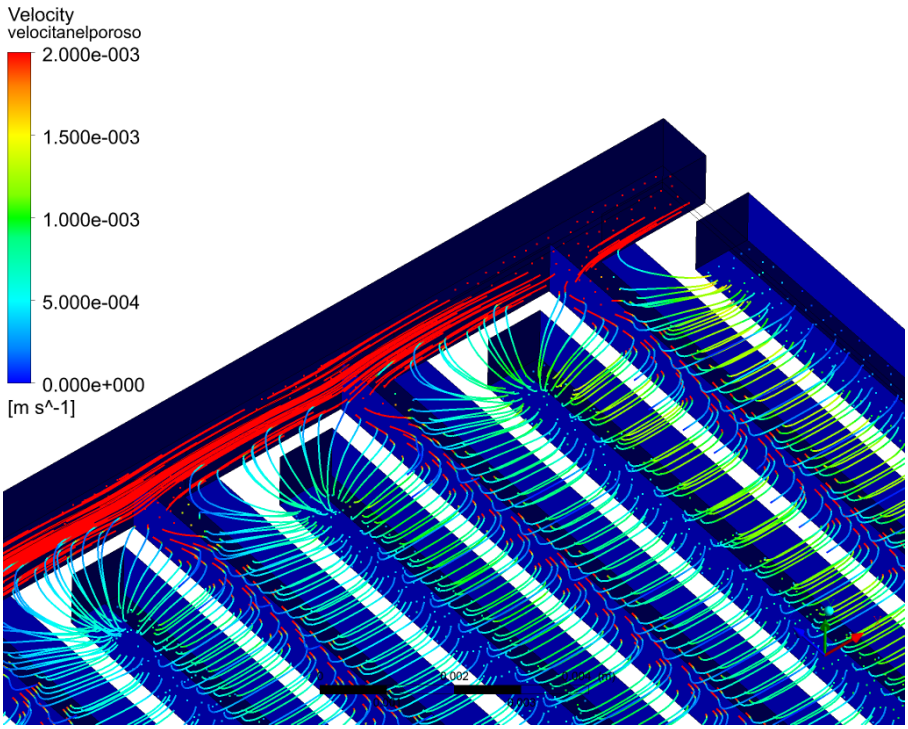

Fig. 4.22: Streamlines of velocity in porous medium

4.4 Influence of the rib size

According to this study, up to this point, not much effort has been made to clarify the influence of the rib on the overall performance of the cell and for this reason a modified architecture for the interdigitated geometry has been proposed. The channel size is kept at *1 mm* while the rib dimension is lowered down to *0.6 mm*: this turned out in a flow field with 32 digits. According to what is found out for the interdigitated geometry the lower

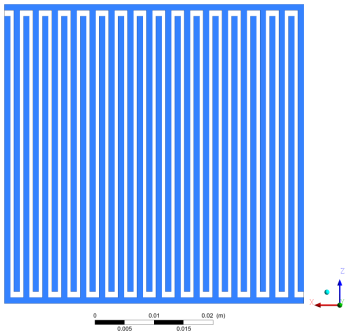

Fig. 4.23: Interdigitated flow field with smaller rib

area of the rib stands for a lower area of the cell over which the potential is actually fixed. Furthermore the central digits will experience a much lower velocity with respect to the lateral ones. This fact is testified by the trend of the scaled velocity in the channels visible in 4.25.The non uniform distribution is penalizing also the performance of the cell in its center as the trend of the reaction rate is testifying.

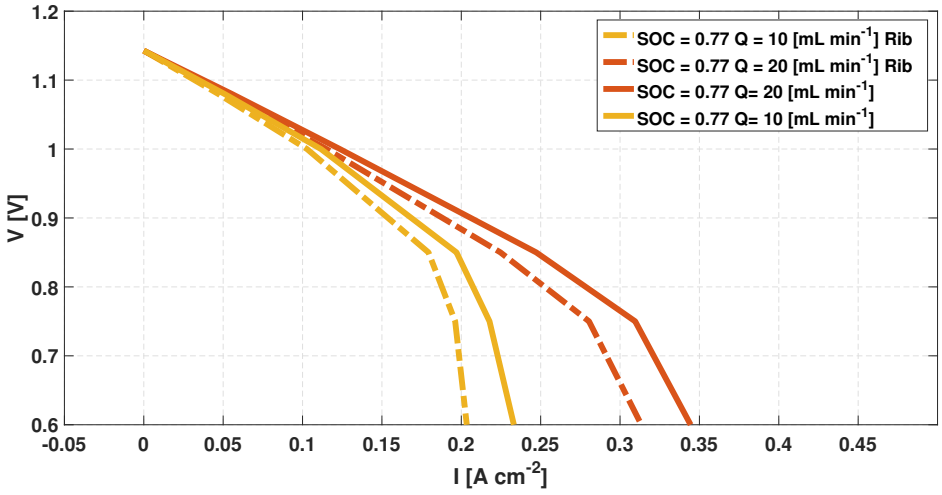

Fig. 4.24: Performance of the interdigitated flow field with smaller rib

This two effects combine and coherently give rise to a lower performance of the cell as visible in 4.24. Both the simulated flow rate experience a decrease of performance when

the size of the rib is lowered. This cell with a lower rib area is tested in the experimental facility in *MRT Fuel Cell Lab* and its performance compared in chapter 5.

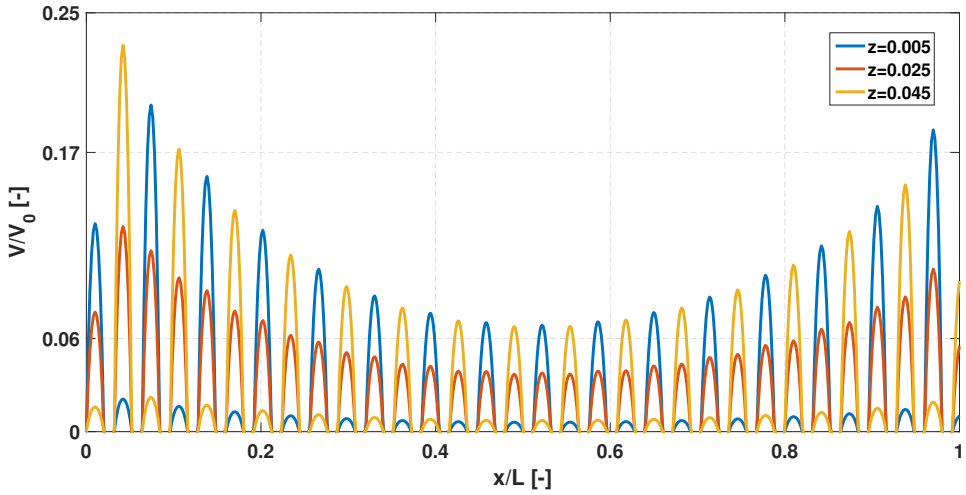

Fig. 4.25: Velocity on a plane passing through the center of the channels

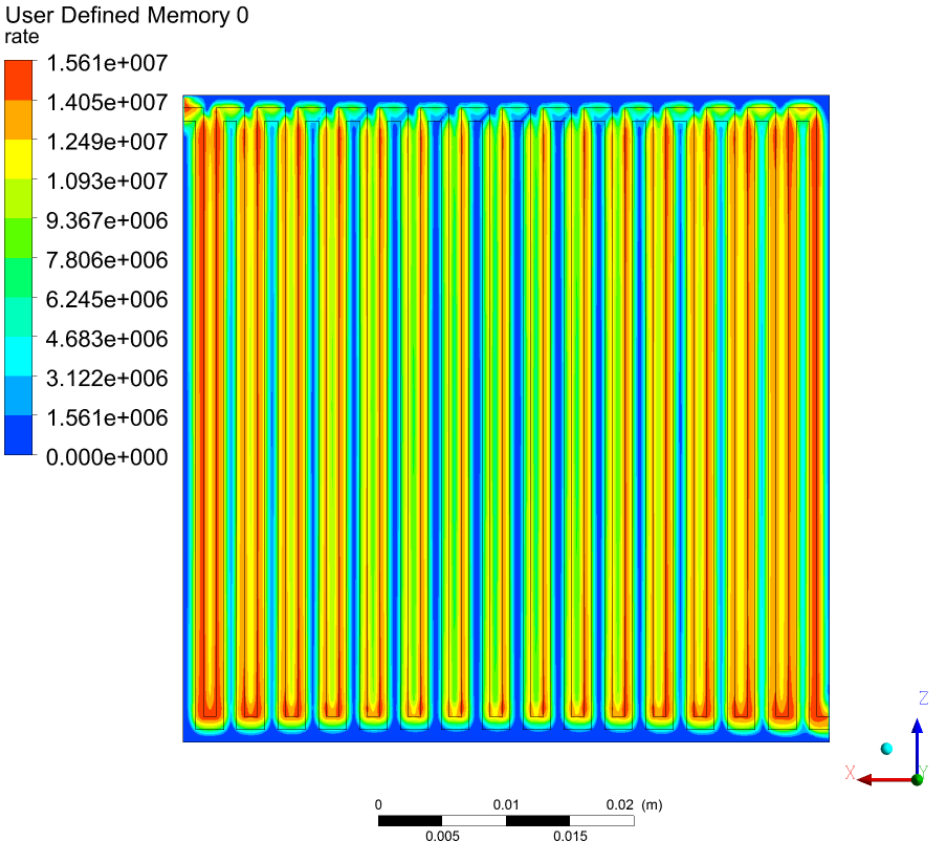

Fig. 4.26: Reaction rate in the interdigitated flow field with small rib

4.5 Double outlet geometry

A novel geometry has been proposed starting from the interdigitated geometry, that was proved to be an alternative for the designed cell. Relying on the experience got modeling the phenomenon, the interdigitated flow field is able to have slightly better performance with respect to the serpentine flow field. The under the rib fluxes are enhanced in this geometry and during this work a novel design is proposed. Its geometry is designed according to two main principles.

- The idea of keeping feeding channels and discharge channels was kept from the interdigitated flow field.
- Since the pressure gradient was found to influence the distribution of reactants it was developed the idea to give a direction to the pressure gradient. Particularly it was decided to shape a flow field in which the pressure gradient would be perpendicular to the direction of the channel in order to force an uniform distribution of the cell.

The geometrical solution to give such effects was a double outlet geometry shown in 4.27.

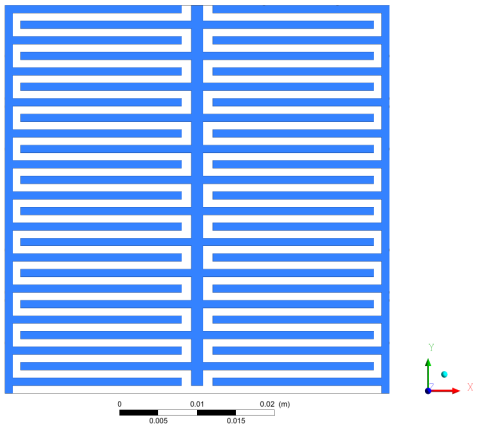

Fig. 4.27: Novel geometry proposed

The inlet is in the center of the higher part of the flow field while the outlets are placed in the lower corners. Changing inlet with outlets would give a cell in which the pressure gradient would be approximately the same but the velocity components in the feeding part would be lower due to the higher inlet area. Due to its more difficult geometry the mesh was not done using $GAMBIT$ but using $Solid\ Works$ for the design part and the *ANSYS Workbench Mesher*" for the meshing part. This process took a very big effort as the procedure to import a multi-zone domain in the mesher is not straightforward since the software tends to distinguish different zones and considers their interface as made

by two different walls one sided by the other. The distribution of velocity of this new flow field is able to give a slight improvement in the performance with respect to the interdigitated one, probably due to the sum of the effects caused by the pressure gradients and the novel shape of the channels. The geometrical parameters chosen are set in order to have a squared channel whose side is *1mm* while the central channel is larger and has a cross-section of *1mm x 1.5mm* . Its characteristic is reported in the following figure and, although the differences are limited, a small improvement is proven numerically for this flow field. What is more the pressure drop caused by this flow field is proved to be in the same order of magnitude of the interdigitated one and slightly lower.

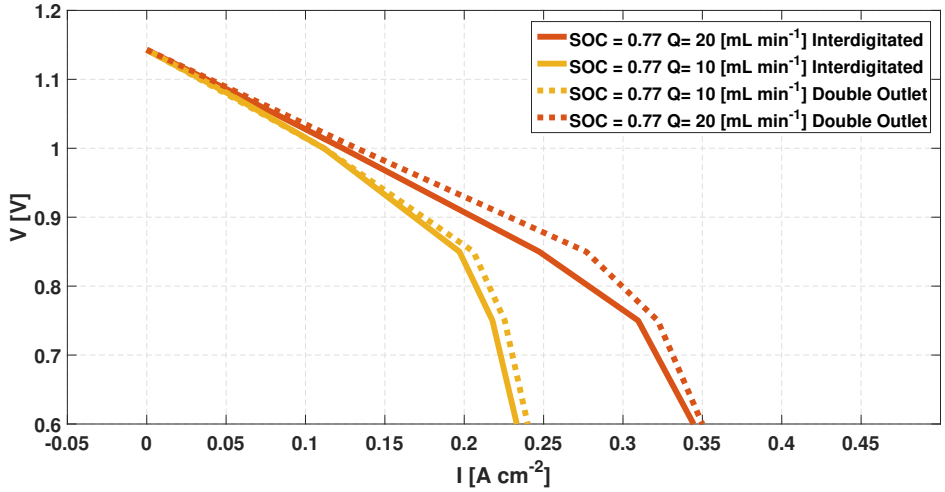

Fig. 4.28: Performance of the double outlet geometry

The velocity on a plane at half heigth of the electrode is also reported for sake of clarity to see how the shape of the flow field influences the current distribution and the velocity one. The lower part of the figure have higher velocities and higher rate but the distribution of reactants is uniform and the reaction rate is dropping less in the interdigitated channels. Under the central channel due to the absence of actual spots in which the potential is fixed the reaction rate goes to very low values on this plane. This flow field has been realized and tested and its performance will be analyzed in the following chapter.

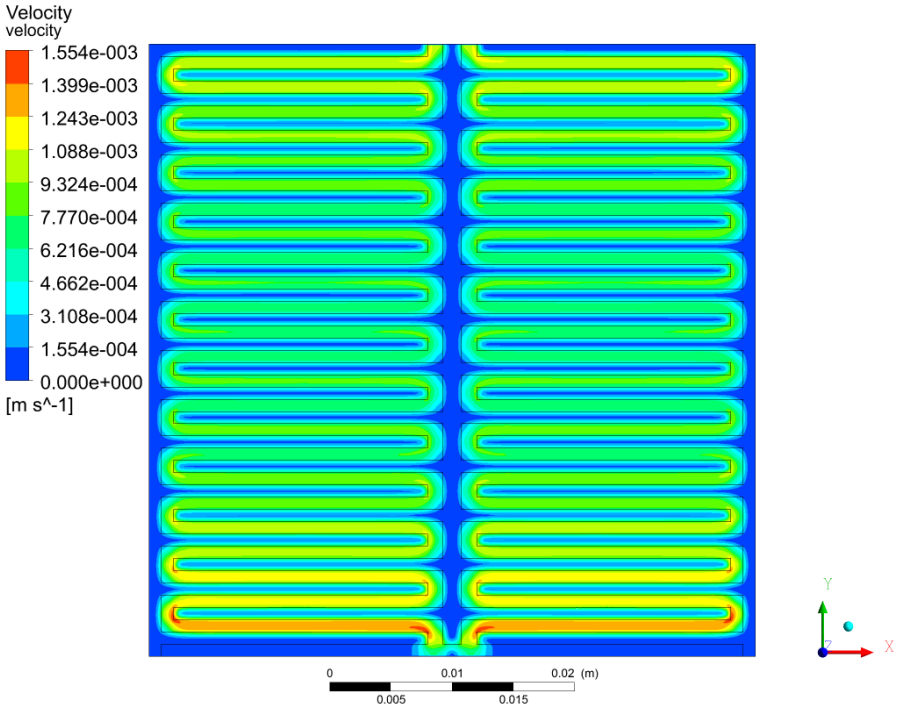

Fig. 4.29: Velocity on a plane at half height for the porous medium

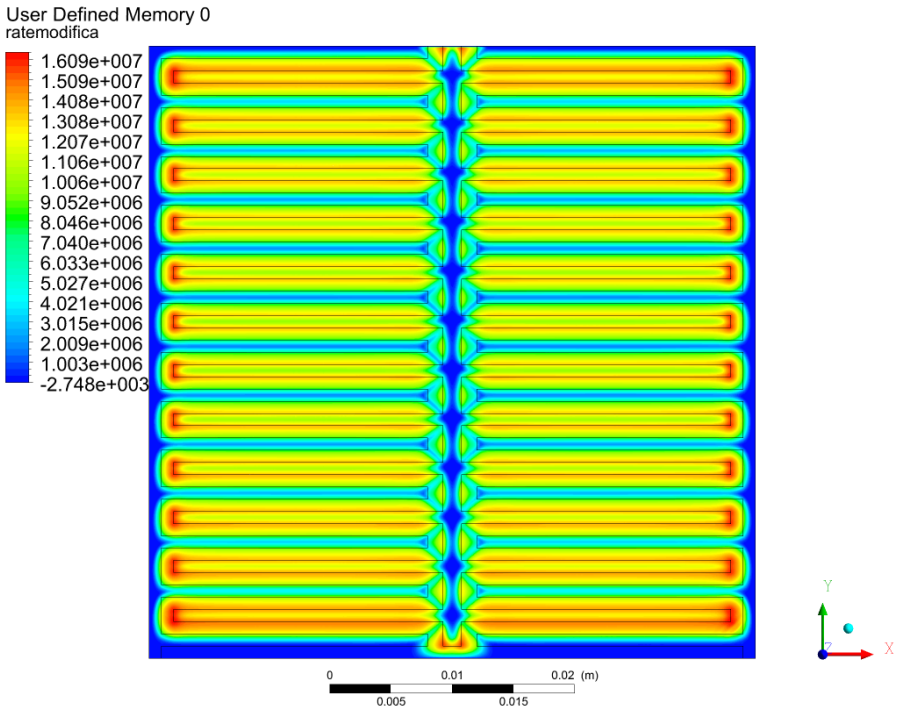

Fig. 4.30: Reaction rate on a plane at half height for the porous medium

4.6 Comparative analysis

In order to end this part a comparative analysis is performed trying to understand which are the geometries that are more suitable for the use in a flow battery system. The model developed and presented in this chapter is able to forecast a difference in the current-voltage characteristic of different flow fields and the entity of this change is visible in the figures presented up to this point: if the parallel flow field does not perform well, the three other flow fields are able to guarantee a similar performance. The results of the model, developed for $Sigracet\ 10\ AA$ reveal some interesting features in the way to feed reactants to a porous medium and are tested in an experimental setup described in the next chapter. Unfortunately, the gas diffusion layer $Sigracet\ 10\ AA$ was not made available by the provider of the materials at the time of the experimental campaign and for this reason a different electrode was used: the $Sigracet\ 39\ AA$. This electrode has the same properties of the previous one as stated in its datasheet [31], but has a lower thickness of 280 μm. In the experimental facility this electrode has been compressed down to 75 % of its thickness. For this reason models are changed and adapted in order to have a smaller electrode: the procedure is eased by using $GAMBIT$ journals.

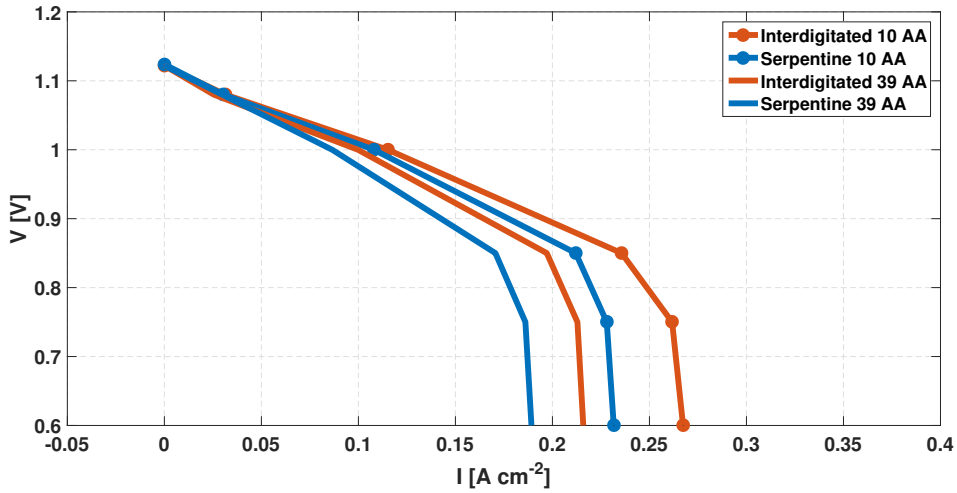

Fig. 4.31: Polarization curves at $20\ ml\ min^{-1}$ for $Sigracet\ 10\ AA$ and $Sigracet\ 39\ AA$ with $SOC\ = 0.6$

The effect of the electrode is not easy to be quantified as its size changes the velocity field and hence the ways in which the electrolytes effectively move through the porous medium. The entity of this change is not easy to be understood a priori, but when one considers the new electrode, what it is natural to think is that being physically smaller it will have less area for the reactions to take place and for this reason it will have lower current generation. This trend is presented also by models as shown in figure 4.31, where the polarization curves are compared for the serpentine and interdigitated flow field with two different electrodes. Regarding the pressure drop introduced by the cell simulated

values are visible in figure 4.32 for both electrodes and the serpentine has a difference of pressure between the inlet and the outlet which is one order of magnitude larger than the three other geometries in all flow rate conditions.

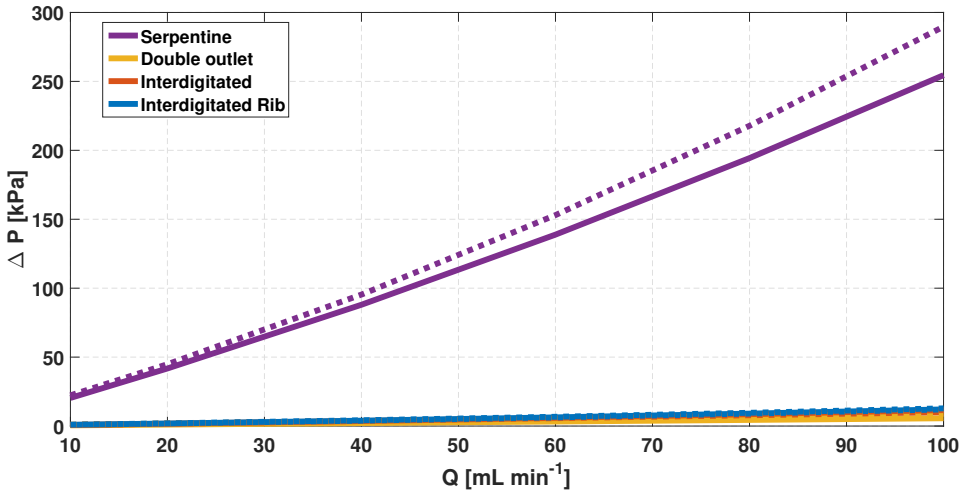

Fig. 4.32: Pressure drop of the cell with $Sigracet\ 10\ AA$ (solid line) and $Sigracet\ 39\ AA$ (dotted line)

The interdigitated based designs have significantly lower pressure drops and among them the base case is proved to have a smaller pressure drop with respect to the small rib flow field and the double outlet geometry. The differences between these flow field are very limited.

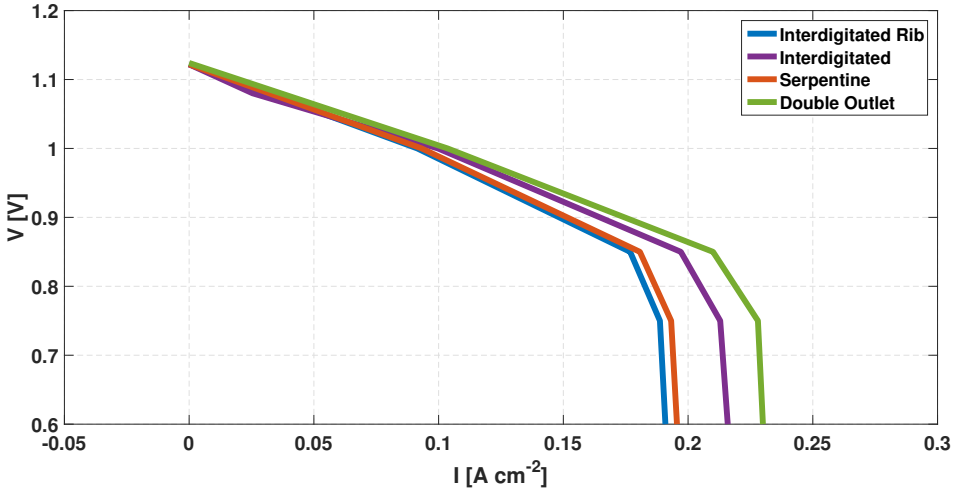

Fig. 4.33: Performance difference for a flow rate of $20\ ml\ min^{-1}$ and $SOC\ = 0.6$ with different flow fields

The new electrode provides a lower current density for each flow field, but when considering all the flow fields the comparison is still slightly in favour of the interdigitated

geometry. It has to be noticed that the numerical entity of the difference tends to decrease with the new electrode. The pressure drop of the cell changes with the new electrode, as figure 4.32 shows, and there is an increase of pressure drop when using the smaller electrode for all flow fields. The causes of this behaviour are found in the complex coupling of the flow field in the porous medium and in the channel and yield to this conclusion. The higher pressure drop for the serpentine flow field gives a starting point for a consideration regarding the possible weight of the power consumption of auxiliaries on the performance of the system. At this point simulations were performed to clarify the differences of the flow fields with the new electrode for two different values of state of charge, coherently with the experimental procedure proposed in chapter 5 and, in order to clarify the different performances, graphs with low flow rate and low state of charge are reported in figure 4.33. This choice is made to enlighten the differences of mass transport in an unfavorable condition. Although the curves are evidencing mass transfer problems as the state of charge is not very high, there are differences in the performance for a given flow rate.

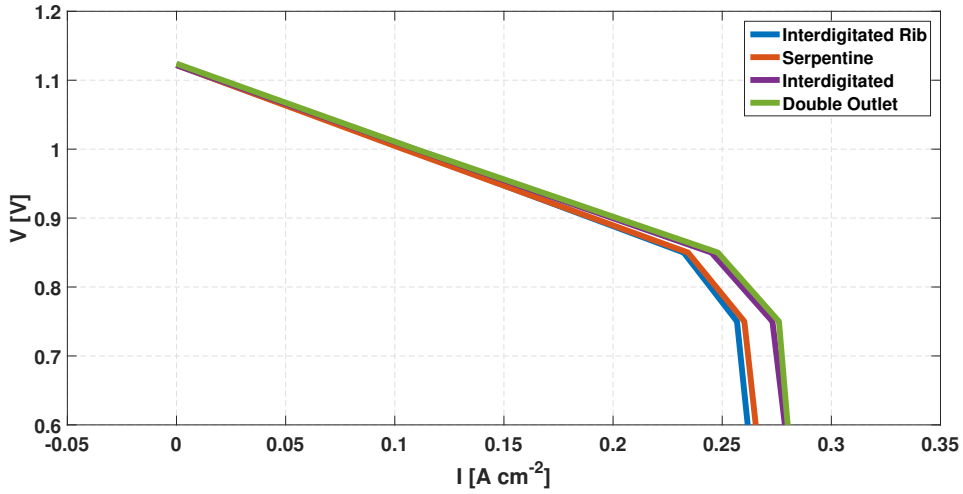

Fig. 4.34: Performance difference for a flow rate of $60\ ml\ min^{-1}$ and $SOC\ = 0.6$ with different flow fields

When the flow rate increases, as shown in 4.34, where polarization at a flow rate of $60\ ml\ min^{-1}$ are presented, the differences in the performance become smoother and the variability decreases. Yet the interdigitated flow field is able to perform slightly better than the serpentine one.

4.6.1 Efficiency of the ideal distributor

The model developed in this work gives some insights on how the quantities inside the battery are changing and provides an estimation of its pressure drop. As the geometries are changing and their shape influences the values of velocity, it is developed a methodology to quantify the performance in a different way. As a reference an ideal distributor is defined: it is a flow field able to deliver in every point of the electrode a solution with the same state of charge. The procedure of the determination of the efficiency of the distributor is presented: it is based on the charge conservation principle and a Butler-Volmer kinetic model. The variables needed are the operating condition of the cell: voltage V_0, current I_0, state of charge SOC_0 and flow rate Q_0. Considering the cell as a reactor and writing a conservation equation (I_0 is positive during the discharge phase) one gets:

$$(c_{VO_2^+,out} - c_{VO_2^+,in})FQ_0 = -I_0 \qquad [A] \tag{4.2}$$

The same equation can be written for the other vanadium specie as follows:

$$(c_{VO^{++},out} - c_{VO^{++},in})FQ_0 = I_0 \qquad [A] \tag{4.3}$$

Therefore for each specie it is possible to calculate the mean concentration at which the cell is operating.

$$c_{VO^{++},mean} = \frac{c_{VO^{++},out} + c_{VO^{++},in}}{2} \qquad c_{VO_2^+,mean} = \frac{c_{VO_2^+,out} + c_{VO_2^+,in}}{2} \tag{4.4}$$

The ideal distributor would give a total current equal to I_0 but operating with constant rate i_{r0} and with a uniform concentration of vanadium species. The calculation is done as follows and allows finding the value of the overpotential $\tilde{\eta}$ from the Butler-Volmer equation 5.6

$$I_0 = V_{electrode} \cdot i_{r0}(c_{VO^{++},mean},\ \ c_{VO^{++},mean}\ \ ,\tilde{\eta}) \qquad [A] \tag{4.5}$$

According to this approach the voltage of the ideal cell operating at the same current I_0 would be:

$$V_{ideal} = E_0 - \tilde{\eta} - \frac{t_m}{\sigma_m A_{cell}} \cdot I_0 \qquad [V] \tag{4.6}$$

Where the third term of the equation is the loss due to the membrane, that includes its conductivity σ_m, its thickness t_m and the area of the cell. The efficiency of the distributor is therefore defined:

$$\eta_{dist,id} = \frac{V_0}{V_{ideal}} \tag{4.7}$$

This quantity is a measure of how far the cell is from ideality and is used as a tool to understand the loss sources in the system and to quantify the impact of a non uniform reactants distribution. At this point, since the quantities are analyzed in a broader sense, the excess of reactants is also calculated from the value of state of charge. At first the

maximum current is calculated and this quantity is the current that the cell would produce if the state of charge would be null at the outlet.

$$I_{max} = c_{VO_2^+,in} F Q_0 \qquad [A] \tag{4.8}$$

Therefore the excess of reactants can be calculated as:

$$\lambda = \frac{I_{max}}{I_0} \tag{4.9}$$

A more convenient expression of the same quantity is given:

$$\lambda = \frac{c_{VO_2^+,in}}{(c_{VO_2^+,in} - c_{VO_2^+,out})} \tag{4.10}$$

What is more, since the data of the pressure drop are collected and analyzed, a second efficiency is proposed in this chapter and it is related to the pressure drop introduced by the flow field. The power produced by the cell is influenced by the consumption of the pump to move the reactants and an energy efficiency is defined and analyzed.

$$\eta_{energy} = \frac{P_{cell}}{P_{cell} + P_{pump}} \tag{4.11}$$

Where the power of the pump is calculated from a measured or calculated pressure drop.

$$P_{pump} = Q_0 \frac{\Delta P}{\eta_{en}} \qquad [W] \tag{4.12}$$

The results of this analysis are reported briefly plotting the values of both efficiency of the distributor and the energy efficiency of the system on simulated polarization curves but before it a comparative plot is shown in figure 4.35 to see the impact of the flow rate on two different flow fields.

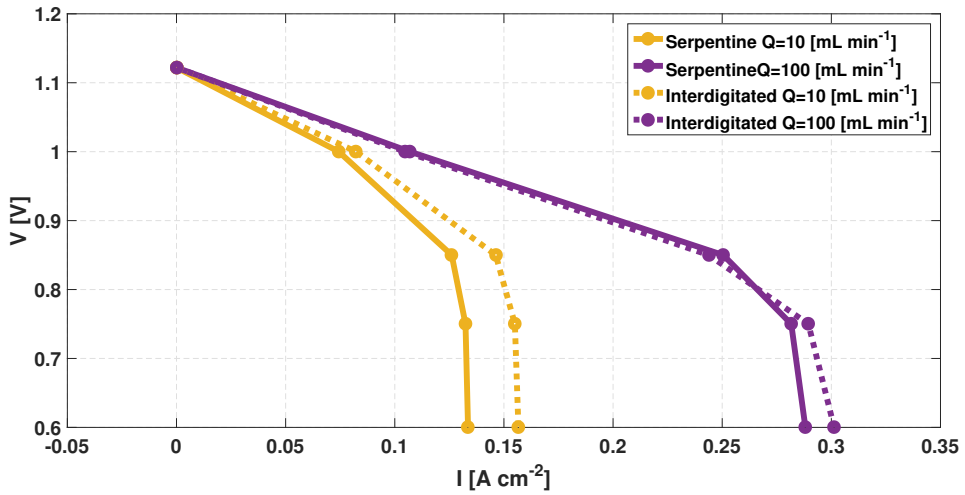

Fig. 4.35: Comparative analysis between interdigitated and serpentine flow field

At both high and low flow rate there is a difference in the performance of the systems even if when the cell is operated with very high flow rate this difference is very smooth and present just when the current is significantly high.

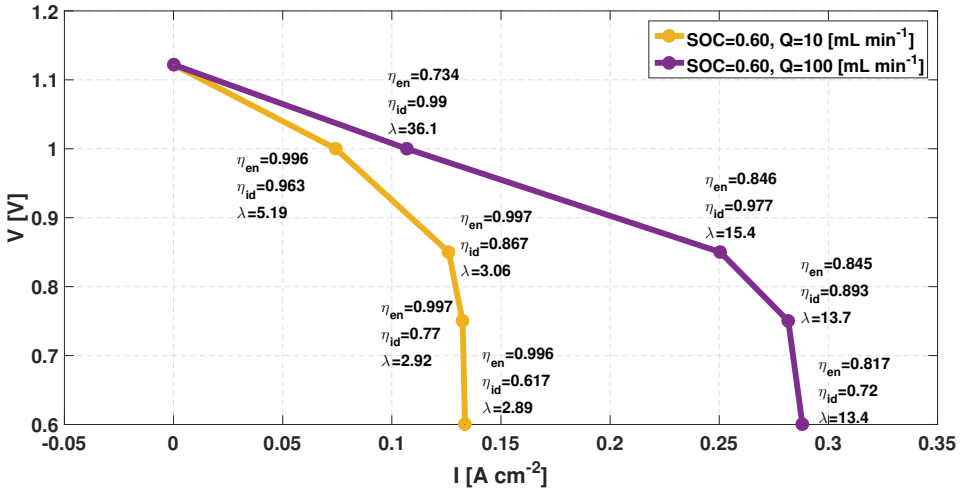

Fig. 4.36: Serpentine data elaboration

This visualization of the serpentine flow field performance in figure 4.36 allows better comprehension of the working condition of the cell for two different flow rates. As one may notice in all conditions the cell is working with excess of reactants, even if at very low flow rate the values of this parameter are not higher than 5. Considering the low flow rate, the pressure drop caused by the cell is not enough to make the energy efficiency change from the value of one, while a complete different situation is present at high flow rate where the impact of the cell counts up to 20 percent. Regarding the ideal distributor efficiency, the higher the current the lower the value of the parameter as the local differences of mass transport impact the flow field. The same analysis is made for an interdigitated flow field and the results are reported in figure 4.37. The performance of the interdigitated flow field at low flow rate is slightly better than the serpentine flow field as it is able to distribute reactants more efficiently and has a slightly higher efficiency with respect to the ideal distributor. At high flow rate the differences in the performance are actually almost null and the two cells are operating with a very similar voltage-current characteristic this is due to the fact that the excess of reactants is large enough to give sufficient reactants to the redox reaction. What changes is how the pump consumption is impacting the energy efficiency and the interdigitated flow field is able to limit the energy loss to very low values and hence to work with energy efficiency close to unity in all points of the purple curve. This result enables the comprehension of the problem from a different perspective. Since the system is not fed by a fuel whose loss would be undesired, the goal of the work should not be increasing the mass transport characteristic of the flow field with a given flow rate but the best configuration in terms of flow rate, geometry and energy efficiency has to be found. No irreversible loss is introduced in the system if the solution is recirculated.

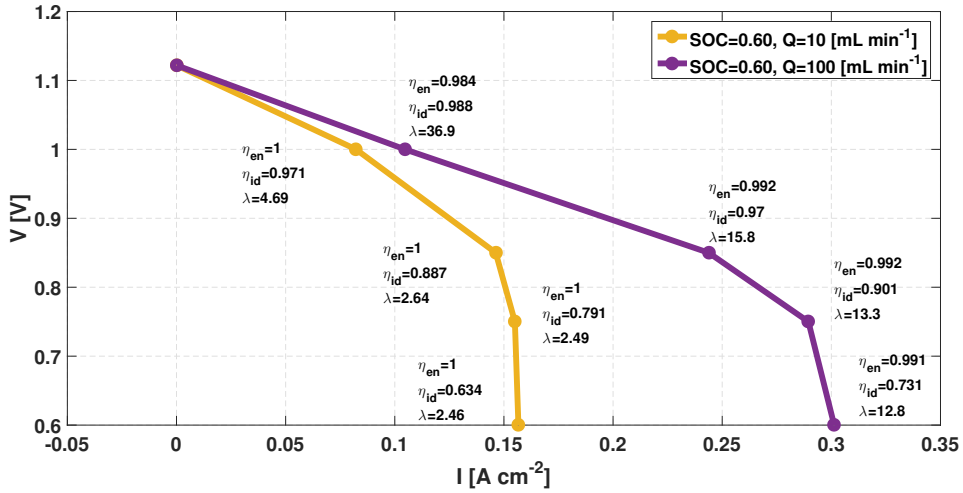

Fig. 4.37: Interdigitated data elaboration

Increasing the flow rate means lowering the variation of state of charge inside the cell and making it work with a more uniform concentration. This increases the distributor efficiency but has to be paid with a higher pressure loss. Therefore the optimal flow field has a different aim: it has to allow a good distribution of reactants while keeping the pressure loss low. The interdigitated is able, according to numerical models, to do such thing. Since the geometry characteristic have been analyzed and the model forecast some trends, an experimental campaign is performed to understand up to which point the analysis here presented is applicable to a real case.

5 Experimental campaign

In this chapter it is presented the experimental campaign which included the testing procedure of 4 flow fields. The experimental setup is described along with the procedure to obtain measures with high repeatability. Results of the experimental campaign are presented and compared with the results of the models. A new fitting procedure is performed aimed at introducing a convective resistance in the modelling of the mass transport problem.

5.1 Experimental setup

In $MRT\ Fuel\ Cell\ Lab$ it has been installed a facility to test the hydrogen-vanadium cell. The experimental setup used in this work is similar to the one used in [32] but some modifications are made. In figure 5.1 it is possible to see a photo of the experimental setup, whose schematic is proposed in figure 5.2.

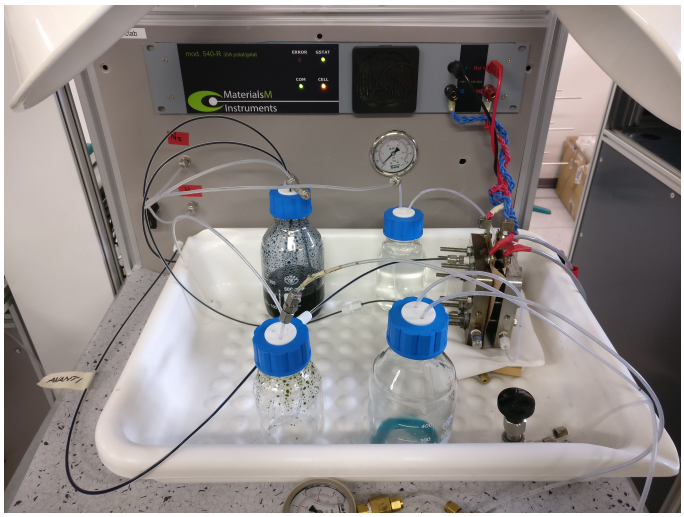

Fig. 5.1: Experimental setup

The cell has two different sides and the circuit of vanadium consists of a tank, a peristaltic pump and acid resistant tubing. Hydrogen is taken from a line at 3.5 bar and its flow is regulated using a flow meter controlled by the software $LabView$. The anodic and cathodic electrodes are connected to a potentiostat/galvanostat that is able to impose current and voltage and characterize the electrochemical behaviour of the cell. Its parameters are

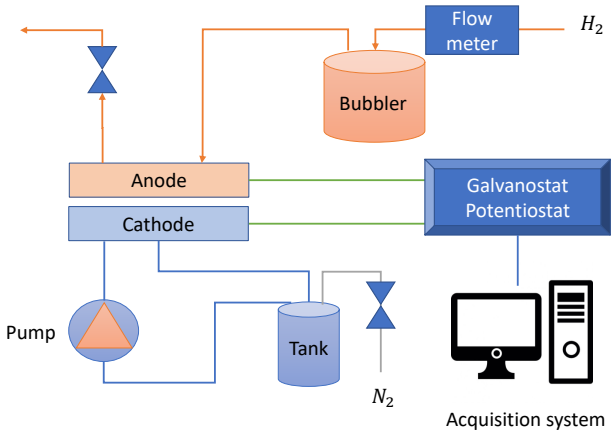

Fig. 5.2: Scheme of the experimental setup in $MRT\ Fuel\ Cell\ Lab$

controlled by a control system using the software $LabView$. Since the acid solution is able to corrode the metal plates of the cell, the cathodic hydraulic circuit is built to avoid contact between the solution and the supports of the electrochemical cell. Pumps characteristic curves are built using acid solution as a working fluid to relate the revolutions per minute of the pump to the flow rate. It is important to place the cell in the pressure side of the pump, in case it would be on the suction side it might happen that the pressure drop of the cell could be too high and the pump could not guarantee the flow rate. For this reason the pump has a preferential sense of rotation. The instruments characteristics can be found in [32]. A modified circuit architecture is built to allow the use of a pressure transducer to measure the pressure drop of the circuit as shown in figure 5.3. An additional tank is used for two purposes: the first is to provide a reference for the pressure transducer and the second is to guarantee uniform flow rate to the cell. Since the pump is peristaltic, there can be some fluctuations in the flow rate. The dampener is a closed system able to keep the pressure. Starting from a situation in which the dampener is empty, imposing the flow rate the dampener will be filled up to a point in which the situation stabilizes. In this point the pressure of the air (or equivalentely of the liquid) inside the tank is equal to the pressure drop caused by the circuit. The fluctuation of the flow rate caused by the peristaltic pump is effectively dampened by a sudden compression of the air in the tank. As a result, electric quantities of the cell will suffer less the variability of the flow rate and are proved to be stable.

Nitrogen is taken from a 3.5 bar line and it is used, by means of a valve, to pressurize the vanadium circuit up to a pressure of $1.2\ bar$. This procedure is aimed at avoiding oxygen from entering the tank as it may react with the solution, discharging it. The materials used in the cell are:

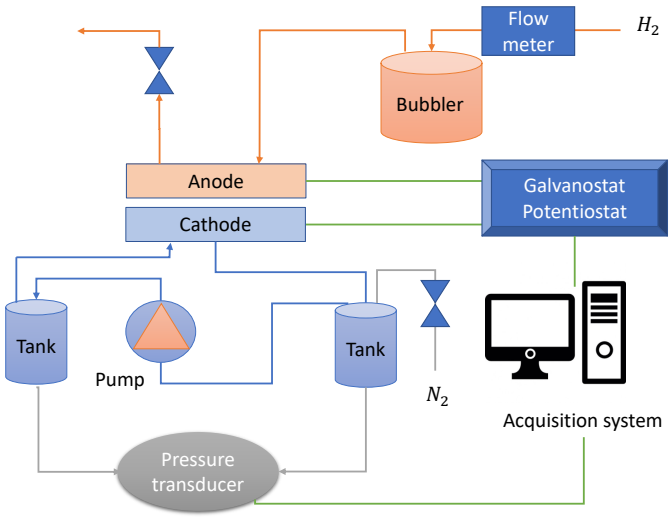

Fig. 5.3: Scheme of the experimental facility $MRT\ Fuel\ Cell\ Lab$ to measure pressure drop

- $Sigracet\ 39\ AA$ for the cathodic electrode.
- $Nafion$ membrane with a thickness of $125\ \mu m$;
- $Baltic\ GDE\ S10CC$ electrode with $0.5\ mg\ cm^{-2}$ of platinum catalytic support;

The flow fields tested are four and their characteristics are listed in chapter 4: single serpentine flow field, interdigitated flow field, interdigitated flow field with smaller rib and a double outlet architecture. In case of this last geometry a slight modification has been done from what visible in figure 4.27. In fact two additional channels are added to adapt the flow field to the existing support, that has just two holes for the solution to enter and exit the cell as figure 5.4 testifies. In the real cell gaskets are placed close to the plate and effectively avoid liquid from the feeding channels from going into the porous medium.

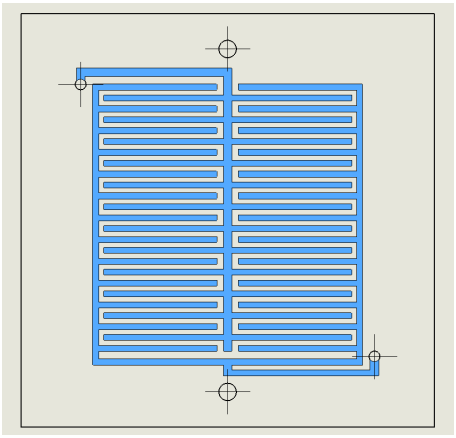

Fig. 5.4: Adapted geometry for the double outlet flow field.

5.2 Experimental data

Polarization curves are collected and the procedure to get them is aimed at guaranteeing the repeatability of the curves. It is observed during the experimental campaign that leaving the cell in air for two or three days may change its performance. The most influencing parameter is found to be the not perfect behaviour of the negative electrode. The cross contamination process of vanadium changes the characteristic of the operation of the negative electrode. For this reason an improved procedure to have the polarization curves is built. A bubbler, a tank with water in which hydrogen is injected at the bottom, is used to hydrate the hydrogen. Before each measure, the pump of the vanadium circuit is stopped and hydrogen is fluxed for 5 minutes. During the operation of the system the hydrogen flow rate is kept at $90\ mL\ min^{-1}$ as this values guarantees a high excess of reactants at the negative electrode. The measurement itself consists of a sequence of measures:

- Open circuit voltage is measured for 45 seconds,
- Current steps of $-1.25\ A$ are imposed incrementally to the cell every 45 seconds while the voltage is recorded by the acquisition system. This gives points every $0.05\ A\ cm^{-2}$.

The number of points each curve is made of is related to the capability of the system to produce current staying in the limits of voltage needed for the safe operation of the cell and that are 1.6 V and 0.5 V. The procedure is performed for various values of flow rate ranging from $10\ mL\ min^{-1}$ to $100\ mL\ min^{-1}$. In this section polarization curves are presented, particularly the interdigitated flow field performance is reported in figures 5.5 and 5.6.

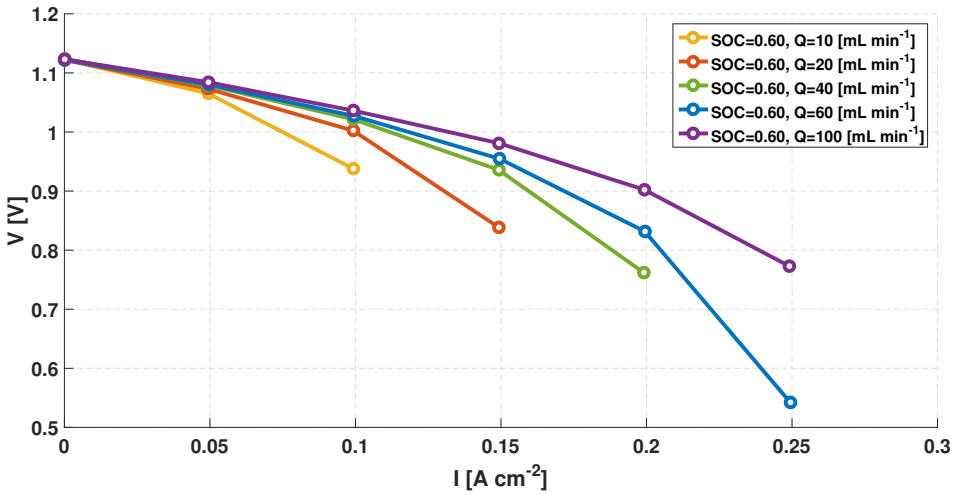

Fig. 5.5: Performance of interdigitated flow field SOC=0.6

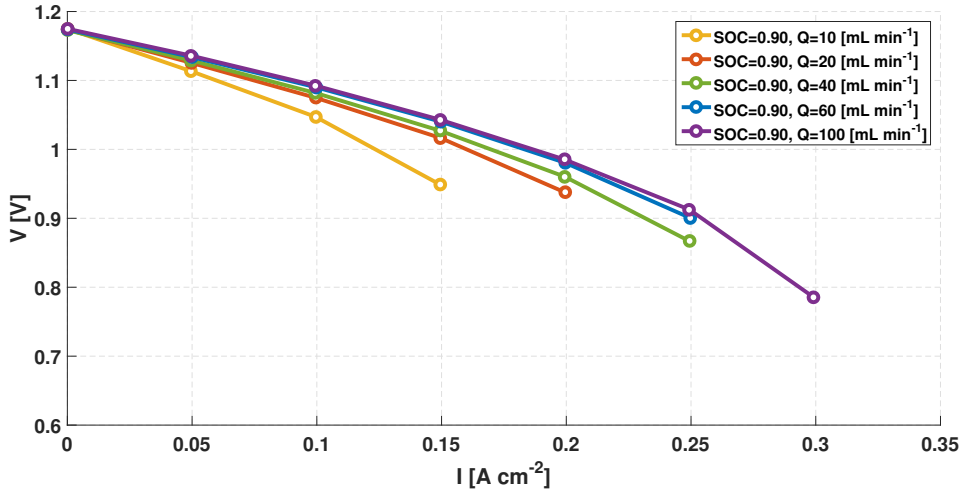

Fig. 5.6: Performance of interdigitated flow field SOC=0.9

The first thing to see is that the influence of the state of charge is present and a higher SOC increases the capability of the system to give current when discharged. All curves in figure 5.5 and 5.6 present an improvement of performance when the state of charge is higher. Another important fact related to the concentration of the vanadium species is that when the state of charge decreases the variability with respect to the flow rate increases. The problems of mass transport are more and more evident in this condition: taking the $10\ mL\ min^{-1}$ curve at low state of charge it is possible to state how this is not able to reach high current densities. Coherently to what done with models, the influence of the rib width is quantified experimentally and the trend seems to be the same as forecast by the numerical model: a smaller rib penalizes the performance of the system and this is more visible when the flow rate is very low. At higher flow rate as one may notice from figure 5.7 any difference is not visible.

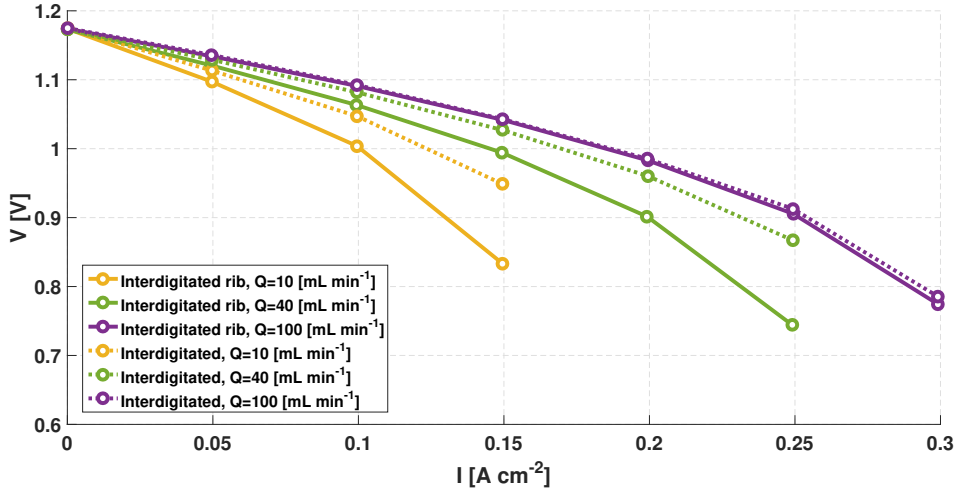

Fig. 5.7: Performance of interdigitated flow field SOC=0.9

At a lower state of charge the situation does not exhibit a large variation from what stated for figure 5.7 and therefore is not shown. The higher the flow rate the lower the difference between the two tested flow fields as the mass transport phenomena are less limiting. At higher state of charge a similar consideration can be stated and the two flow fields are proved to be equivalent in terms of performance. The double outlet flow field is tested and its performance is characterized for four different flow rates and two states of charge. Its performance in relation with the interdigitated one is reported in figure 5.8, where, for sake of clarity, just three flow rates are visualized. At low state of charge the novel flow field developed in this work is able to perform better than the base interdigitated geometry. For $10\ mL\ min^{-1}$ and $20\ mL\ min^{-1}$ the differences are more marked than what happens at $100\ mL\ min^{-1}$. At higher state of charge the differences are much more limited even if the double outlet geometry performs slightly better than the interdigitated flow field.

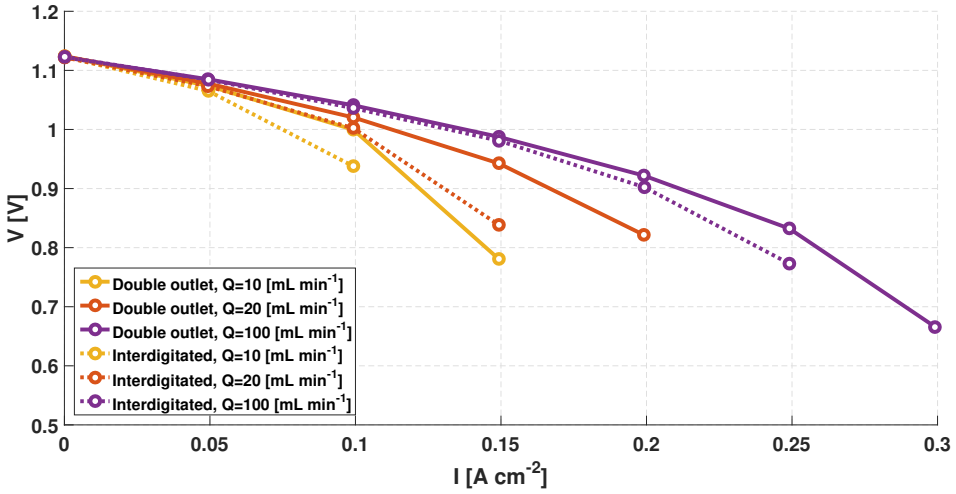

Fig. 5.8: Performance of double outlet geometry and interdigitated flow field at SOC=0.6

This novel flow field was proposed and designed in this work as a modification of the interdigitated flow field and hence this result is important for the aim of the work as in the literature, according to the knowledge of the writer, similar flow fields are not present. The study of the mechanism through which the interdigitated flow field works enabled the development of such new flow field and represented a very limited, yet existing innovation to the problem of flow field design for flow battery systems.
Up to this point the trends of the performance of the flow fields were forecast by the model and last flow field presented is the single serpentine for both the states of charge considered in this work.

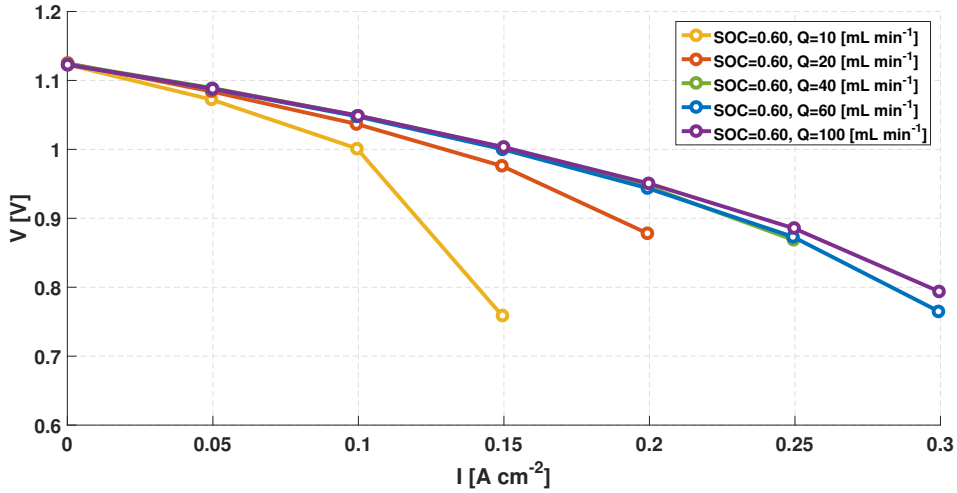

Fig. 5.9: Performance of serpentine flow field SOC=0.6

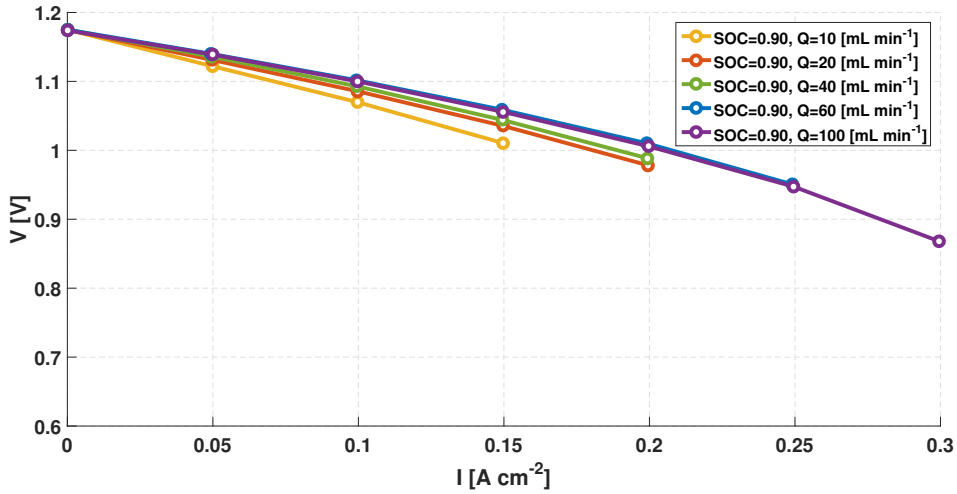

Fig. 5.10: Performance of serpentine flow field SOC=0.9

This flow field has a characteristic trend when the state of charge is high. It seems that mass transport problems are not present and all curves collapse while this is not completely true. Considering the yellow curve in figure 5.10, the last point is corresponding to a current density of $0.15A\ cm^{-2}$. What happens is that, if a current density of $0.2A\ cm^{-2}$ is applied, the cell is not able to operate in the voltage limits and therefore the the voltage is dropping between $0.15A\ cm^{-2}$ and $0.2A\ cm^{-2}$. Future works should focus on the improvement of the $LabView$ procedure to get curves and consequently to better characterize the polarization curve. Comparing the performance of the interdigitated flow field and the serpentine one emerges a better performance of the second. This is experienced both at high flow rate and at high state of charge even if the entity of the difference in this two cases is lower. This result is not in accordance with the analysis done with the numerical model and needs to be investigated.

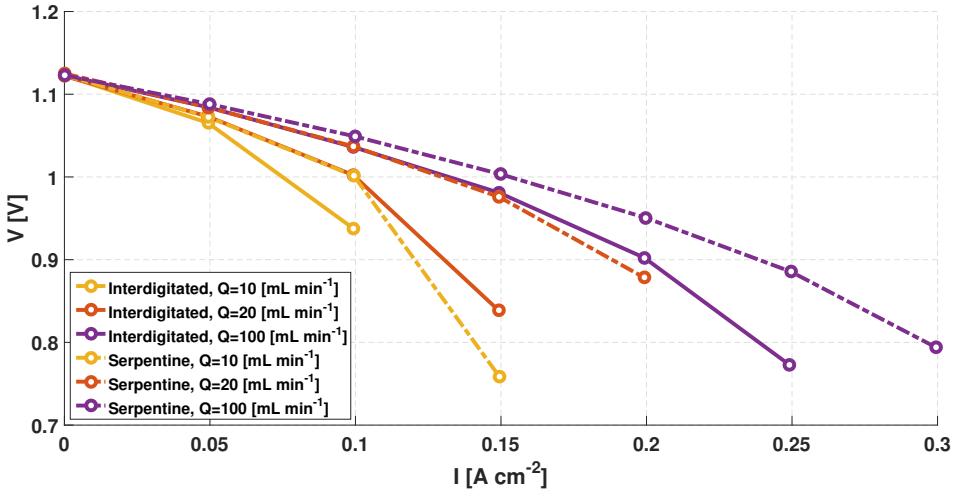

Fig. 5.11: Comparison of the performance of serpentine and interdigitated flow field SOC=0.6

The double outlet cell performance, even if better than the interdigitated's one, is not able to overcome the serpentine flow field, which is the best configuration examined in the experimental campaign.

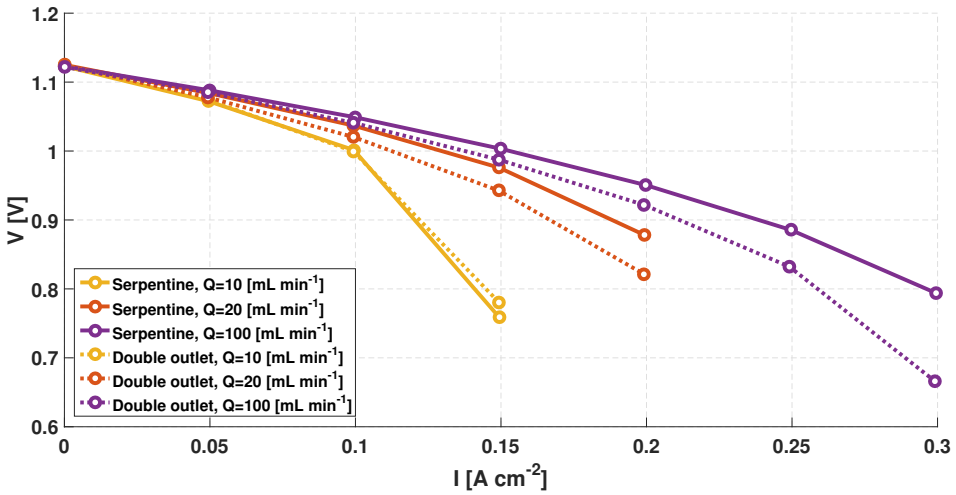

Fig. 5.12: Comparison of the performance of serpentine and double outlet flow field SOC=0.6

As a last result of this section, a measure of the pressure drop of the cell is presented. This values are measured in the experimental facility as the difference between the pressure drop of the whole circuit and the pressure drop of the circuit without the cell. The measure of the pressure drop of the circuit is obtained using a proper configuration for the vanadium circuit as visible in figure 5.3. In figure 5.13 it is reported the trend of the pressure drop of the cells: lines represent the simulated results while the dots are measured values. The model forecast a higher the pressure drop of the serpentine flow field while over predicts the effective loss of the interdigitated-derived flow fields.

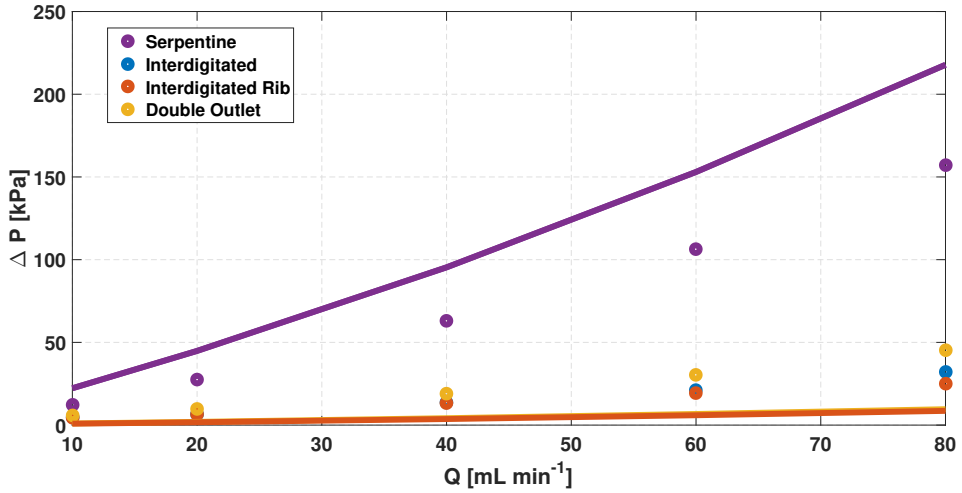

Fig. 5.13: Pressure drop of the cell for various flow rates, dots are experimental measured points, lines are numerical results.

Simulated curves are overlapped in figure 5.13 as their values are much lower than the serpentine's ones. A partial explanation of this fact can be found for the interdigitated flow fields as a high pressure drop is caused by the feeding tubes and curves going from the circuit to the cell itself. These parts are effectively measured in the experimental setup while are not modelled in the numerical code. Particularly the double outlet flow field may have a higher pressure drop due to the fact that additional channels were added to adapt the geometry to the existing plate. On the other side, the serpentine pressure drop is overestimated by the model and reasons for this behaviour are very probably related to the modelling of the flow inside the porous medium and also to the parameters taken into account.

5.3 Refitting

The numerical results have to be discussed, since the model is able neither to forecast numerically the electrochemical behaviour of the cell nor the trend between different flow fields. It seems evident how some phenomena are influencing the result in a way that is not in line with the real cell one and need further investigation. For sake of simplicity just two flow fields will be considered in this part: the serpentine and the interdigitated geometry and for the same reason the focus is on the curves with lower state of charge.

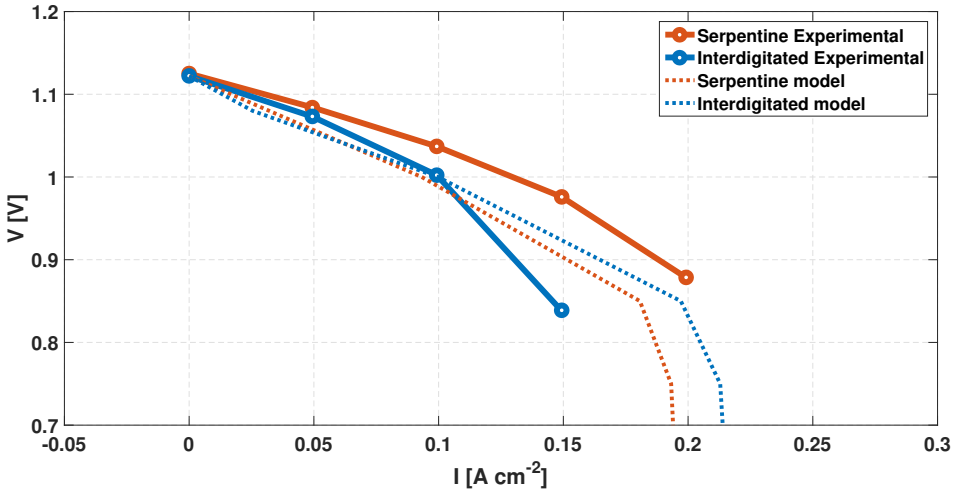

Fig. 5.14: Simulated and experimental polarizations for serpentine and interdigitated geometry for a flow rate of $20\ ml\ min^{-1}$ and SOC = 0.6

Figure 5.14 shows the numerical differences between the experimental results and the model for the operating conditions mentioned. The differences are marked but it has to be kept in mind that the parameters used in the threedimensional model are taken from a fitting procedure done on the bidimensional model presented in chapter 2. The only significant difference is regarding the different permeability of the material. Therefore this difference might be caused by an erroneous value of the parameters that describe the kinetic of the reaction or the fluid dynamic behaviour of the solution. Consequently, to reach a better result, the first attempt performed deals with the determination of the parameters that describe the kinetic of the reaction: density, viscosity and permeability are supposed to be close to the real values as their values are shared by most of the authors in this field [37] [13] [40]. The procedure started with the fitting of the performance for the serpentine flow field and, with the parameters found, the interdigitated flow field was simulated. Values for the new parameters are shown in table 5.1 along with the values used in previous simulations.

Parameter	Previous value	Fitted value
Active area a $[m^{-1}]$	35000	50000
Pore radius r_p $[\mu m]$	32	70
Velocity of the reaction k_{agar} $[\frac{m}{s}]$	1.8e-6	1.8e-6

Tab. 5.1: Parameters used for the fitting procedure

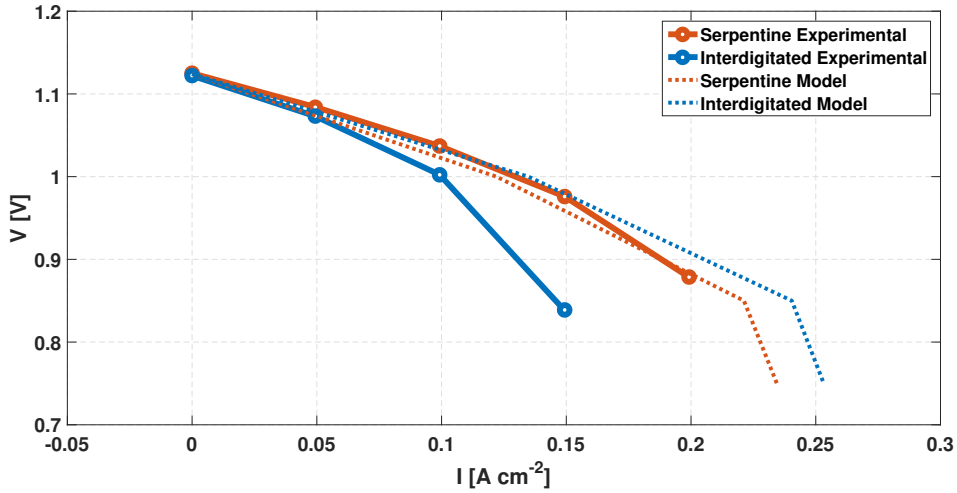

Fig. 5.15: Refitting procedure for the serpentine and interdigitated flow field

The dashed curves in figure 5.15 are the results of the model with the parameters of table 5.1 for serpentine and interdigitated geometry. As one can see, even if the red curve is not far from the experimental result, the performance of the interdigitated flow field is not forecast correctly. Since the parameters' influence has been analyzed in this way, the next step in trying to understand the behaviour of the cell is changing the way in which phenomena are modelled. If the kinetic model based on a Butler-Volmer equation is used by all authors in this field, studying the literature a considerable difference in the approach of the mass transfer problem was found out. Some authors used to model the mass transfer problem using just diffusion while other works [37] and [40] apply a different correlation to model the mass transport losses. To relate the bulk and surface concentration the use of a convective resistance is proposed and widely used. The theoretical basis for this approach is reported in [27]. A convective mass transport correlation is proposed to characterize the properties of felts and basically this includes actively the velocity in the determination of the mass transfer characteristic. This relation is evaluated experimentally and links the following adimensional groups:

$$Sh = 7Re^{0.4} \qquad [-] \tag{5.1}$$

The author of the paper develops the correlation for a mass transfer limited reaction using just one fiber of material and states it can be used as a first approximation for carbon felts.

The details of the experimental facility used are reported in [27]. Therefore the mass transfer coefficient can be calculated according to the following equations.

$$\frac{h_m d_f}{D} = 7\Big(\frac{\rho u d_f}{\mu}\Big)^{0.4} \qquad [-] \tag{5.2}$$

$$h_m = 7\frac{D\rho^{0.4}}{d_f^{0.6}\mu^{0.4}}u^{0.4}\,[\frac{m}{s}] \tag{5.3}$$

$$h_m = Au^{0.4}\,[\frac{m}{s}] \tag{5.4}$$

This approach changes the pore impact on the local difference between the surface and bulk concentration and introduces an explicit dependence from velocity of the mass transport phenomena.

$$h_m(c_{VO^{2+}}^{surface} - c_{VO^{2+}}^{bulk}) = \frac{i_r}{aF} \qquad \left[\frac{mol}{s\cdot m^2}\right] \tag{5.5}$$

The equation 5.5 is used to express the link between surface and bulk concentration and the reaction rate can be written as follows.

$$i_r = \frac{k_0 aF}{1+\frac{k_0}{h_m}\cdot\left(e^{\frac{\alpha F\eta^*}{RT}} + e^{-\frac{(1-\alpha)F\eta^*}{RT}}\right)}\left(c_{V^{4+}}^b \cdot e^{\frac{\alpha F\eta^*}{RT}} - c_{V^{5+}}^b \cdot e^{-\frac{(1-\alpha)F\eta^*}{RT}}\right)\left[\frac{A}{m^3}\right] \tag{5.6}$$

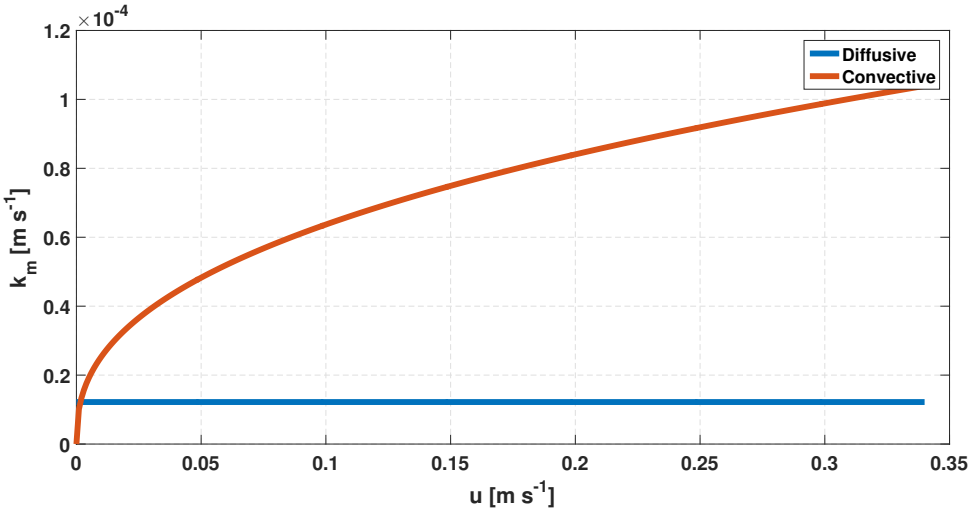

Fig. 5.16: Diffusive and convective mass transfer coefficient

Figure 5.16 shows the different values of the mass transfer coefficient when the approach is diffusive or convective. In the first case all the points in the domain will experience the value for the diffusive coefficient equal to the ratio of vanadium diffusivity to the pore radius, while in the second the variability of the velocity field causes a variability in the resistance to mass transfer. The range of velocity reported is taken from the model for

$20\ ml\ min^{-1}$, considering the maximum velocity value in the porous medium. What is done in this work it was to use the mass transfer correlation reported by [37] and by [40] and to include it in the code used for the models. The most important results are shown in figure 5.17. The procedure was aimed at the fitting of the curve of the serpentine flow field and with the same parameters the interdigitated flow field was simulated. The numeric values for the parameters used for the fitting are reported. The parameter A is taken directly from [37] and [40] since both authors use the same number.

Parameter	Previous value	Fitted value
Active area $a\ [m^{-1}]$	35000	17000
Pore radius $r_p\ [\mu m]$	32	Not present
Velocity of the reaction $k_{agar}\ [\frac{m}{s}]$	1.8e-6	7e-6
A	Not present	1.6e-4

Tab. 5.2: Parameters used in the fitting procedure

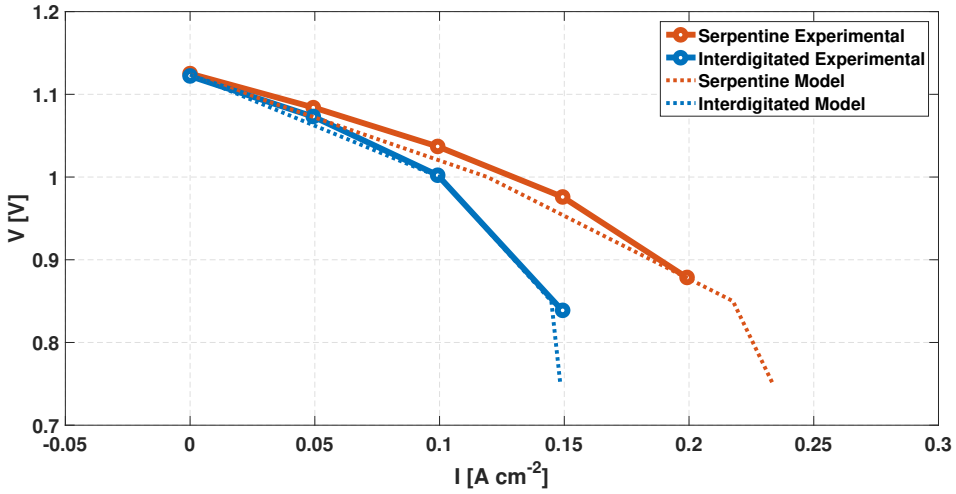

Fig. 5.17: Comparison of the performance between experimental and models for $20\ ml\ min^{-1}$ and SOC=0.6

Regarding the working condition considered, with the new parameters and the new kinetic model, the results of the simulated cell are close to the real one and this is very remarkable. It is possible to state that there was an issue in the way in which mass transport was modelled previously. Anyway, when moving out of the working condition considered, the accuracy of the analysis decreases and significant differences emerge. The behaviour of the serpentine flow field is forecast with lower accuracy by the model at lower and higher flow rate but even if the numerical entity is not the same, the trend between the interdigitated and the serpentine is well forecast.

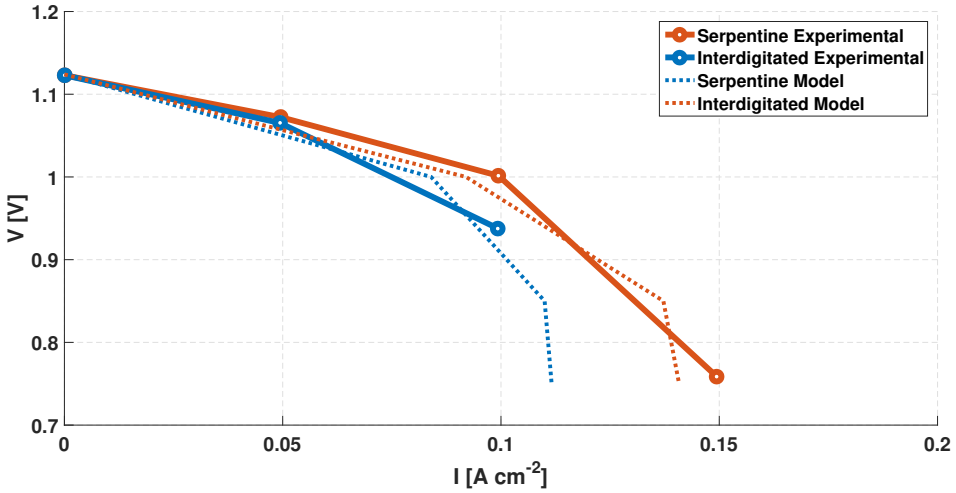

Fig. 5.18: Comparison of the performance between experimental and models for $10\ ml\ min^{-1}$ and SOC=0.6

When the flow rate is low, as reported in figure 5.18, the simulated cell is similar to the real one, but when the voltage decreases the model gives lower current density with respect to the real cell. When instead the flow rate is increased up to $60\ ml\ min^{-1}$, the performance of the simulated serpentine is significantly far from the real cell but the interdigitated flow field is seen as less performing also by the model.

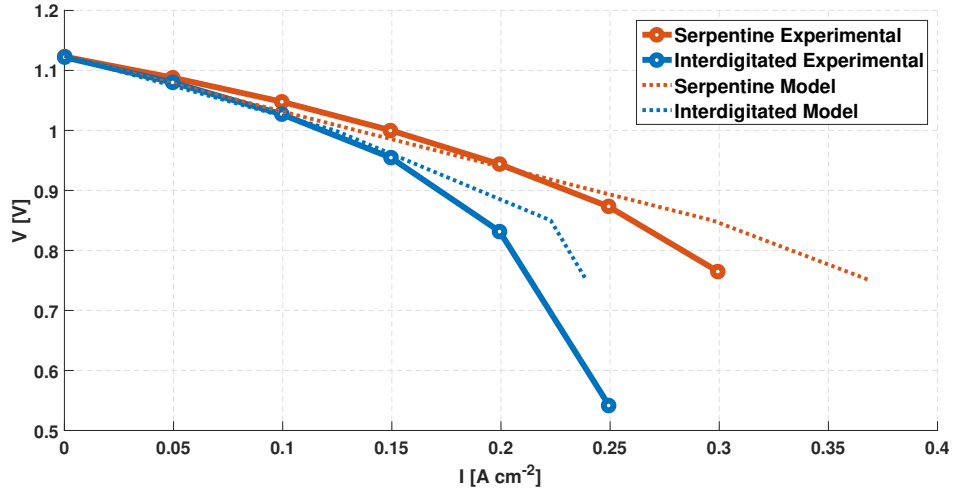

Fig. 5.19: Comparison of the performance between experimental and models for $60\ ml\ min^{-1}$ and SOC=0.6

As a last result regarding this state of charge, the performance of the double outlet geometry is presented when modelled with convective mass transport correlation and the same parameters of table 5.2. Also in this case the modification of the model is able to

forecast accurately the performance of the cell when the flow rate is low but significantly overestimates the values of the current density with high flow rate.

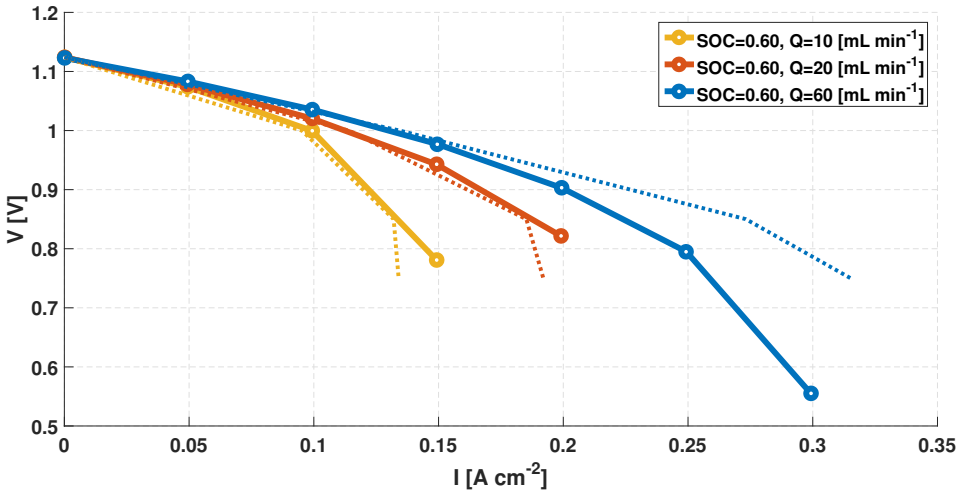

Fig. 5.20: Comparison of the performance between experimental and models for double outlet geometry

To increase the validity of the model curves for high state of charge have also been simulated and the results are reported in figure 5.21 and 5.22. In the graph it is presented a comparison of the performance of the three most influencing flow fields analyzed in this work between the real polarization curves and modelled points.

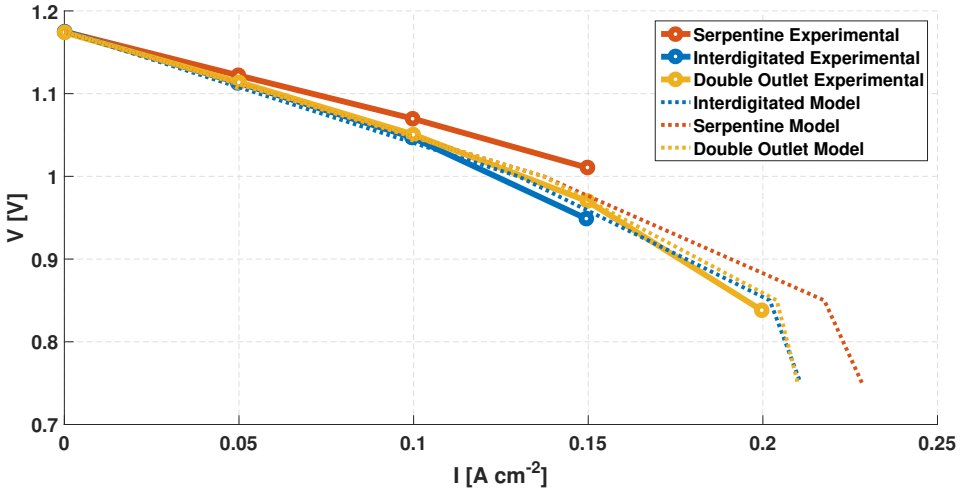

Fig. 5.21: Comparison of the performance between experimental and models for $10\ ml\ min^{-1}$ and SOC=0.9

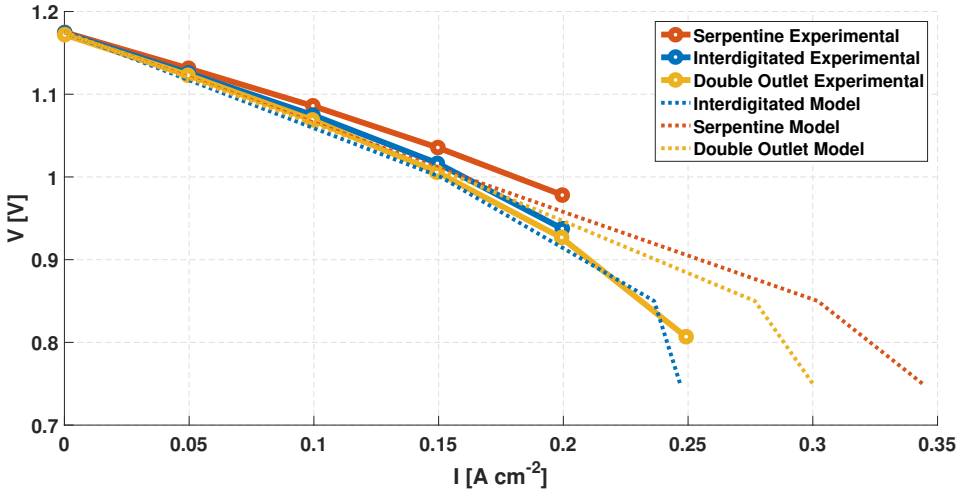

Fig. 5.22: Comparison of the performance between experimental and models for $20\ ml\ min^{-1}$ and SOC=0.9

The models tend to overestimate the performance of all the cells when the state of charge is higher and this effect is more evident when the flow rate is equal to $20\ ml\ min^{-1}$: the points with low voltage present high values of current density. A possible explanation of this fact might be found in the values used for the model and from the fact that the set of parameter used was identified taking into consideration a flow rate of $20\ ml\ min^{-1}$ and a state of charge of 0.6. Therefore the accuracy of the model is expected to decrease out of this working conditions. Further improvements should aim at the identification of more accurate sets of parameters probably not considering the perfect pairing on just one curve but the fitting of two conditions (two different flow rates or two different states of charge), like done in this work for the bidimensional model presented. The huge computational effort made this procedure difficult to be performed effectively with a three dimensional model in the time available for this work. Anyway it has to be kept in mind that is very difficult to numerically understand the performance of these system in all working conditions with just one set of parameters in a threedimensional model.

6 Conclusions

The aim of this work was to understand and quantify the impact of the geometry and design of a flow field on the operation of a Vanadium Redox Flow Battery. In order to accomplish this goal effort has been made to develop numerical models and an experimental campaign has been made. The first part of the work dealt with the development of a bidimensional model using $COMSOL\ Multiphysics^{®}$ simulating in a potentiostatic way the performance of a cell tested in a previous work [32]. The fitting procedure brought to the determination of a set of parameters used throughout the work and gave the opportunity to understand which are the most influencing phenomena and how they are modelled using the constitutive equations of the electrochemical cell. The weight of the parameters on the cell behaviour was clarified and a procedure to solve together electrochemistry and fluid dynamics was developed. The characteristics of the electrode were its active area, the mean pore radius, the permeability and the porosity. These last two influence the fluid dynamic behaviour of the electrode while active area and mean pore radius are involved in the electrochemical reaction kinetics. Other key parameters were the speed of the reaction and the value of charge transfer coefficient. An additional fitting procedure was performed to analyze the characteristic of a thicker electrode and to point out its different behaviour. In all this work the influence of the negative electrode is not taken into account and these hypotheses are justified in the first chapters. The results of the first chapter enlighten how it is difficult to relate the local behaviour of species' fluxes to the overall performance of the cell and how convection plays a major role in the porous domain. Since in the experimental facility in $MRT\ Fuel\ Cell\ Lab$ different flow fields were tested on a Hydrogen-Vanadium cell and caused a significant difference on its performance, the limits of a bidimensional model are identified as they cannot analyze and forecast the influence of the threedimensional effects. A threedimensional code has been developed using $ANSYS\ Fluent^{®}$ with the use of $User\ Defined\ Functions$ and $User\ Defined\ Scalars$. This model solves both electrochemistry and fluid dynamics inside a *5 cm x 5 cm* domain. Such level of detail allows the visualization of the phenomena that occur in the porous electrode and in the channels. What emerges is that the flow in porous medium is not easy to be modelled and its link with electrochemical quantities is complicated: the solid part of the domain is not physically present in the models. Anyway this work clarifies, according to the assumptions made, the phenomenon of the under the rib fluxes, visualizing this quantity inside the electrode domain. The analysis presented is relevant from the scientific point of view as just one example of a fully coupled and full cell threedimensional model is found to exist in the literature [37] and therefore the

knowledge of the problem is not fully investigated. Not much effort has been done to relate locally the performance of the cell to the fluid dynamic condition whereas in this work this aspect is analyzed. The first case studied is the serpentine channel: the pressure distribution inside the cell is heavily influenced by the geometry of the flow field and forces some fluid to pass under the rib in certain zones close to the switchbacks. The model also forecasts for a given flow rate, coherently with the experimental data [32], a lower performance of a triple serpentine with respect to the single one. The analysis of the under the rib fluxes pointed also out that locally the concentration of reactants is crucial for the capability of the system to operate with high current densities. The geometrical characteristics of the domain have been investigated performing a sensitivity analysis with respect to the channel dimension pointing out that for a serpentine flow field the smaller the channel the higher the performance and the pressure drop for a given flow rate and state of charge. According to the experimental analysis present in the literature, a parallel flow field is presented as an example of a situation in which mass transport phenomena are limiting heavily the performance of the battery. A different design is presented: the interdigitated. Its different properties force all electrolyte to move under the rib to reach the outlet. A sensitivity analysis with respect to the dimension of the channel is proposed and the trends of main quantities are also critically analyzed, finding that exists a dimension of the channel that maximize the performance. There are significant differences between the velocity values among the channels for the interdigitated geometry, while the variability of reaction rate and state of charge is heavily dependent on both the geometry of the flow field, the state of charge and the flow rate. The comparison between the interdigitated and serpentine flow field forecasts a better performance of the interdigitated flow field. Thanks to the experience gained in the initial phase of the modelling part, a novel geometry is proposed as a modification of the interdigitated flow field shaping a double outlet geometry. The ideas that drove the process were aimed at giving a direction to the pressure gradient between inlet and outlet and limiting the unevenness of velocity in the channels. The numerical results forecast a certain trend of electrochemical performance but also quantified the pressure drop of the cell, a key parameter for the operation of a real cell as it impacts on the consumption of the auxiliaries and hence has an impact on the energy efficiency of the system. It was found that serpentine design introduces a pressure loss that is one order of magnitude larger than the interdigitated's one in all working conditions. A dedicated procedure was developed to quantify both the energy efficiency of the system and the efficiency with respect to an ideal distributor. The conclusion of this process was that the influence of the flow field has to be taken into account along with the operating condition of the cell and, since in these system there is the possibility of recirculating the electrolyte, in order to have more uniform distribution of reactants one has to operate the cell at low current density or increase the excess of the reaction by means of a higher flow rate. The flow field has to guarantee a uniform distribution of reactants limiting the pressure drop. The flow field that is able to do both these things is proved numerically to be the interdigitated flow field. In order to validate the model with real data an experimental campaign is performed in $MRT\ Fuel\ Cell\ Lab$ testing four different

flow field by means of polarization curve and measuring the pressure drop introduced by the cell. The trend forecast by the model were confirmed by the experimental campaign regarding the performance of the three flow fields derived from an interdigitated design: a base case, the double outlet and an interdigitated flow field with smaller rib and higher number of channels. The influence of a smaller rib is quantified to be penalizing the cell as on one side it has a lower area of the cell over which the potential is fixed and on the other side it causes a higher unevenness of the velocity in the channels giving a lower velocity component in the central digits. The double outlet design is proved to improve the performance of the cell with respect to the interdigitated base case when operated at low state of charge and low flow rate. The experimental campaign pointed also out how the serpentine flow field, whose performance was numerically forecast to be lower than the interdigitated, outperformed all other flow fields in all working conditions tested. The values of pressure drop measured in the experimental facility had the same trend of ones of the simulated cells even if the numerical values were not the same. As a last procedure, since no dedicated fitting procedure was performed on the threedimensional model, an attempt to understand the numerical entity of the performance was considered. Despite the fact that the performance of the serpentine was fitted with a new set of parameters, the simulation regarding the interdigitated were still favoring this last flow field. Effort has been made to understand which could be the reason of such behaviour and it was found out that the way in which mass transport was modelled could effectively change the shape of performance of the simulated cells. A new fitting procedure was therefore put in place considering a convective model for the characterization of the mass transport inside the porous medium and this brought to a better pairing with the experimental data.
The possibility to have an answer in a few hours regarding the performance and the pressure drop of a flow field starting from its drawing in a commercial CAD software makes the model developed in this work a powerful tool for the design of novel geometries for the use in flow batteries. On the other hand what emerged in this work is that the relation of the fluid dynamic flow field and the electrochemical quantities is rather complex and is heavily dependent on which phenomena are taken into account, the way in which these phenomena are modelled and the parameters chosen. A significant analysis has been carried out on the local trends of the most significant quantities in the cell for several working conditions. The results are found to be heavily dependent on both the area of the cell and the thickness of the electrode. Future works are likely to explore the variability of the conclusions of this study with respect to the dimension of the cell and with respect to the way in which the main phenomena are modelled. The absence of the negative electrode is without any doubt another aspect in which the model can be improved, along with a better approach to the modelling of the membrane. There could also be the possibility of writing the model using different softwares such as $Star\ CCM+$ or, if there will be the need of increasing the user capability of customizing the model, $OpenFOAM$ could be a viable solution. The intrinsic complexity of this problem is without any doubt a limit to the capability of models to be fully predictive but their validity as a tool for the comprehension of the working principles of flow battery systems is crystal clear.

7 Appendix

In this appendix several curves are reported that are not directly inserted into chapter 5 for sake of brevity. These data do not present different trends from what stated in the analysis of the experimental campaign. Particularly, here are reported the polarization curves obtained for the interdigitated rib geometry and the double outlet geometry. At first the additional curves for the interdigitated with smaller rib are reported.

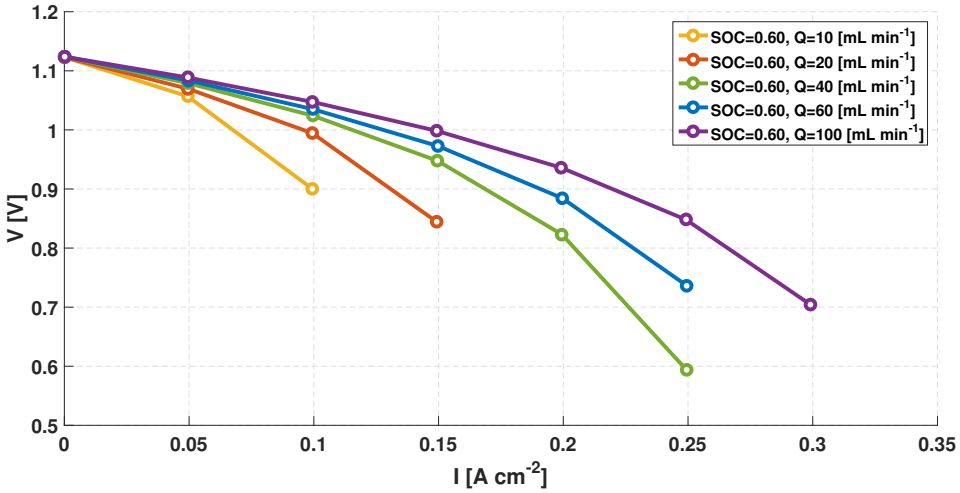

Fig. 7.1: Polarization curves for the interdigitated with smaller rib flow field, SOC=0.6

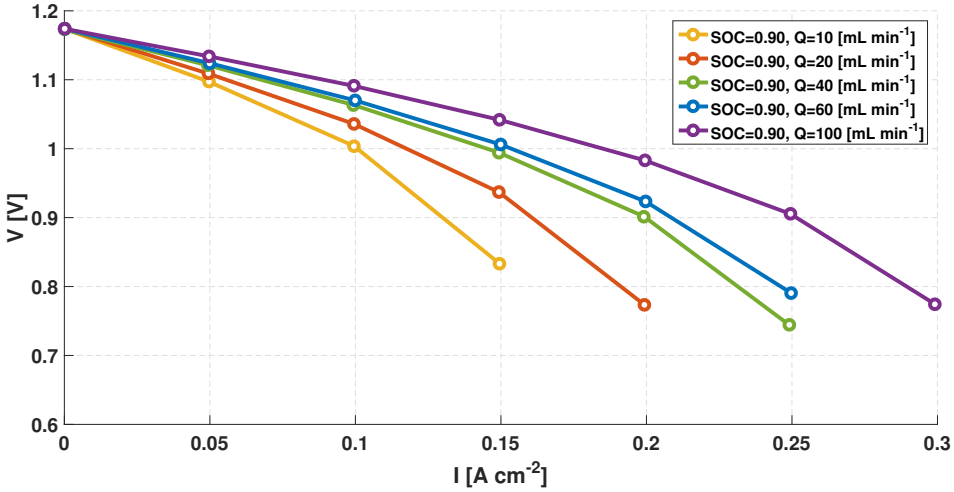

Fig. 7.2: Polarization curves for the interdigitated with smaller rib flow field, SOC=0.9

Secondly polarization curves for the double outlet geometry are reported for both the states of charge considered in this work.

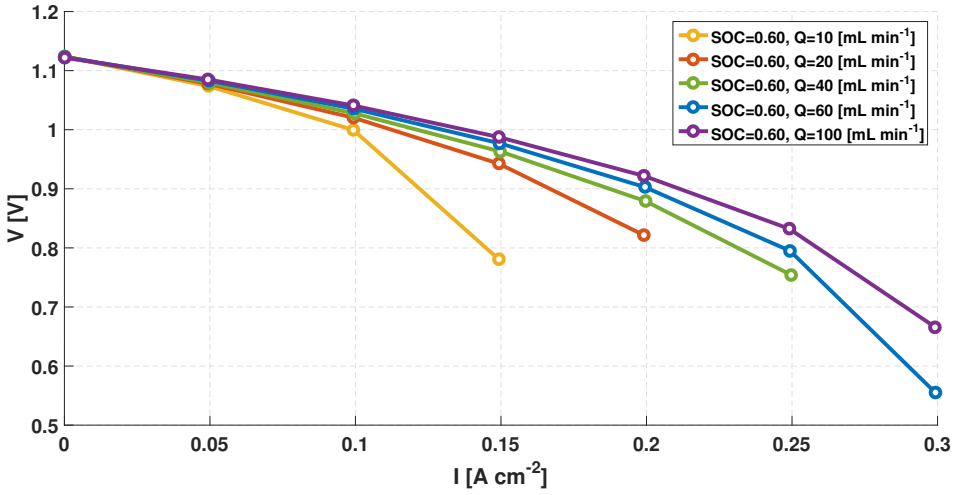

Fig. 7.3: Polarization curves for the double outlet flow field, SOC=0.6

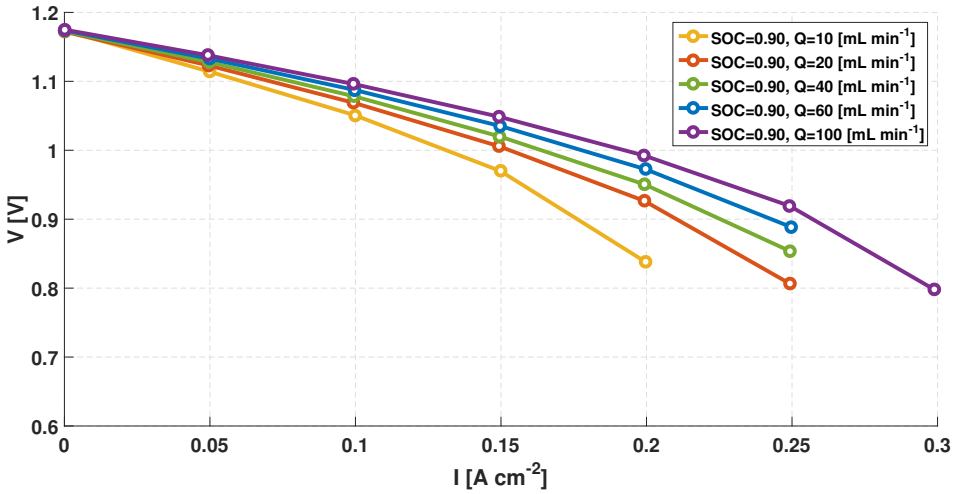

Fig. 7.4: Polarization curves for the double outlet flow field, SOC=0.9

Their comparison among the various flow fields is very significant and is presented previously into the details. When comparing the performance of the simulated flow field in this work two figures have been presented in chapter 4, while to have a complete overlook of the variability of the cell performance simulations were performed. For sake of brevity these figures were not reported but one can have a look on the variability of the performance of the flow fields when the flow rate changes.

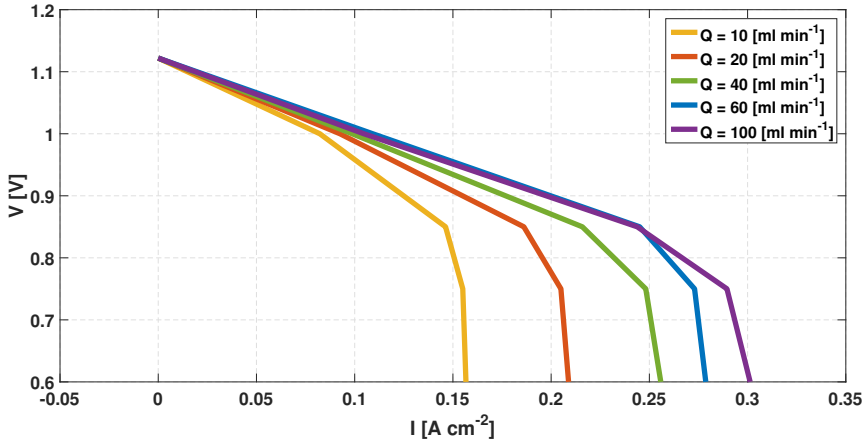

Fig. 7.5: Simulated polarization curves for the interdigitated flow field, SOC=0.6

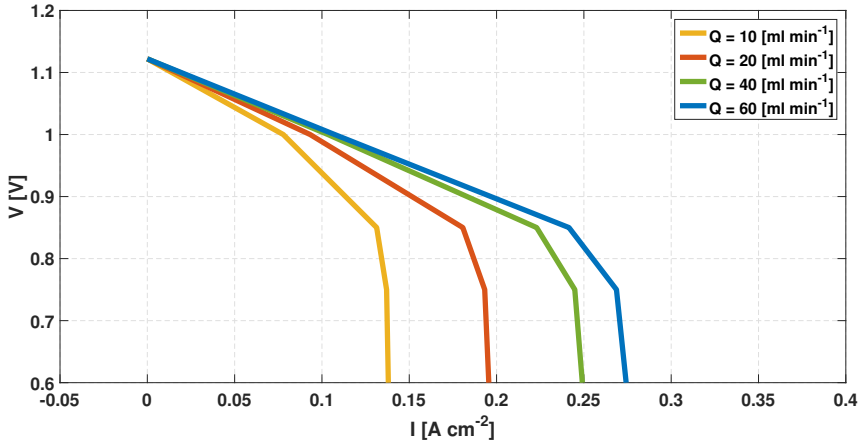

Fig. 7.6: Simulated polarization curves for the serpentine flow field, SOC=0.6

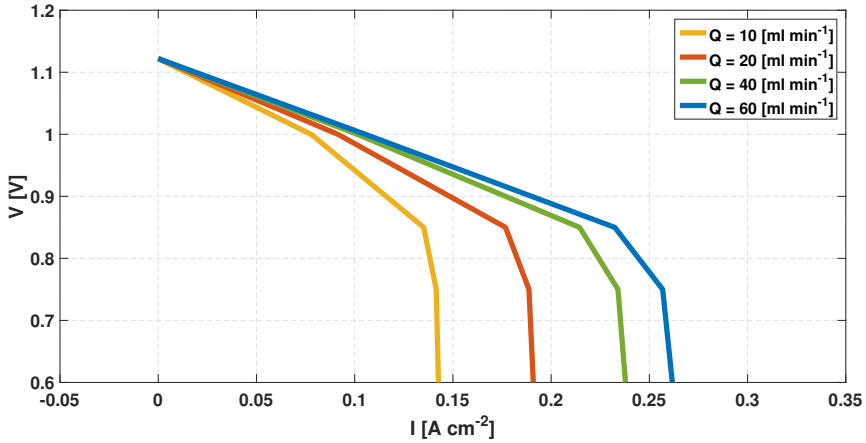

Fig. 7.7: Simulated polarization curves for the interdigitated flow field with smaller rib, SOC=0.6

Bibliography

[1]D. S. Aaron, Q. Liu, Z. Tang, et al. „Dramatic performance gains in vanadium redox flow batteries through modified cell architecture“. In: *Journal of Power Sources* 206 (2012), pp. 450–453 (cit. on pp. vii, xiii, 16).

[2]Doug Aaron, Zhijiang Tang, Alexander B Papandrew, and Thomas A Zawodzinski. „Polarization curve analysis of all-vanadium redox flow batteries“. In: *Journal of Applied Electrochemistry* 41.10 (2011), pp. 1175–1182 (cit. on p. 41).

[3]Dewan Hasan Ahmed and Hyung Jin Sung. „Effects of channel geometrical configuration and shoulder width on {PEMFC} performance at high current density“. In: *Journal of Power Sources* 162.1 (2006), pp. 327 –339 (cit. on p. 16).

[4]Piergiorgio Alotto, Massimo Guarnieri, and Federico Moro. „Redox flow batteries for the storage of renewable energy: A review“. In: *Renewable and Sustainable Energy Reviews* 29.C (2014), pp. 325–335 (cit. on pp. 8, 10, 13).

[5]Allen J Bard and Larry R Faulkner. *Electrochemical Methods: Fundamentals and Applications*. Vol. 677. 2001, p. 833 (cit. on p. 25).

[6]S Bortolin, P Toninelli, D Maggiolo, M Guarnieri, and D Del Col. „CFD study on electrolyte distribution in redox flow batteries“. In: *Journal of Physics: Conference Series* 655.1 (2015), p. 012049 (cit. on pp. 17, 48).

[7]Ching Liang Chen, Hak Koon Yeoh, and Mohammed Harun Chakrabarti. „An enhancement to Vynnycky's model for the all-vanadium redox flow battery“. In: *Electrochimica Acta* 120 (2014), pp. 167–179 (cit. on p. 22).

[8]Sara Corcuera and Maria Skyllas-Kazacos. „State-of-Charge Monitoring and Electrolyte Rebalancing Methods for the Vanadium Redox Flow Battery“. In: *European Chemical Bulletin* 1.12 (2012), pp. 511–519 (cit. on p. 7).

[9]C. R. Dennison, Ertan Agar, Bilen Akuzum, and E. C. Kumbur. „Enhancing Mass Transport in Redox Flow Batteries by Tailoring Flow Field and Electrode Design“. In: *Journal Of The Electrochemical Society* 163.1 (2016), A5163–A5169 (cit. on pp. 17, 73, 74).

[10]Bruce Dunn, Haresh Kamath, and Jean-Marie Tarascon. „Electrical Energy Storage for the Grid: A Battery of Choices“. In: *Science* 334.6058 (2011), pp. 928–935. eprint: `http://science.sciencemag.org/content/334/6058/928.full.pdf` (cit. on pp. 8–10).

[11]„Examining Spatial (Grid) Convergence“. In: () (cit. on p. 65).

[12]Giulia Fontana. *Studio sperimentale e modellistico di una batteria a flusso vanadio-vanadio*. 2015 (cit. on pp. 21, 33).

[13]Jacob Houser, Jason Clement, Alan Pezeshki, and Matthew M. Mench. „Influence of architecture and material properties on vanadium redox flow battery performance“. In: *Journal of Power Sources* 302 (2016), pp. 369 –377 (cit. on pp. 74, 76, 104).

[14]Ke-Long Huang, Xiao-gang Li, Su-qin Liu, Ning Tan, and Li-quan Chen. „Research progress of vanadium redox flow battery for energy storage in China“. In: *Renewable Energy* 33.2 (2008), pp. 186–192 (cit. on p. 15).

[15]Jiin-Yuh Jang, Chin-Hsiang Cheng, and Yu-Xian Huang. „Optimal design of baffles locations with interdigitated flow channels of a centimeter-scale proton exchange membrane fuel cell“. In: *International Journal of Heat and Mass Transfer* 53.4 (2010), pp. 732 –743 (cit. on p. 16).

[16]T. Jyothi Latha and S. Jayanti. „Hydrodynamic analysis of flow fields for redox flow battery applications“. In: *Journal of Applied Electrochemistry* 44.9 (2014), pp. 995–1006 (cit. on pp. 17, 48, 59).

[17]K W Knehr, Ertan Agar, C R Dennison, A R Kalidindi, and E C Kumbur. „A Transient Vanadium Flow Battery Model Incorporating Vanadium Crossover and Water Transport through the Membrane“. In: *Journal of The Electrochemical Society* 159.9 (2012), pp. 1446–1459 (cit. on pp. 15, 19, 22, 24, 33).

[18]E. Knudsen, P. Albertus, K.T. Cho, A.Z. Weber, and A. Kojic. „Flow simulation and analysis of high-power flow batteries“. In: *Journal of Power Sources* 299 (2015), pp. 617 –628 (cit. on p. 48).

[19]Andrei A Kulikovsky. *Analytical modelling of fuel cells*. 2010 (cit. on p. 25).

[20]S. Kumar and S. Jayanti. „Effect of flow field on the performance of an all-vanadium redox flow battery“. In: *Journal of Power Sources* 307 (2016), pp. 782 –787 (cit. on p. 17).

[21]Y. Lei, B.W. Zhang, B.F. Bai, and T.S. Zhao. „A transient electrochemical model incorporating the Donnan effect for all-vanadium redox flow batteries“. In: *Journal of Power Sources* 299 (2015), pp. 202 –211 (cit. on p. 19).

[22]M.Reed. „Stack Developments in a kW Class All Vanadium Mixed Acid Redox Flow Battery at the Pacific Northwest National Laboratory“. In: *Journal of Industrial and Engineering Chemistry* 45 (2017), pp. 387 –390 (cit. on p. 14).

[23]Donald A. Nield. *Convection in porous media*. 2013 (cit. on p. 48).

[24]O.M. Orogbemi, D.B. Ingham, M.S. Ismail, et al. „Through-plane gas permeability of gas diffusion layers and microporous layer: Effects of carbon loading and sintering“. In: *Journal of the Energy Institute* (2017), pp. – (cit. on p. 50).

[25]Dong-Jun Park, Kwang-Sun Jeon, Cheol-Hwi Ryu, and Gab-Jin Hwang. „Performance of the all-vanadium redox flow battery stack“. In: *Journal of Industrial and Engineering Chemistry* 45 (2017), pp. 387 –390 (cit. on p. 14).

[26]Eugenio Rovera. *Sviluppo di un modello di una batteria a flusso vanadio-vanadio*. 2014 (cit. on pp. 13, 15, 21, 22, 28, 30, 52).

[27]D. Schmal, J. Van Erkel, and P. J. Van Duin. „Mass transfer at carbon fibre electrodes“. In: *Journal of Applied Electrochemistry* 16.3 (1986), pp. 422–430 (cit. on pp. 105, 106).

[28]A. A. Shah, M. J. Watt-Smith, and F. C. Walsh. „A dynamic performance model for redox-flow batteries involving soluble species“. In: *Electrochimica Acta* 53.27 (2008), pp. 8087–8100 (cit. on p. 6).

[29]A. A. Shah, H. Al-Fetlawi, and F. C. Walsh. „Dynamic modelling of hydrogen evolution effects in the all-vanadium redox flow battery“. In: *Electrochimica Acta* 55.3 (2010), pp. 1125–1139 (cit. on p. 22).

[30]Sigracet. URL: http://fuelcellsetc.com/helpful-tools/gas-diffusion-layer-gdl-comparison-chart/ (cit. on p. 33).

[31]Sigracet. *SIGRACET Gas Diffusion layers for PEM Fuel Cells, Eletrolyzers and Batteries* (cit. on p. 87).

[32]Matteo Tagliabue. *Caratterizzazione sperimentale e analisi modellistica del catodo di una batteria a flusso al vanadio* (cit. on pp. 16, 17, 22, 33, 41, 42, 44, 47, 95, 96, 111, 112).

[33]Ao Tang, John McCann, Jie Bao, and Maria Skyllas-Kazacos. „Investigation of the effect of shunt current on battery efficiency and stack temperature in vanadium redox flow battery“. In: *Journal of Power Sources* 242 (2013), pp. 349–356 (cit. on pp. 8, 23).

[34]Vilayanur Viswanathan, Alasdair Crawford, David Stephenson, et al. „Cost and performance model for redox flow batteries“. In: *Journal of Power Sources* 247 (2014), pp. 1040 –1051 (cit. on pp. 8, 10–12).

[35]M. Vynnycky. „Analysis of a model for the operation of a vanadium redox battery“. In: *Energy* 36.4 (2011), pp. 2242–2256 (cit. on p. 22).

[36]Jia X. Wang, Thomas E. Springer, and Radoslav R. Adzic. „Dual-Pathway Kinetic Equation for the Hydrogen Oxidation Reaction on Pt Electrodes“. In: *Journal of The Electrochemical Society* 153.9 (2006), A1732 (cit. on p. 19).

[37]Q Xu, T S Zhao, and P K Leung. „Numerical investigations of flow field designs for vanadium redox flow batteries“. In: *Applied Energy* 105 (2013), pp. 47–56 (cit. on pp. ix, 17, 30, 47, 49, 74, 104, 105, 107, 111).

[38]Cong Yin, Yan Gao, Shaoyun Guo, and Hao Tang. „A coupled three dimensional model of vanadium redox flow battery for flow field designs“. In: *Energy* 74 (2014), pp. 886 –895 (cit. on p. 47).

[39]Dongjiang You, Huamin Zhang, and Jian Chen. „A simple model for the vanadium redox battery“. In: *Electrochimica Acta* 54.27 (2009), pp. 6827 –6836 (cit. on p. 22).

[40]Dongjiang You, Huamin Zhang, and Jian Chen. „A simple model for the vanadium redox battery“. In: *Electrochimica Acta* 54.27 (2009), pp. 6827 –6836 (cit. on pp. 104, 105, 107).

[41]Behnam Zakeri and Sanna Syri. „Electrical energy storage systems: A comparative life cycle cost analysis“. In: *Renewable and Sustainable Energy Reviews* 42 (2015), pp. 569–596 (cit. on pp. 5, 8, 10).

[42]Y.K. Zeng, T.S. Zhao, L. An, X.L. Zhou, and L. Wei. „A comparative study of all-vanadium and iron-chromium redox flow batteries for large-scale energy storage“. In: *Journal of Power Sources* 300 (2015), pp. 438 –443 (cit. on pp. 10, 12).

Websites

[30]Sigracet. URL: http://fuelcellsetc.com/helpful-tools/gas-diffusion-layer-gdl-comparison-chart/ (cit. on p. 33).

List of Figures

List of Tables